FY25 NRL DOD HPCMP ANNUAL REPORTS

U.S. NAVAL RESEARCH LABORATORY

FY25 NRL DoD
High Performance Computing Modernization Program Annual Reports

Edited by
Dr. Yu Yu Khine

Prepared by
Beth A. Howell

Center for Computational Science
Information Technology Division

June 1, 2026

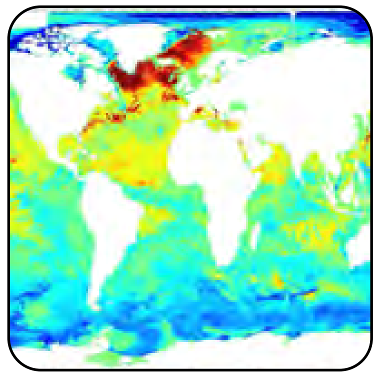
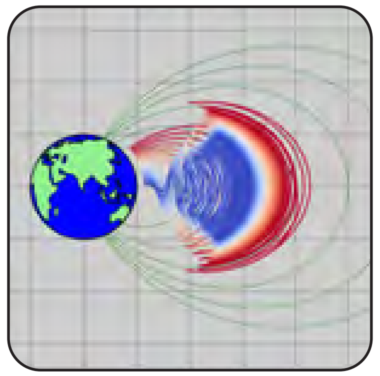
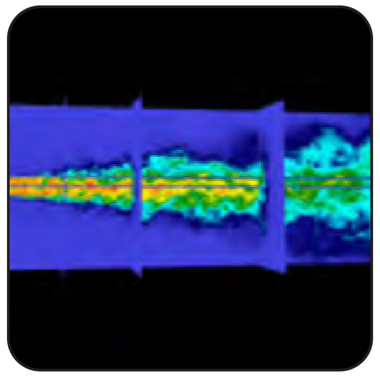

REVIEWED AND APPROVED
NRL/5590/PU--2026/1
IR-5590-26-1-U
May 2026

Center for Computational Science
Information Technology Division

~ *Preface* ~

This volume presents work accomplished by the NRL scientists and engineers and their collaborators using the DoD's High Performance Computing Modernization Program (HPCMP) resources for fiscal year 2025. The reports reflect research performed across NRL's three primary sites: Washington, D.C., Stennis Space Center, Mississippi, and Monterey, California, and are approved for public release.

We publish this book annually to highlight recent findings, methodological advances, and engineering insights that enhance the capabilities of the defense community and support the mission of the department. These efforts are made possible through the technical and financial resources provided by the HPCMP.

The reports are organized according to the primary Computational Technology Areas (CTAs) defined by the HPCMP and document the use of computational resources at the DoD Supercomputing Resource Centers (DSRCs) and at the Affiliated Resource Centers (ARCs). For ease of reference, this volume includes three indices: an author index, a site index, and an NRL hierarchical index organized by branch and division.

Please contact us for additional copies of this volume or for further information regarding high-performance computing (HPC) activities at NRL.

Respectfully,

Center for Computational Science, Code 5590
US Naval Research Laboratory
4555 Overlook Ave SW
Washington, DC 20375
www.nrl.navy.mil

This page intentionally left blank

Table of Contents

Computational Biology, Chemistry, and Materials Science (CCM)

<u>Computational Electromagnetics and Acoustics (CEA)</u>

Climate Weather Ocean Modeling (CWO)

THIS PAGE INTENTIONALLY LEFT BLANK

CSM

Computational Structural Mechanics

The Computational Structural Mechanics (CSM) Computational Technology Area (CTA) focuses on high-resolution, multidimensional modeling of materials and structures subjected to a broad spectrum of loading conditions, including quasistatic and dynamic loads, electromagnetic effects, shocks, penetrations, and blasts. The field also encompasses materials design, an inherently interdisciplinary area that relies on multiscale modeling spanning atomistic to macroscopic length scales. High-performance computing enables the accurate numerical solution of governing conservation laws, equations of motion, equations of state, and constitutive models across simple to highly complex geometries and material systems, subject to realistic boundary conditions and loading scenarios.

Representative defense applications include underwater explosions and ship response, structural acoustics, coupled multiphysics problems, propulsion system analysis, and weapon simulations. CSM also underpins lethality and survivability assessments for weapon systems — including aircraft, ships, submarines, and ground vehicles — as well as theater missile defense analyses, design optimization, and real-time, large-scale soldier- and hardware-in-the-loop simulations.

Title: Geometric, Constitutive and Loading Complexities in Structural Materials
Author(s): S.A. Wimmer,[1] N. Wade,[2] and A. Arcari[1]
Affiliation(s): [1]U.S. Naval Research Laboratory, Washington, DC; [2]American Society for Engineering Education Postdoctoral Fellow at the U.S. Naval Research Laboratory, Washington, DC
CTA: CSM

Computer Resources: HPE Cray EX [AFRL, OH], [ARL, MD], [NAVY, MS]

Research Objectives: This project focuses on developing efficient, accurate computational models for complex material interactions. Many Navy materials of interest have complexities that require coupled material responses and in many of these cases, analytical models and techniques cannot fully account for the complex geometries or the multiphysics involved. In order to accurately model the nonlinear response of conventional structural materials, rate dependence, large deformation, and damage accumulation mechanisms, additional computational tools are needed. The primary research objective of this project is to develop these tools in support of internal and external data collection.

Methodology: The project uses finite element methods (FEM), as these methods are highly versatile and represent the current best practice in many cases. However, due to nonlinear complexities, coupled material responses, and complex multiphysics iterations, these models can be very large and can have extended run times. Using CUBIT, ABAQUS/CAE, and/or in-house software, new methods for efficient, accurate modeling of these effects are tested. The work also expands into alternative methods for solving these problems, which includes developing neural networks using TensorFlow. These physics-informed neural networks (PINNs) allow for the pretraining and embedding of the physical laws, resulting in a faster feed-forward calculation.

Results: While this project encompassed several studies, an illustrated result for a PINN trained to solve stochastic boundary value problems (BVPs) is presented. Stochastic BVPs are especially computationally expensive, as they require repeated evaluation of the computational models. PINNs are potentially ideal for solving such problems because once trained, a PINN can produce model predictions for a random set of parameters in a fraction of the time it would take to solve a FEM model. However, training these models is quite complex and challenging. After initial testing and hyperparameter tuning, a PINN model was constructed that can closely approximate a known finite element solution (see Fig. 1). From here, different network architectures and training methods were tested to determine which would best function as a surrogate model (see Fig. 2). Ultimately, it was found that a PINN could produce accurate solution fields and outperformed other model architecture on a like-for-like basis.

Defense Impact/Significance: This project provides several key benefits to the Department of the Navy (DON). First, the expertise gained in building and testing advanced finite element models bolsters the DON’s capacity to both diagnose and engineer solutions to many complete problems. Second, the experience gained in training these machine learning models can be applied across a range of artificial intelligence/ machine learning applications. This, in turn, will help the DON’s capacity to develop, train, and leverage similar models in the future. Third, the improved computational efficiency of these models can help reduce the computational demands on high-performance computing systems in future.

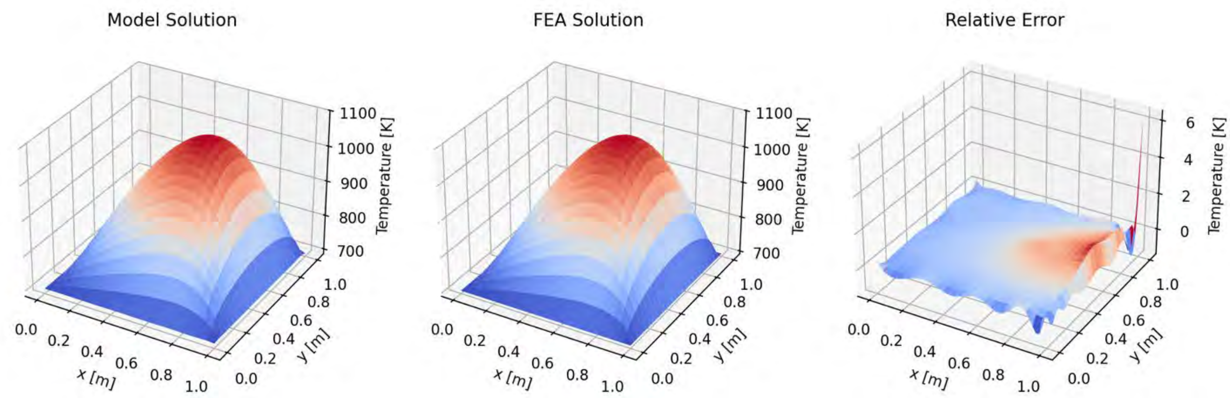

Figure 1. The PINN solution (left) is shown to closely predict the finite element solution (middle), resulting in small absolute errors. The relative error between the models was less than 1% and was contained near the boundary.

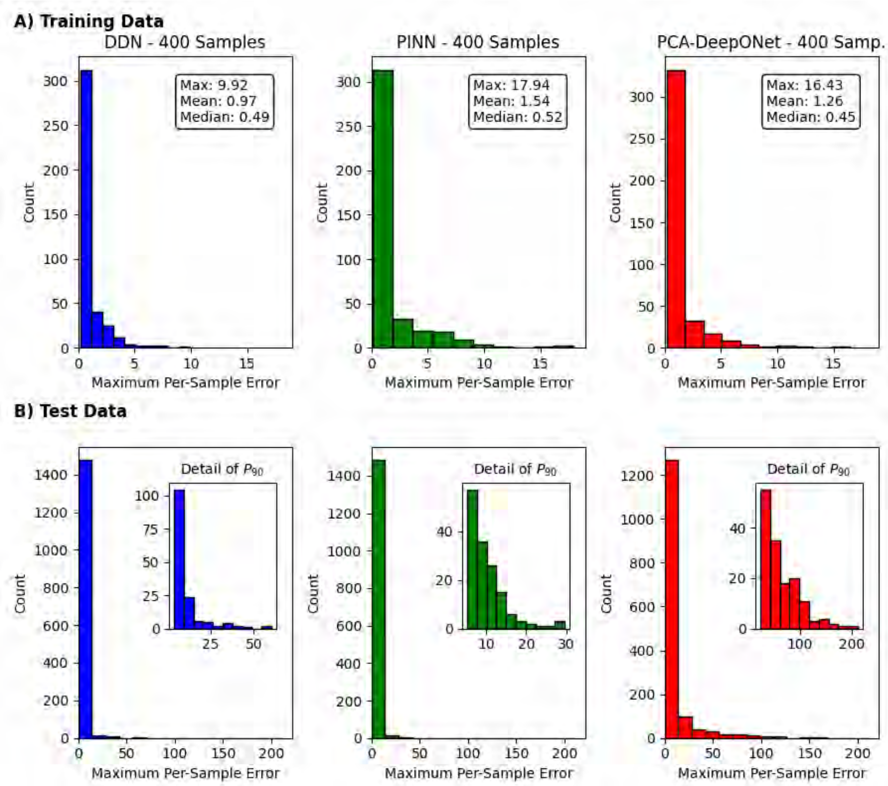

Figure 2. A comparison of different model architectures. While the training data showed comparable results between all three different models, the testing data showed a marked improvement for the PINN architecture. One key accomplishment was the improved performance over a purely data-driven network, something that has been very hard to demonstrate.

Title: Stochastic Methods for Uncertainty Quantification in Computational Mechanics
Author(s): K. Teferra,[1] N. Wade,[2] and A. Chadwick[1]
Affiliation(s): [1]U.S. Naval Research Laboratory, Washington, DC; [2]American Society for Engineering Education Postdoctoral Fellow at the U.S. Naval Research Laboratory, Washington, DC
CTA: CSM

Computer Resources: HPE Cray EX [ARL, MD], [NAVY, MS]; HPE Cray EX 4000 [ERDC, MS]

Research Objectives: The research objective for the work in FY25 that is highlighted in this report is the development of a technique to represent material stress/strain behavior through a general neural network expression rather than classical algebraic expressions that have limited expressivity. The focus on this work is on rate-independent elastoplasticity, where the stress is confined to reside on the surface of a convex domain during plastic increments, resulting in a constrained optimization problem to update the material state variables given a strain update. The structure of the system of equations to solve prevents establishment of a loss function for training the neural network material model from which gradients can be analytically derived, precluding the use of the ubiquitous stochastic gradient descent method (SGD). Therefore, non-gradient-based optimization of large parameter vectors is sought, and the ensemble Kalman inversion (EKI) numerical optimization method for solving inverse problems is investigated. The EKI is a particle method that translates well to HPC systems because of the large number of embarrassingly parallel calculations involved.

Methodology: The general approach proposed to achieving a machine learning material model for rate-independent plasticity involves the generation of stress-strain data (which represents either experimental data or computational data of homogenized stress-strain curves in multiscale modeling), establishment of the target architecture of convex neural network models for the plastic potential, and the performance of a two-stage optimization involving SGD followed by EKI. An initial SGD step must be performed based on a “dummy” material model that approximates the data, which can be a classical model. This approach is necessary because the neural network material model needs a good starting point for its parameters to produce a numerically stable stress update. After this starting point is achieved, EKI is executed to minimize the loss between the stress history of the data and that produced through the neural network model.

Results: During FY25, progress was made in implementing and benchmarking the codes required to execute the methodology. A Von Mises material model was implemented to be used as the stress/strain data. The SGD for the neural network model for setting up the initial parameter set was implemented using TensorFlow. Also, two forms of the EKI algorithm were implemented: the generic EKI algorithm and a version that enables inequality constraints on its parameters. These algorithms were implemented using MPI and have been benchmarked on multiple examples. Sample results from this study are presented in Figs. 1 and 2.

Defense Impact/Significance: The enhanced structural material performance in terms of durability, strength-to-weight ratio, and manufacturability are essential ingredients toward transforming fleet capabilities. Improved representation of material models is essential to optimizing material and structural performance. Further, advanced manufacturing techniques, such as additive manufacturing, contain processing effects that lead to complex material response that classical models fail to fully capture. Further, machine learning constitutive models are a key feature in multiscale models by enabling engineering-scale material models that are derived directly from small-scale representative volume element analyses that incorporate fundamental material response mechanisms. These models are crucial for the development of high-throughput models for exploring material and structural design space.

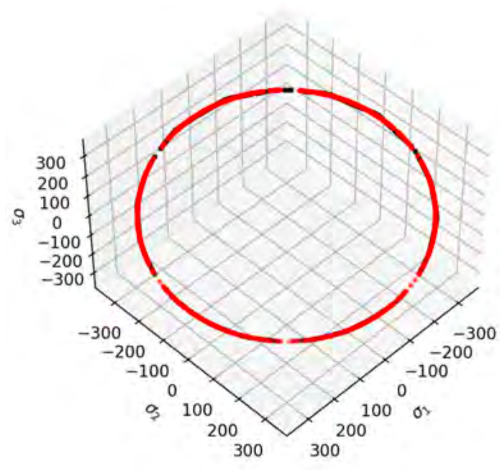

Figure 1. Von Mises yield surface in principal stress space. Red dots represent the analytical model and black dots represent the machine learning model.

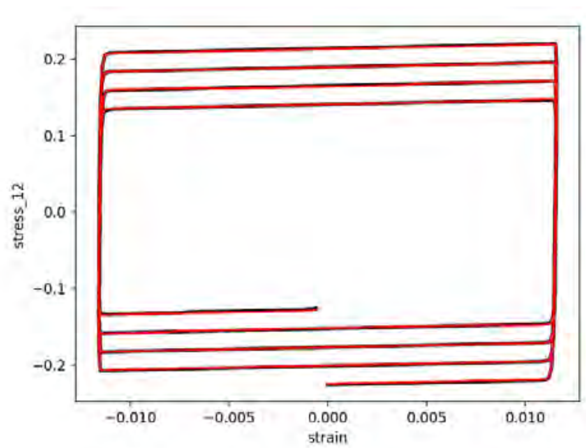

Figure 2. Example stress strain curve of Von Mises material model comparing ground truth (red curve) with Von Mises model with material parameters determined through EKI algorithm (black curve).

Title: Computational Analysis of Warfighter Brain Injury and Protective Equipment
Author(s): X.G. Tan and A.E. Moser
Affiliation(s): U.S. Naval Research Laboratory, Washington, DC
CTA: CSM

Computer Resources: HPE Cray EX [AFRL, OH], [NAVY, MS]; HPE Cray EX 4000 [ERDC, MS]

Research Objectives: The research objective of this project is the development of methods to prevent and mitigate injury to warfighters. This involves computational analysis of ballistic/blunt impacts on personal protective equipment (PPE) and blast-induced traumatic brain injury (TBI). Computational methods, such as finite element analysis, are used to conduct the simulation analysis. The use of HPC resources is vitally important to this project due to the high fidelity of the models of interest. A typical model to analyze traumatic brain injury requires approximately 24 hours on 128 CPUs. One of the primary outcomes of this research will be the accumulation of a significant number of simulations that will be used to construct the corresponding relationship between humans and animals and to optimize the design of protective equipment.

Methodology: The project uses finite element methods extensively, but the work is not restricted to finite element methodologies. Nonlinear material mechanical constitutive response features are highlighted in much of the work performed. Implicit and explicit solution methods are used as appropriate. The primary finite element codes used are CoBi, Abaqus, and CTH. User subroutines are used for specialized material constitutive response when applicable. Multiphysics analysis is used to capture the fluid/acoustic-structure interaction and electromagnetic (EM)-induced thermomechanical effects. Typically, ParaView, Abaqus/Viewer, VisIt, IDL, and Matlab are used for visualization of results in formats such as VTU and HDF5, including animation. For model development, the project typically uses CUBIT, ABAQUS/CAE, Simpleware, IDL and in-house code. Large run times and large model sizes are often required for the multiphysics/multistep nonlinear finite element/volume analysis jobs.

Results: This project involves work in several topical areas. Research has been conducted on the numerical investigation of hearing-loss mechanisms induced by blast exposure, with emphasis on bone-conducted impulse-noise transmission into the inner ear. A key question is how a small air bubble trapped in the fluid-filled inner ear of the head surrogate model that was observed experimentally affects inner ear fluid pressure measurement when the head is exposed to blast overpressure. Understanding this effect can help guide strategies to prevent bubble formation and to enhance experimental quality. To address this, we developed a high-fidelity finite element (FE) model of the head surrogate to simulate the biomechanical response of the inner ear to impulse noise. The submillimeter air bubble in the fluid was explicitly represented using a locally refined mesh in the inner ear regions. Appropriate material models for the skull, the brain tissue, and the air-fluid system in the inner ear, along with loading conditions derived from recorded incident data, were incorporated into the simulations. By varying the size and location of the air bubble, we evaluated its influence on pressure transmission. Figure 1 shows that the air bubble can substantially alter inner ear fluid pressure compared with a no-bubble model. An air bubble only a few percent of the inner ear's length can significantly reduce pressure amplitude and can introduce oscillations in the inner ear fluid.

Defense Impact/Significance: Insights gained from this project are essential for advancing the technology from concept to application. Expected outcomes include a deeper understanding of the mechanisms underlying traumatic brain injury and impulse noise-induced hearing loss relevant to naval and other defense operations. New insights will be achieved by quantifying the effects of anatomical and material variability on the mechanical responses associated with these injuries. These findings will enhance warfighter health by contributing to the development of improved protective gear and advancing understanding of the relationship between mechanical response thresholds and injury onset. The development of techniques to model population-wide anatomical variability will provide insight into the importance of the fit of protective gear.

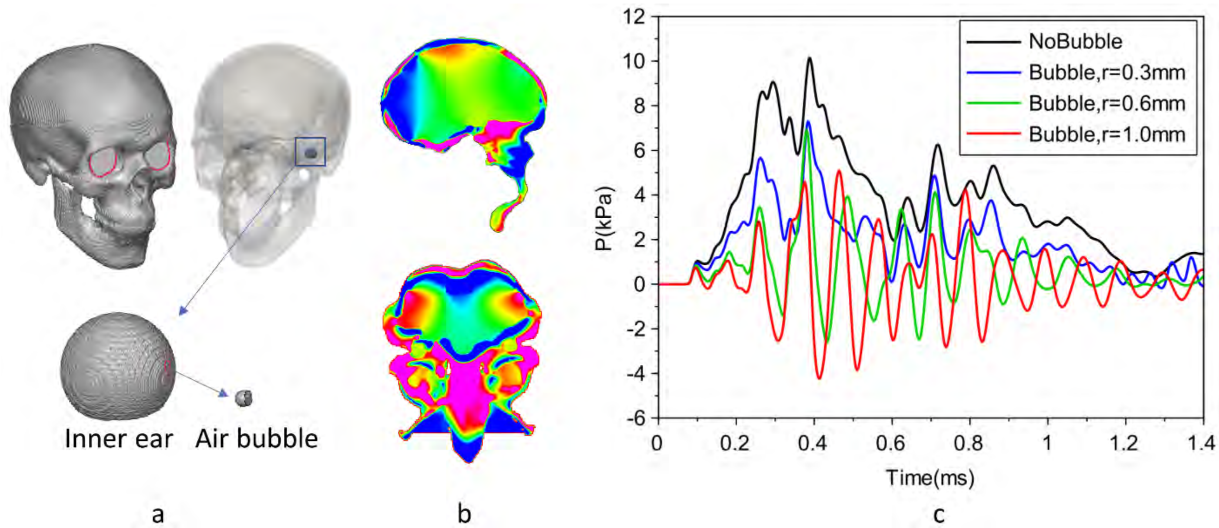

Figure 1. Simulation of NRL's head surrogate model exposed to impulse noise: (a) finite element (FE) model of the head surrogate with a mesh resolution of 0.9 mm and locally refined elements of 0.1 mm in the inner ear regions, (b) pressure distributions in the sagittal and transverse planes of the head subjected to frontal blast loading, and (c) pressure histories in the inner ear fluid with and without an air bubble.

Title: Atomistic Simulations of Structural Materials
Author(s): E. Antillon
Affiliation(s): U.S. Naval Research Laboratory, Washington, DC
CTA: CSM

Computer Resources: Penguin Open Compute Platform (OCP) [AFRL, OH]

Research Objectives: The specific objectives of this program are to use first-principles plane-wave codes employing density functional theory (DFT) calculations to understand magnetostructural effects present in austenitic steel alloys. In structural metals, the type of the deformations largely determines the materials' response to mechanical load within the plastic domain, which is generally carried out by glide of preexisting dislocations. When the applied local net shear stresses reach the critical resolved shear stress of the slip system, slip will occur, but other competing mechanisms, such as twinning, can also become a viable deformation mechanism if the value of the intrinsic stacking fault energy (SFE) is sufficiently low that a transformation to a local hcp transformation becomes favorable. In this study, we would like to precisely measure the value of the intrinsic stacking fault energy for a range of compositions of austenitic steel alloys.

Methodology: We will use the VASP and SPHInX codes to perform all density functional theory calculations. While VASP is the method of choice to solve ab initio calculations in most systems, SPHInX has emerged as an alternative, with the additional advantage of providing atomic spin constraints along with robust, fast minimizers that can allow for faster convergence on calculations for magnetically frustrated systems. Because of the high iron content in steels, various sampling methods on magnetic moments are necessary to approximate the fully disordered magnetic states present in these types of alloys. Our calculations will measure energies associated with various chemical and magnetic arrangements, allowing us to better characterize materials properties of metallic alloys.

Results: A significant discrepancy has been found between experimentally measured stacking fault energies and those obtained through ab initio calculations, especially in alloys with large magnetic moments. It recently has been argued [1] that this discrepancy is due to neglecting the contribution of longitudinal spin fluctuations to the energy calculations, which can be composition- and temperature-dependent. Spin-constrained calculations provide a pathway to measure effective spin coupling to the lattice by performing several calculations to approximate the paramagnetic state, where the magnetic moments can be varied independently while remaining in a disordered arrangement. Other alternative methods that mimic the paramagnetic state initialize the moments randomly and allow their magnitudes to float to find the ground state energy. However, these two methods yield very different results. In the case of FCC-Fe, Fig. 1(a) (bottom panel) shows the longitudinal energy landscape obtained by fixing the magnitude of the magnetic moment while the direction of the moments is assigned randomly. The top panel also illustrates the probability density function of the distribution expected at 300 K and 1200 K. Using this information, values of the SFE can be predicted at a given temperature and volume, where the moments either incorporate the longitudinal spin fluctuation or use floating spins, where the moments find the lowest energy value according to that specific volume. Constrained-spin calculations are evidently closer to the range of experimentally observed values. With this approach, we hope to better describe magnetostructural interactions at finite temperatures on a variety of austenitic steel compositions.

Defense Impact/Significance: The aforementioned objectives have direct relevance to military interests, particularly in the design of superior steel alloys for surface and underwater naval vessels. Our calculations will provide fundamental inputs into the integrated computational materials engineering (ICME) framework, connecting accurate, atomic-scale calculations to processing-property-performance relationships. By implementing a novel approach to account for longitudinal spin fluctuations, which are known to play a critical role at finite temperatures in paramagnetic austenitic steels, we aim to develop a robust, predictive, first-principles methodology for calculating stacking fault energies across a range of austenitic steel compositions. This ICME approach has the potential to significantly reduce the cost and time required to design new materials.

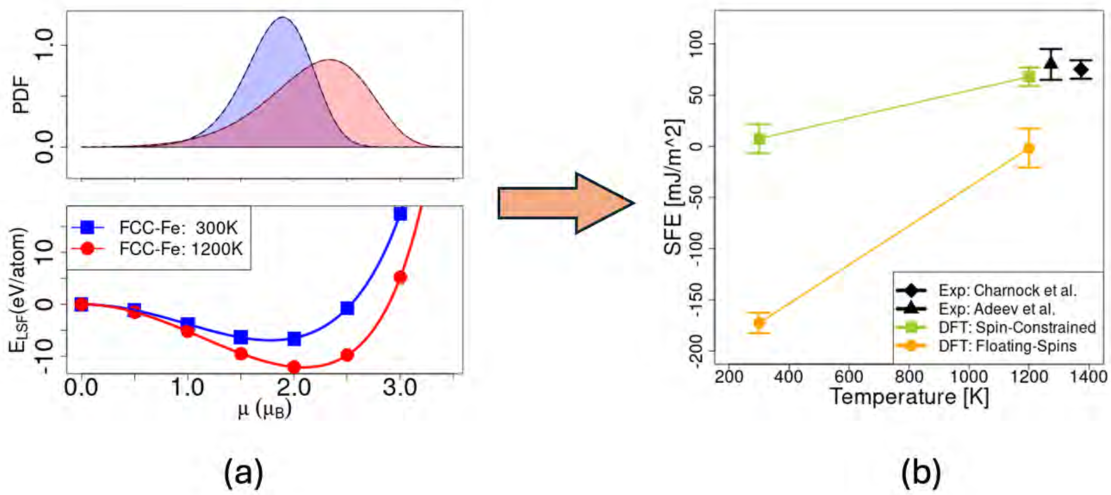

Figure 1. (a) (Top panel) Sample probability density function showing the distribution of moments expected at a given temperature and volume. (Bottom panel) Longitudinal spin fluctuation (LSF) energy, E_LSF, as a function of the local magnetic moment. (b) Intrinsic stacking fault using constrained and floating-spin calculations at 300 K and 1200 K on γ-Fe, compared to experiments at 1273 K and 1373 K, respectively [2,3].

References

[1] Y. W. Choi et al., “Predicting the stacking fault energy of austenitic Fe–Mn–Al(Si) alloys,” Mater. Des., vol. 187, Art. no. 108392, 2020.
[2] V. M. Adeev and Y. N. Petrov, “Influence of carbon on the stacking fault energy of austenite in plain carbon steel,” Ukr. Fiz. Zh., vol. 20, no. 12, pp. 2004–2007, 1975.
[3] W. Charnock and J. Nutting, “The effect of carbon and nickel upon the stacking-fault energy of iron,” Metal Sci. J., vol. 1, no. 1, pp. 123–127, 1967.

THIS PAGE INTENTIONALLY LEFT BLANK

CFD

Computational Fluid Dynamics

Fluid dynamics involves inherently complex phenomena, including boundary layers, the transition to turbulence, and fully developed turbulent flow. The Computational Fluid Dynamics (CFD) CTA addresses these challenges by using high-performance computing to accurately solve the governing equations of fluid and gas motion. Modern computing architectures enable CFD to support both fundamental research and engineering design for complex flow configurations. CFD also plays a key role in interpreting experimental data and extending predictions into flow regimes that are difficult, impractical, or too costly to study experimentally.

Defense-relevant research within the CFD CTA spans the full range of velocity regimes. Incompressible flows dominate low-speed systems, such as underwater hydrodynamics, slow-moving aircraft, internal flows, and environmental air circulation, while compressible flows govern higher-speed systems, including transonic, supersonic, and hypersonic systems, missiles, and projectiles. Realistic CFD simulations often require additional coupled physics to represent operational environments accurately. These include external force fields; interactions with surface chemistry, atomic-scale processes, and microphysics; phase changes; chemical reactions; and multiphase effects in heterogeneous flows. In summary, CFD can handle complex geometries and can account for moving or deforming solid boundaries, allowing realistic simulations of dynamic, mission-relevant scenarios.

Title: The Impact of Foam and Aerosol Dynamics on Fire, Explosion Safety, and Suppression
Author(s): R. Ananth and J. Cramer
Affiliation(s): U.S. Naval Research Laboratory, Washington, DC
CTA: CFD

Computer Resources: HPE Cray EX [AFRL, OH]; Penguin Open Compute Platform (OCP) [AFRL, OH]

Research Objectives: To develop machine learning (ML) methods to predict the fire-suppression capabilities of novel nonfluorinated surfactant concepts prior to synthesis, thus both streamlining and otherwise enhancing the development of alternatives to fluorinated fire-suppression materials.

Methodology: In-house firefighting foam performance data collections were collated and reformatted into an expansive and ever-expanding database upon which to train future ML models. Discrete applications during the course of the majority of the research program involved supervised ML (specifically, artificial neural networks, or ANN) to directly and quantitatively predict the performance of surfactants and formulations thereof based on archived experimental data and the molecular descriptors of the individual chemical components associated with that experimental data. However, the coding infrastructure for utilizing unsupervised ML (specifically, self-organizing maps, or SOMs) also was developed to allow for less targeted, and thus potentially more widely scoped, go/no-go pattern-recognition results. SOMs are essentially neural networks trained in an unsupervised fashion, i.e., grids of ANN-type neurons that heuristically envelop multidimensional “blobs” of data to find similarities and differences between individual data points without predefined performance targets. However, there are a large number of potential design parameters associated with SOMs, and these parameters need to be assessed repeatedly to account for randomized initial model states. HPC resources were thus deployed to assist in efficiently optimizing the in-development coding infrastructure in a reasonable time frame.

Results*:* Figure 1 shows an example of a nonlinear data cluster output produced in house via SOMs while addressing firefighting foam development. The blue data points represent high-performing materials containing per- and polyfluoroalkyl substances (PFAS), and the nonblue points lying close to blue points represent non-PFAS materials that share similarities with the PFAS materials as determined via the unsupervised modeling. While the unsupervised nature of the SOM modeling outputs shown in Fig. 1 means that the modeled similarities are not explicitly available to the end user, modeling operations such as this remain a complementary alternative methodology by which to predict which non-PFAS materials, and formulations thereof should be the subject of follow-up data collections and/or development work by subject matter experts.

Defense Impact/Significance: PFAS in aqueous film-forming foam (AFFF) firefighting materials pose environmental and health problems. PFAS must be replaced per the National Defense Authorization Act (NDAA, passed by the U.S. Congress in 2020). However, while fluorine-free foams can be much more environmentally friendly, these materials do not normally meet the exacting fire-suppression requirements set forth in MIL-PRF-24385F. Research into producing a robust pool of suitable fluorine-free surfactants is ongoing, but trial-and-error empirical development approaches are both inefficient and dependent upon preexisting expert knowledge. An ML-based capability to accurately screen fire-suppression material concepts prior to synthesis will allow for accelerated development cycles, which, in turn, will allow for a much faster investigation of promising concepts both well-informed by expert knowledge and completely novel in the context of fire suppression.

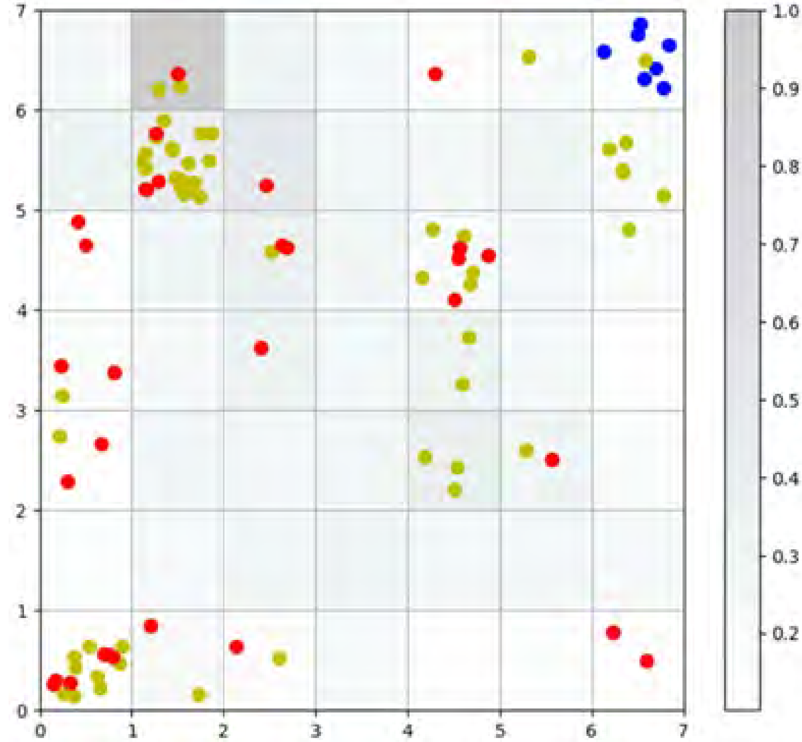

Figure 1. Nonlinear data cluster output produced in house via SOM while addressing firefighting foam development. Blue data points are outputs associated with PFAS-containing materials, and data points lying close to these blue points are outputs associated with non-PFAS materials that share similarities with the PFAS materials. Distinctions between red and green data points are the subject of ongoing research.

Title: Applications of FEFLO Incompressible Flow Solver
Author(s): K. Viswanath
Affiliation(s): U.S. Naval Research Laboratory, Washington, DC
CTA: CFD

Computer Resources: HPE Cray EX [AFRL, OH]; HPE Cray EX 4000 [ERDC, MS]

Research Objective: Perform three-dimensional (3D) numerical simulations of flow past complex configurations. The proposed studies will investigate hydrodynamics of extra-large unmanned underwater vehicles (XLUUVs) during docking and recovery operations at different angles of attack (AoAs) of the incoming flow and vehicle configurations. This will include multibody simulations of smaller UUVs in the vicinity of the large vehicle at different paths of approach for recovery.

Methodology: A finite element solver, called FEFLO, is used for 3D incompressible flows based on unstructured grids. The flow solver is combined with adaptive remeshing techniques for transient problems with moving grids and also is integrated with the rigid-body motion in a self-consistent manner that allows the simulation of fully coupled fluid-rigid-body interaction problems of arbitrary geometric complexity in three dimensions. NRL has developed a coupled fluid-structure interaction solver for simulating moving surfaces in propulsion for operations.

Results: The study examined the unsteady hydrodynamic environment surrounding an XLUUV with an open docking bay, Fig. 1, and what a smaller UUV positioned in the wake region will experience approaching the bay at nonzero angles of attack. The geometry of the XLUUV was varied between a closed hull, a rectangular bay, and a trapezoidal bay to assess their respective influences on wake structure and flow stability. The results, Fig. 2, show that the presence of a docking cavity alters the downstream flow field, introducing flow separation and vortical structures that can affect a smaller UUV. The rectangular and trapezoidal bays both generate low-velocity, high-vorticity regions near the bay lip, with the trapezoidal bay exhibiting slightly smoother reattachment characteristics. The study also emphasizes the importance of resolving flow features near sharp edges. The results reveal complex, time-dependent flow features near the docking bay that significantly influence the approach dynamics of the trailing UUV.

Defense Impact/Significance: Simulations have enabled characterization of the unsteady flow behind an extra-large unmanned underwater vehicle (XLUUV) at flow conditions. These findings provide insights into design considerations and control strategies for reliable UUV recovery operations. The next step will expand the simulation space to introduce a second, smaller UUV close to the bay opening to investigate hydrodynamic challenges to docking. The relative vehicle motion and UUV trajectories within the unsteady wake of the XLUUV will be simulated, and docking bay geometry changes will be considered.

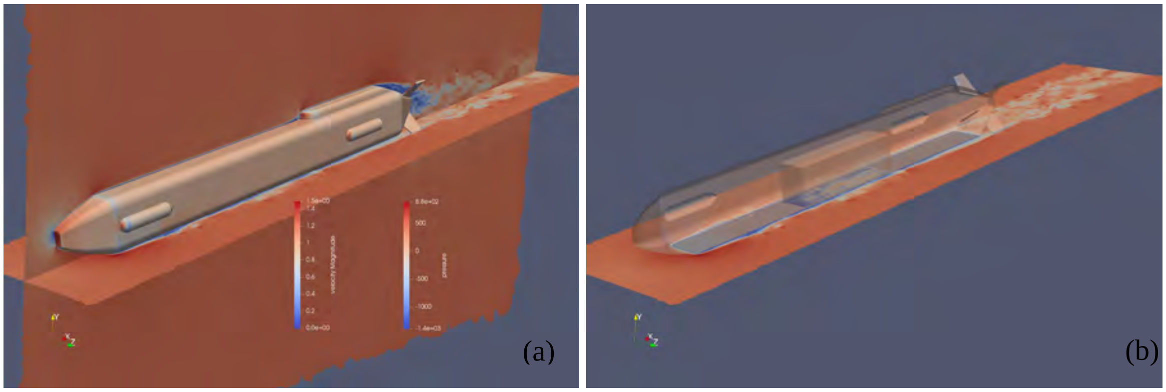

Figure 1. (a) Cross-sectional planes showing the instantaneous velocity magnitudes (m/s) and the XLUUV body showing pressure (Pa) contours at 10° AoA, pitched-down body position with incoming flow. (b) The interior geometry of the XLUUV with rectangular bay configuration and plane slice extracting flow data through the bay opening.

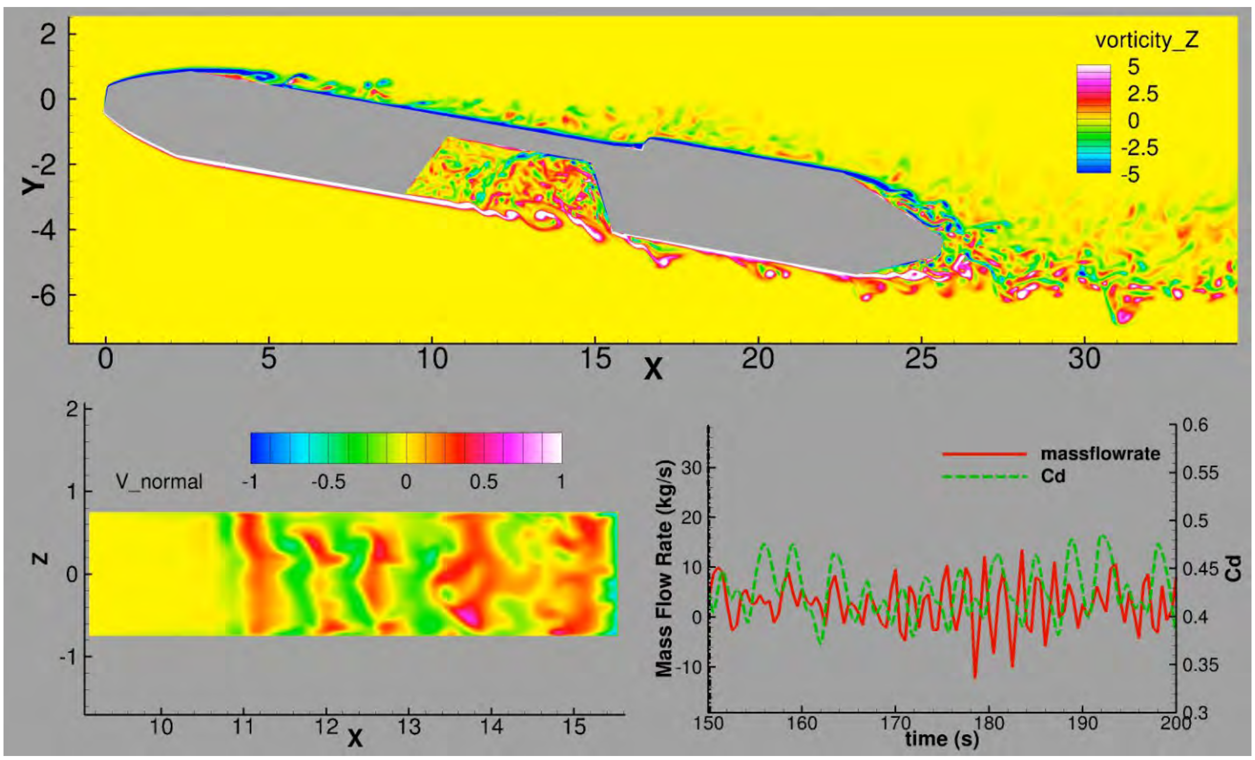

Figure 2. Top: Flow contours of vorticity (z-direction) around the XLUUV with open trapezoidal bay, and incoming flow from the left, at −10° pitch angle. Bottom left: Trapezoidal bay opening plane slice showing contours of normal velocity (m/s). Bottom right: Instantaneous mass flow through the bay opening and drag coefficient of the XLUUV.

Title: Numerical Simulations of Noise Generated by Non-Circular Advanced Military Aircraft Nozzles
Author(s): K. Viswanath
Affiliation(s): U.S. Naval Research Laboratory, Washington, DC
CTA: CFD

Computer Resources: HPE Cray EX [AFRL, OH], [NAVY, MS]; HPE Cray EX 4000 [ERDC, MS]

Research Objectives: Use HPC computational resources to predict details of turbulent flow structures and noise generation in supersonic noncircular asymmetric exhaust jets from representative military aircraft jet engine nozzles. This information will be used to investigate and assess promising jet noise reduction concepts in support of the ongoing testing program.

Methodology: Simulations are performed using the JENRE® Multiphysics Framework, developed by the Naval Research Laboratory (NRL) with collaborating institutions. This U.S. Government-owned code provides unsteady compressible flow-solver capabilities that support various numerics, cell-centered finite volume or nodal finite element methods, while delivering high throughput on calculations. It was developed with an emphasis on raw performance and the ability to exploit emerging massively parallel, high-performance computing (HPC) architectures. It supports different HPC parallel-programming paradigms for message passing such as MPI, OpenMP, CUDA, HIP, and hybrid models depending on the HPC cluster architecture. A key bottleneck of HPC throughput is data input-output (IO). The code supports parallel IO via MPI/IO to further complement the multiple levels of parallelism. The noise source simulation data is fed into a Julia-based code for ship deck surface noise heat map calculations. The existing implementation of the heat map code is designed to run on high-performance computing (HPC) hardware and makes use of threading and distributed computing. The code is being systematically optimized for modern parallel computing architectures, including GPUs.

Results: Simulations of a rectangular supersonic jet for various operating conditions were investigated to understand asymmetric noise characteristics and to evaluate noise-reduction techniques. The nozzle, with an aspect ratio of 2, models future nozzle requirements of aircraft frame integration and provides input for reduced-order models for ship deck noise heat maps using the noise spectra recorded. 3D isosurfaces (Fig. 1) of qcriterion show the strong self-induction and stretching of the large-scale coherent azimuthal structures, especially at the corners, that dominate the mixing features of the rectangular jet. The noise from the flow is recorded on a surface outside this plume, enclosing it without impinging, and is projected from there to any listener location. Figure 2 shows a projection of the noise from a single jet source across a nominal ship deck geometry. This noise heat map code is being developed for understanding noise distribution across the carrier deck for typical conditions, where there are multiple jets readying for operation, and the ability to quickly simulate the hot spots given relevant data. This data will also be used to understand areas of prolonged noise exposure for a given deck geometry.

Defense Impact/Significance: The results of our work will provide better understanding of the noise production for both industrial and military aircraft and will aid the current effort of noise reduction, especially for supersonic aircraft, to reduce the impact of jet noise on shipboard health and safety issues.

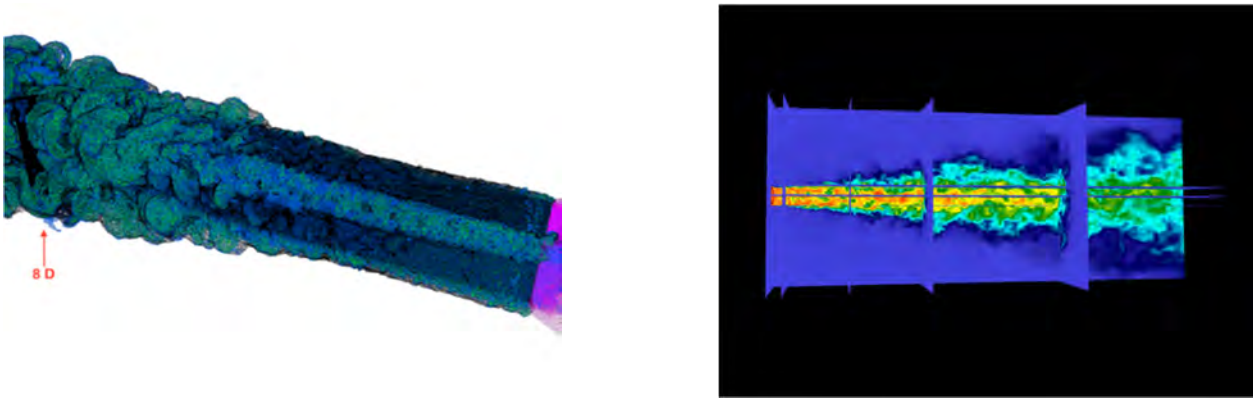

(a) Isosurfaces (b) Extracted plane surfaces in the plume

Figure 1. (a) Dynamics of the azimuthal vortex ring for the aspect ratio 2 rectangular jet at temperature ratio (TR) 1.0 and nozzle pressure ratio (NPR) 3.67. The isosurfaces of vorticity and qcriterion are shown till 8 D axial distance, where D is diameter. The jet direction is from right to left. (b) Temperature contours of the jet plume and extracted plane data at NPR 3.0.

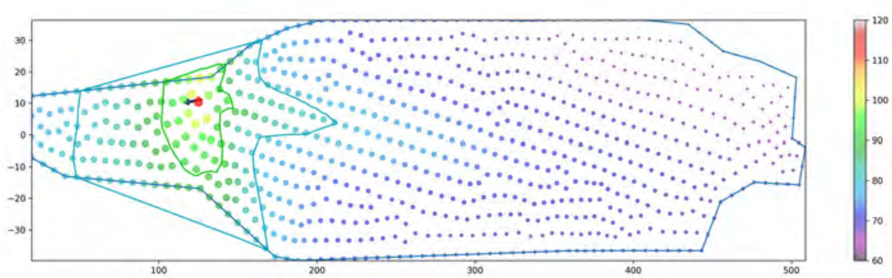

Figure 2. Ship deck noise heat map using a nominal deck surface geometry, with the arrow showing an active jet noise source location and orientation relative to the ship. The contours show greater than 95 dB (green) and 75 dB (blue) noise levels. Distance is in meters.

Title: Numerical Simulations of Turbulence Impact on Optical Signal Transmission and Near-Surface Turbulence
Author(s): S. Matt
Affiliation(s): U.S. Naval Research Laboratory, Stennis Space Center, MS
CTA: CFD

Computer Resources: Penguin TrueHPC [NAVY, MS]; Liqid [ARL, MD]

Research Objectives: The objective is to provide companion numerical simulations that complement laboratory experiments conducted at multiple research facilities. These include the large University of Miami SUrge-STructure-Atmosphere INteraction (SUSTAIN) facility, as well as the Simulated Turbulence and Turbidity Environment (SiTTE) laboratory and the laminar-to-turbulent-flow channel facility at Naval Research Laboratory. This effort supports projects focused on the dynamics of near-surface turbulence and air-sea interaction processes, with the goal of improving air-sea flux parameterizations for the next generation of coupled forecasting models. It also advances research in boundary layer control, drag reduction, and the development of novel fiber-sensor technologies for measuring ocean temperature in support of acoustics and related applications.

In addition, the project aims to develop a downscaling effort for ocean models to realize a model system that captures oceanographic dynamics that range from a domain size on the order of 1 km by 1 km down to the meter-to-centimeter scale, including nonhydrostatic internal dynamics and phase-resolved surface wave fields. This model system will be designed to bridge the gap between larger-scale geophysical regional and global models and the purely fluid dynamics-focused models employed in engineering-centered applications.

Methodology: To accurately reproduce the turbulence dynamics, the representation of the numerical tanks is accomplished using large-eddy simulation (LES) and the full physical domain size of the respective tanks. In addition, a nonhydrostatic ocean model, the "Stanford unstructured-grid, nonhydrostatic, parallel coastal ocean model" (SUNTANS) was built on a system at Navy DSRC to provide a bridge from large-scale geophysical representations in general circulation models toward the smaller scales of hydrodynamics models.

Results: Simulations of a numerical wind-wave tank and flow over roughness elements and near deformable surfaces resumed on Jean (ARL DSRC). Numerical simulations of flow over roughness elements (denticles) on an airfoil and deforming wall elements in channel flow were compared to laboratory experiments (Figs. 1, 2). Model code was also ported to other systems and architectures (Navy DSRC). The SUNTANS model was built on the system at Navy DSRC, with a build geared toward multiple users and portability. Preprocessing routines were developed to generate grid and boundary/initial conditions to set up the model for a Navy region of interest with complex coastline, watershed, and bathymetry. Python code was modernized and developed to generate boundary and initial conditions from NCOM for input to SUNTANS. A twin setup was run in Delft3D to support the nonhydrostatic solution.

Defense Impact/Significance: Numerical tanks and nested nonhydrostatic ocean and wave models are critical to advancing research on air-sea interface and coastal dynamics, as well as to the development of novel approaches for boundary layer control and drag reduction, optical communications, and fiber-optics sensing technologies, that play a key role in improving ocean forecasting models.

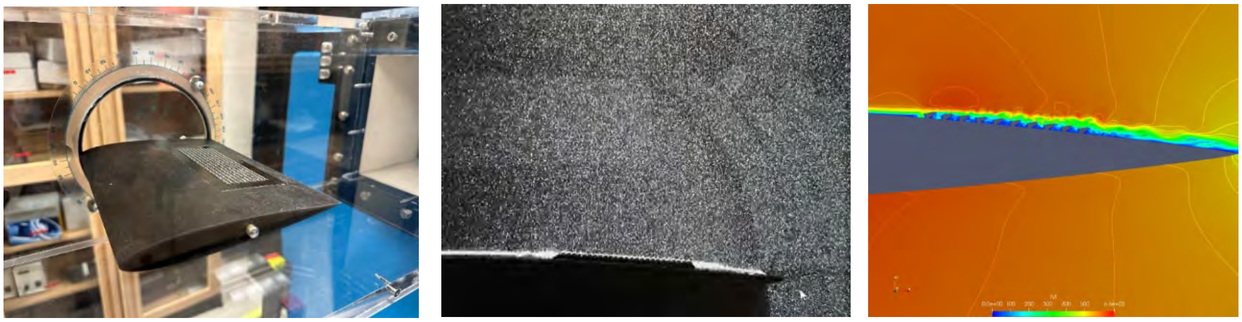

Figure 1. Simulations of flow over an airfoil emulating companion laboratory experiments. Laboratory setup of airfoil with denticle-covered insert (left), raw image from particle image velocimetry (PIV) showing airfoil and denticle insert (middle) and numerical simulation of flow over denticles (right) (from Matt, S., J. Geder, J. Stocking, R. Ramamurti, "Bio-inspired surfaces for turbulence reduction," Proceedings IEEE Int. Symposium on Underwater Technology (UT2025), Taipei, Taiwan, March 2–5, 2025).

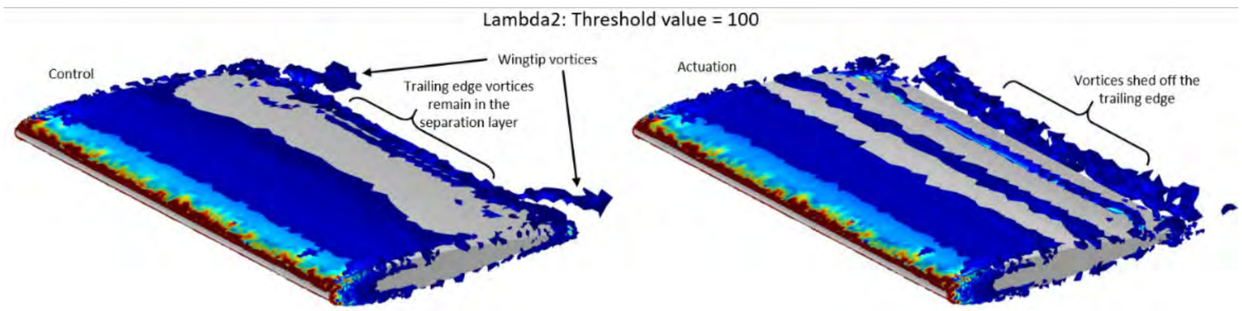

Figure 2. Vortical structures along the NACA0012 airfoil with (right) and without (left) boundary actuation in the region of flow transition/separation using COMSOL. Simulations support work on development of novel bioinspired methods of drag reduction for UUVs.

Title: Towards New Generation of Physical Models for Gaseous and Liquid-Fuel Detonations

Author(s): V.N. Gamezo[1] and A.Y. Poludnenko[2]
Affiliation(s): [1]U.S. Naval Research Laboratory, Washington, D.C.; [2]University of Connecticut, Storrs, CT

CTA: CFD

Computer Resources: Penguin Open Compute Platform (OCP) [AFRL, OH]; Liqid [ARL, MD]; HPE Cray EX [AFRL, OH], [NAVY, MS]; Liqid Matrix XT-4 [ARL, MD]; Penguin TrueHPC [NAVY, MS]

Research Objectives: High-fidelity numerical modeling of detonations in gaseous mixtures and liquid fuel sprays is essential for designing the next generation of defense and Navy-relevant detonation-based propulsion and fuel-safety systems. This present effort builds on our previous work, in which a comprehensive survey of detonation characteristics was performed for a wide range of gaseous fuels, including hydrogen, methane, acetylene, ethylene, and Navy-relevant fuels such as JP10. That prior work demonstrated that numerical simulations employing existing state-of-the-art, multistep chemical kinetics are unable to accurately reproduce key macroscopic detonation properties, including detonation cell size and detonability limits, under practically relevant conditions, with errors often exceeding an order of magnitude. The primary objective of the current work is to develop a new, state-of-the-art, multistep chemical kinetics model for hydrogen combustion that accurately reproduces a wide range of experimental metrics from laminar flame speeds to detonation properties. Furthermore, to address more practically relevant systems, this effort also includes the first high-fidelity three-dimensional (3D) simulations of jet-fuel spray detonations, employing the state-of-the-art shock-droplet interaction models together with the advanced chemical kinetics for *n*-dodecane.

Methodology: In FY25, a new state-of-the-art, multistep chemical kinetics mechanism for hydrogen combustion (GDP mechanism) was developed based on the Stanford FFCM-1 family of reaction kinetics models. The new mechanism was validated to reproduce key combustion properties, including laminar flame speeds, Chapman-Jouguet detonation velocities, and standard hydrogen benchmarking targets reported in the literature. With this mechanism, a large suite of 2D and 3D high-fidelity simulations of freely propagating detonations in rectangular channels was performed. The simulations covered a broad range of equivalence ratios, diluent mass fractions, and initial mixture pressures and temperatures, for which experimental data are available, spanning both subatmospheric and atmospheric conditions. All computations were carried out with the Athena-RFX++ code, a massively parallel, higher-order, structured-grid solver with adaptive mesh refinement that integrates the fully compressible reactive Navier-Stokes equations. Furthermore, a state-of-the-art droplet vaporization model, developed jointly with Stanford University, was implemented in the Athena-RFX code to perform detailed spray detonation calculations.

Results: The new hydrogen chemical kinetics mechanism reproduces all standard hydrogen combustion targets reported in the literature with accuracy comparable to or better than existing complex hydrogen mechanisms widely used in the combustion community. Crucially, it also captures the correct detonation cell size for hydrogen-air mixtures over a broad range of conditions (Fig. 1), demonstrating predictive capability for key macroscopic detonation characteristics. These results demonstrate a broader approach for constructing novel chemical kinetics mechanisms that can provide high modeling fidelity for complex hypersonic reacting flows, such as detonations. Finally, this effort resulted in the first systematic 3D simulations of detonations in jet-fuel/air sprays (Fig. 2), providing new insight into the spray-detonation physics, which is directly applicable to practical liquid-fuel detonation-based propulsion systems.

Defense Impact/Significance: This work delivers state-of-the-art numerical models of gaseous detonations that, for the first time, enable a predictive multistep chemical-kinetic description of detonation dynamics in hydrogen-based mixtures. This opens the path for the design of novel chemical-kinetics models for more complex hydrocarbon fuels. Such predictive capability is central to the design and qualification of advanced detonation-based propulsion systems, where detonability limits, minimum channel sizes, and spray dynamics critically define operability, performance, and safety margins. The effort is tightly integrated with the ongoing Navy and DoD initiatives in supersonic combustion, high-speed propulsion, and fuel safety at the U.S. Naval Research Laboratory, the Office of Naval Research, and other defense agencies, thereby providing next-generation modeling tools for system design, risk assessment, and operational planning.

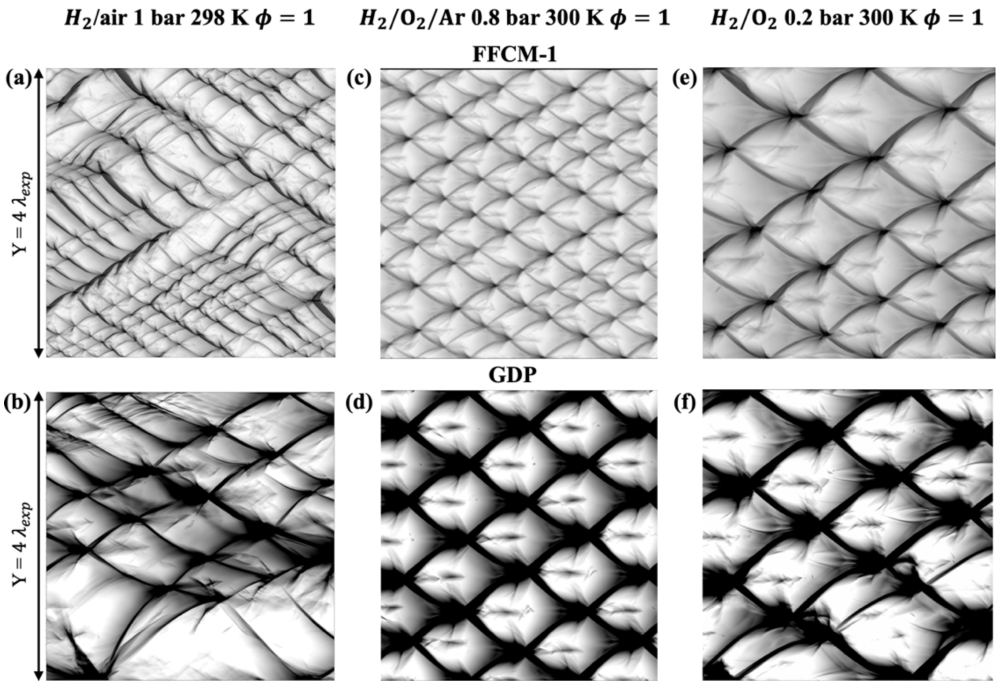

Figure 1. Synthetic soot foils showing the characteristic cellular detonation structure in hydrogen-based mixtures with different diluents, computed using the FFCM-1 (top row) and the newly developed GDP (bottom row) chemical kinetics models. Detonations propagate from right to left, and the channel height in all cases is four times the experimentally measured detonation cell size for a given mixture. The FFCM-1 model reproduces the experimentally observed cell size only for the low-pressure hydrogen-oxygen case, whereas the GDP kinetics model accurately predicts the detonation cell size for all cases.

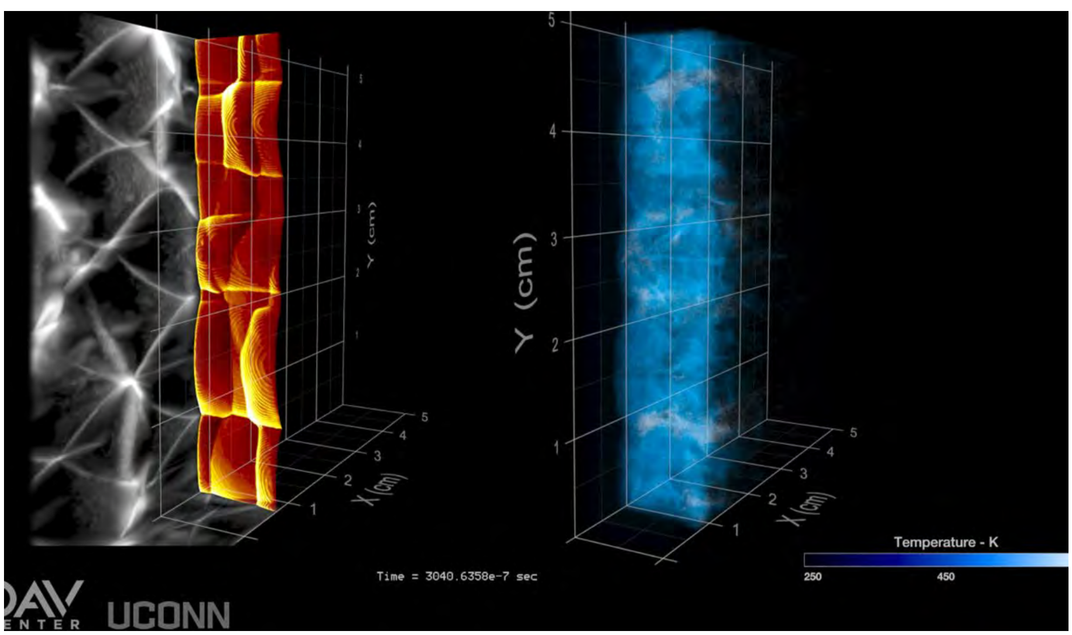

Figure 2. Structure of a 3D spray detonation in a stoichiometric *n*-dodecane spray in air at 1 atm with 10-micron droplets. Shown are the front structure (left) and the droplet temperature distribution (right).

Title: High-Fidelity CFD Simulations of High-Speed Flows in Realistic Atmospheric Conditions

Author(s): D.A. Kessler,[1] R. DeBoskey,[2] B. Bojko,[1] T. Patel,[1] R.F. Johnson,[1] A. Hess[1]
Affiliation(s): [1]U.S. Naval Research Laboratory, Washington, DC; [2] Syntek Technologies, Inc., Fairfax, VA
CTA: CFD

Computer Resources: HPE Cray EX [AFRL, OH], [NAVY, MS]; HPE Cray EX 4000 [ERDC, MS]; Penguin TrueHPC [NAVY, MS]

Research Objectives: Determine the impact of chemical kinetics and multidimensional flow effects on the combustion behavior in an experimental solid-fuel ramjet characterization facility.

Methodology: We are using a modified version of the JENRE® Multiphysics Framework to perform high-fidelity and high-resolution simulations of the chemically reacting flows associated with high-Mach-number supersonic and hypersonic flights.

Results: Recent interest in the use of solid fuels to power ramjet engines for high-speed (greater than Mach 3) propulsion systems has driven the construction of laboratory-scale experimental facilities designed to characterize the performance of these fuels under relevant operating conditions. These facilities can provide a coarse description of the combustion behavior inside these engines. When used in conjunction with high-fidelity numerical simulations, however, a wealth of information about the underlying flame dynamics and chemical kinetics can be deduced. During FY25, a series of three-dimensional simulations of a solid-fuel slab burner facility at North Carolina State University were performed using two different numerical techniques. Implicit large eddy simulations (LESs) using a modified version of the JENRE® Multiphysics Framework resolved the energy-containing scales within the flow and used a finite-rate model for the chemical kinetics. Detached eddy simulations (DESs) using the STAR-CCM+ software package were used to investigate the use of turbulence closure models and reduced-order chemical kinetics using the eddy breakup (EBU) model.

The LESs and DESs show similar levels of flame wrinkling, with smaller structures observed upstream and near the shear and recirculation zones (Fig. 1). As the flow moves downstream, structures increase in size due to the thermal expansion caused by the heat released by combustion. Negative axial velocities are indicative of the recirculation near the air inlet that assists with flame anchoring. The mass fraction of butadiene is highest in the recirculation zone, as isocontours of fuel mass fraction extend above the recirculation zone and follow the shear layer impingement toward the fuel surface. The largest variations in spanwise momentum are observed near the flow reattachment region, which corresponds to the location of highest fuel regression rate. The temperature is higher directly attached to the backward-facing step in DESs compared to LESs. This is due to the EBU chemistry closure, which models the rate of combustion based on the local mixture fraction. As soon as fresh reactants are mixed with hot recirculation products within the shear layer, combustion begins.

In contrast, finite-rate models naturally predict a delay between mixing and ignition based on the characteristics of the relevant chemical reaction kinetics. Overall, LESs and DESs produced similar flow structures and overall flame dynamics that compared well to experimental measurements; however, the resulting fuel regression rates differed throughout the combustor. While the qualitative behavior was reasonable, simulation predictions differed from the experimental measurements for regression rate by up to a factor of two at some locations. Additional work is needed to sort out which physical model is most responsible for the discrepancy.

Defense Impact/Significance: Achieving a long-range strike capability and countermeasures for similar technologies under development by our adversaries are critical for protecting our fleet and maintaining naval superiority. This work will provide a better understanding of how solid fuels can be used in high-speed weapon systems to provide a significant increase in range.

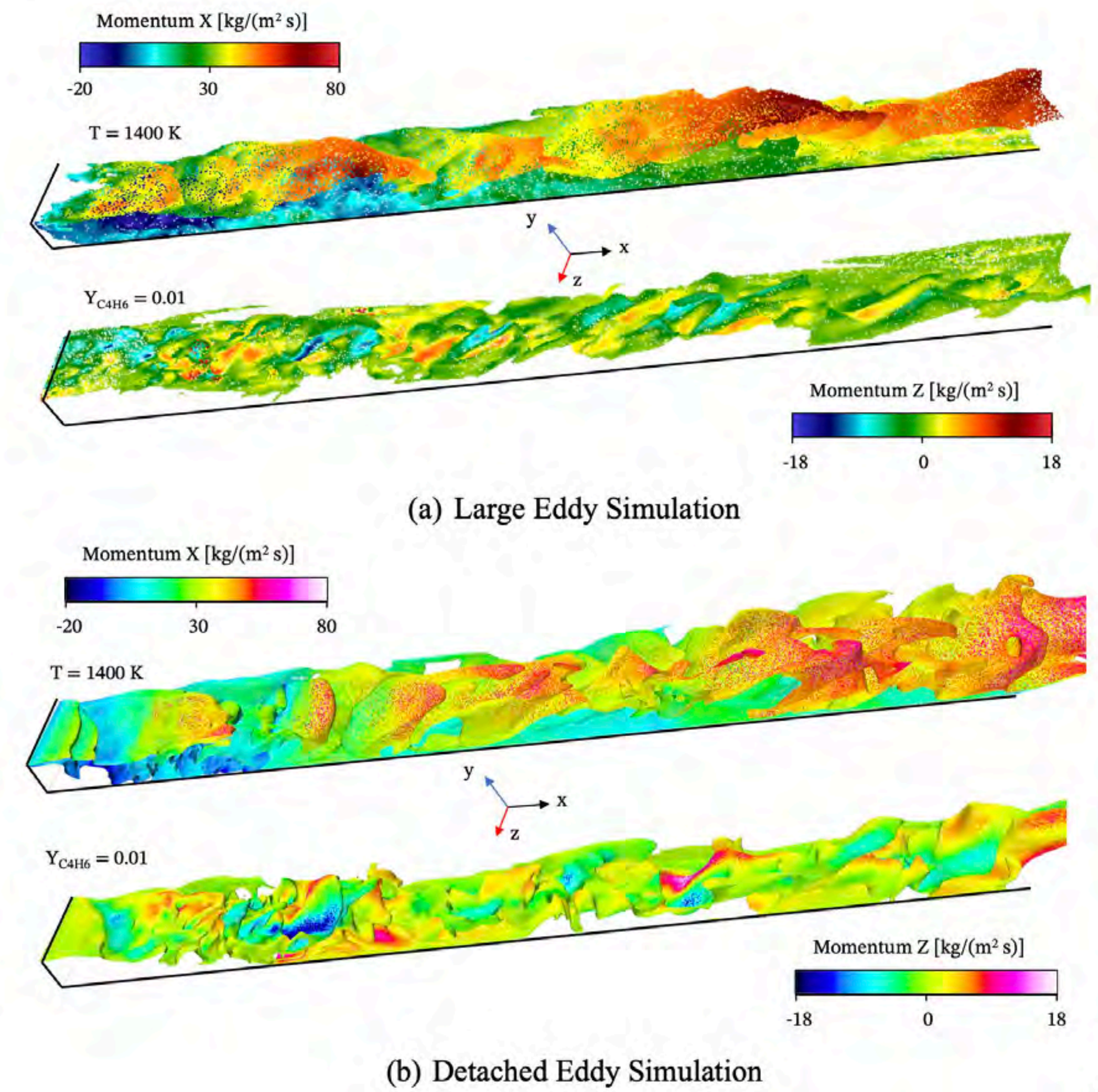

Figure 1. Comparison of instantaneous isosurfaces of temperature and fuel mass fraction computed using (a) large eddy simulation (LES) method and (b) detached eddy simulation (DES) method. Temperature isosurfaces are colored by the magnitude of the streamwise momentum and mass fraction isosurfaces are colored by the magnitude of the spanwise momentum to give a pictorial representation of the complex three-dimensional flow field.

Title: Direct Numerical Simulation of Fluid-Sediment Wave Bottom Boundary Layer
Author(s): J. Simeonov, I. Adams, A. Penko, S. Allen, S. Bateman, K. Edwards, R. Phillip, and J. Veeramony
Affiliation(s): U.S. Naval Research Laboratory, Stennis Space Center, MS
CTA: CFD

Computer Resources: HPE Cray EX 4000 [ERDC, MS]; HPE Cray EX, Penguin TrueHPC [NAVY, MS]

Research Objectives: The objective of this project is high-resolution predictions of wave, currents and sediment transport in coastal environments. Predictive models for nearshore hydrodynamic and bathymetry evolution require a complete understanding of the physics of fluid-sediment interactions in the wave bottom boundary layer (WBBL) and the air-sea physics driving the ocean flows. Since such variable three-dimensional (3D) processes are difficult to quantify in situ, we perform coupled multiphase numerical simulations to increase our understanding of the nearshore hydrodynamics and the resulting sediment transport. Fundamental concepts used in describing the phenomena of sediment transport such as particle size and shape, turbulent bottom stress, hindered settling, bed failure criterion, and bedforms and their effect on bottom stress are addressed with our models. The models produce high-resolution results necessary to gain insight into the small-scale boundary-layer processes and provide new directions needed to improve ocean and seabed predictive capabilities.

Methodology: Utilization and development of a suite of discrete and continuum WBBL multiphase models for simulating sediment transport and hydrodynamics in the nearshore environment from the microscale (cm–m) to the mesoscale (km) is ongoing with HPC resources. At the mesoscale, we use Reynolds-averaged Navier-Stokes simulations (RANS) to predict wave- or current-induced bottom stress and the resulting sediment fluxes (e.g., using the Delft3D model). At this scale, the sediment bed is usually modeled as a continuum and its kinematics and morphology are determined by simple mass conservation. At the microscale (<10 cm), the 3D sediment phase is simulated with a discrete element method (DEM) that allows individual grains and their interactions to be uniquely specified, and the fluid model varies in its complexity. In the eddy viscosity DEM approach, the fluid flow is only resolved at scales larger than individual particles, and as a result, the fluid forces (e.g., drag) induced by the flow are parameterized using drag and lift coefficients. Below, we discuss new parameterizations for the horizontal and vertical transport in a sediment bed mobilized by oscillatory flow.

Results: We used particle velocity and position data from DEM simulations by Drake and Calantoni [1] of a bed of spherical particles mobilized by oscillatory flows to develop formulations that relate the horizontal and vertical sediment transport rates to an easily measurable quantity, such as the free stream velocity. The analysis showed that a simple cubic function of the sediment volume concentration provides a better model for the vertical sediment volume flux compared to more traditional approaches of modeling the vertical flux as a Fickian diffusion flux proportional to the gradient of the volume concentration. The new model for the vertical flux was then used to develop predictions for the rate of change of the sediment volume concentration profile of the dynamic sediment bed by obtaining a theoretical solution of the sediment advection equation. The theoretical profiles of the varying volume concentration of the mobile bed (Fig. 1) were found to agree well in tests with the volume concentration dynamics in the DEM simulations and the laboratory measurements of O'Donoghue and Wright [2]. The theoretical solution for the instantaneous volume concentration was also combined with a simple slip-velocity model for the sediment horizontal velocity to obtain the explicit relationship between the horizontal sediment transport rate and the free stream velocity that was in good agreement with previous empirical formulations.

Defense Impact/Significance: Accurate characterization of the nearshore battlespace for mine warfare (MIW) and Navy special warfare (NSW) is currently limited by shortcomings in fundamental knowledge of the bottom boundary layer physics. Our microscale simulations provide unprecedented details for the study of fluid-sediment interactions that are impossible to obtain with available measuring technologies in the field or the laboratory. These results are utilized to improve parameterizations of small-scale processes in tactical-scale models for seabed mobility and object burial. The computational resources consumed were in direct support of NRL base programs "Modeling sediment sorting in sand-shell environments" and "Predicting wind driven topographic change in sandy, coastal battlespace environments."

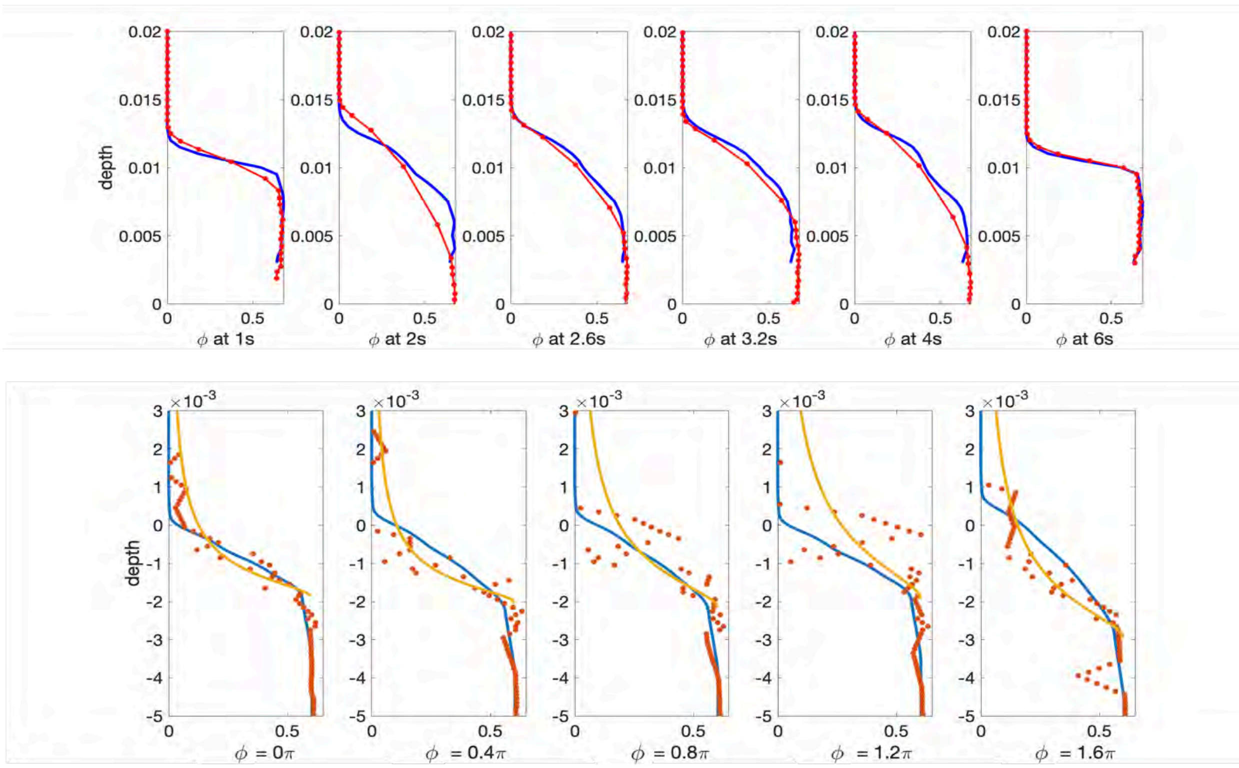

Figure 1. Top panel: Depth profiles of volume fraction at different flow phases for a bed of 1 mm spherical particles mobilized by oscillatory flow with 6 s period and maximum velocity of 1.35 m/s in the DEM simulation (blue) and predicted by our theoretical model (red). The flow is quiescent at $\phi = 0$. Bottom panel: Profiles of predicted (blue) and measured (red points) volume fraction profiles for a laboratory flow with peak velocity of 1.26 m/s and period of 7.5 seconds. Shown for comparison is the volume fraction model (orange line) of O'Donoghue and Wright [2].

References

[1] T. G. Drake and J. Calantoni, "Discrete particle model for sheet flow sediment transport in the nearshore," *Journal of Geophysical Research: Oceans*, vol. 106, no. C9, pp. 19859–19868, 2001, doi: 10.1029/2000JC000611.

[2] T. O'Donoghue and S. Wright, "Flow tunnel measurements of velocities and sand flux in oscillatory sheet flow for well-sorted and graded sands," *Coastal Engineering*, vol. 51, no. 11, pp. 1163–1184, 2004, doi: 10.1016/j.coastaleng.2004.08.001.

Title: Multidimensional Chemically Reacting Fluid Dynamics with Application to Flameless Combustors
Author(s): R.F. Johnson and E. Ching
Affiliation(s): U.S. Naval Research Laboratory, Washington, DC
CTA: CFD

Computer Resources: HPE Cray EX [NAVY, MS]

Research Objectives: Perform large-scale simulations of chemically reacting fluid dynamics in multidimensional settings using high-performance computing. The goal is to advance understanding of complex, multiscale combustion behavior.

Methodology: The Laboratories for Computational Physics and Fluid Dynamics apply high-fidelity simulation tools to compute detailed flow fields across a range of configurations. These tools employ high-order numerical methods that are well suited for unsteady flows involving shocks, chemical reactions, and coupled multiscale processes. This effort centers on advancing algorithms for chemically reacting flows across both low- and high-speed regimes. During the past year, we achieved important progress in demonstrating the robustness of these approaches.

Results: This work employs a positivity-preserving and entropy-bounded discontinuous Galerkin (DG) method for the compressible, chemically reacting Navier-Stokes equations. A key advantage of DG is its ability to attain high-order accuracy while resolving detailed flow structures without excessive mesh refinement. This year, we performed simulations to investigate the effect of ozone sensitization on oblique detonation waves induced by curved ramps. These simulations used HPCMP resources and a modified version of the JENRE® Multiphysics Framework that incorporates the entropy-bounded DG method described above.

We found that the addition of ozone can enhance the initiation and stabilization of oblique detonation waves, which helps address a major challenge of oblique detonation-based propulsion. Figure 1 presents the temperature distribution of an oblique detonation wave induced by a curved ramp with ozone addition. In the absence of ozone, a Mach stem appears downstream of the detonation, which is detrimental to detonation stabilization.

Defense Impact/Significance: Improved numerical approaches for propulsion simulations enhance predictive capability for Navy and defense applications. This year highlighted significant advances in modeling multicomponent reacting flows on fully unstructured grids, reinforcing the relevance of these methods to state-of-the-art propulsion research.

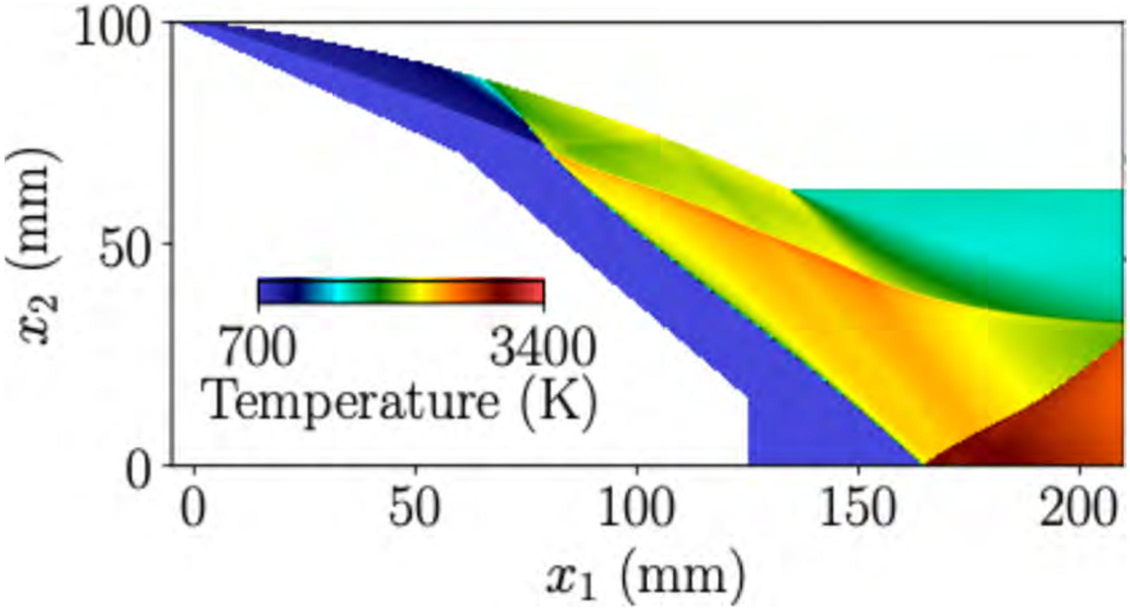

Figure 1. Temperature distribution of oblique detonation wave induced by curved ramp with ozone sensitization.

Title: Detonations with Multi-Phase Flows for Propulsion
Author: D.A. Schwer
Affiliation: Naval Research Laboratory, Washington, DC
CTA: CFD

Computer Resources: HPE Cray Ex [NAVY, MS]

Research Objectives: The main research goal of the present HPC project is to study high- and low-speed multiphase reacting flows for further understanding advanced engine concepts, with the specific application for detonation engines.

Methodology: We have used two modeling codes for our research into blast and detonation engine simulations. Simulations are primarily done using the JENRE® Multiphysics Framework. Due to our extensive experience with using the DET3D codes for detonation propulsion, we continue to use them as a benchmark for comparison with the JENRE® framework. The framework utilizes unstructured meshes and both continuous- and discontinuous-Galerkin finite element method to solve a wide variety of complex fluid dynamical phenomena. It has been built from the ground up to make efficient use of CUDA, HIP, Thread-Building-Blocks, OpenMP, and MPI through the use of template libraries. By utilizing unstructured meshes, the solver can easily handle complex flow paths from rig assemblies and engine concepts while remaining relatively efficient. Extensive work has gone into improving the JENRE® framework for both reacting and multiphase flows during the past several years.

Results: Simulations were conducted investigating the three-dimensional flow structure of a severely underexpanded nozzle with a fluid injector placed in the supersonic wake. Three-dimensional meshes were constructed using the CREATE Capstone tool for a representative geometry, consisting of a straight tube dumping into a large plenum, creating an underexpanded, supersonic jet within the plenum. The intent of these simulations was to elucidate perturbations in the flow field caused by the presence of the injector itself. The JENRE® framework was used to conduct simulations using this geometry and conditions. Results from the simulations showed a strong primary wake that forms before the first Mach disk, about $2.08D$ downstream from the exit of the nozzle, where D is diameter. This portion of the jet is very stable up to the first Mach disk. Instabilities from the nozzle boundary layers are entrained into the jet from the edges after the first Mach disk and cause substantial unsteadiness above the first Mach disk through the rest of the wake. The presence of the injector introduces a large perturbation on the jet, as expected. From the simulations, we note three observations. 1) Perturbations to the injector are restricted to the area close to and downstream of the injector itself and have very little impact on the dynamics of the jet outside of this area. 2) The flow at the tip of the injector (where fluid will be injected in experiments and the simulations) is processed by an oblique shock wave that forms at the tip. 3) Pressures are quite high on the windward side of the injector, about $3.5P_{amb}$, where *amb* is ambient, and so experiments are needed to determine whether the injector can survive that environment and provide a steady injection of fluid into the jet.

Defense Impact/Significance: The physics involved in rotating detonation combustors (RDCs) and other detonation engines is substantially different from that of gas-turbine engines. Simulations of RDC systems from basic concepts all the way to full propulsion devices are necessary to understand these devices, as well as to contribute to the design process. The work accomplished this year relates to understanding RDC fuel injection. Results from these simulations in concert with experimental efforts will help elucidate fuel penetration into a high-velocity stream similar to flow within an RDC and can be used to design new and novel injectors for these engines that optimize the engine performance over conditions of interest.

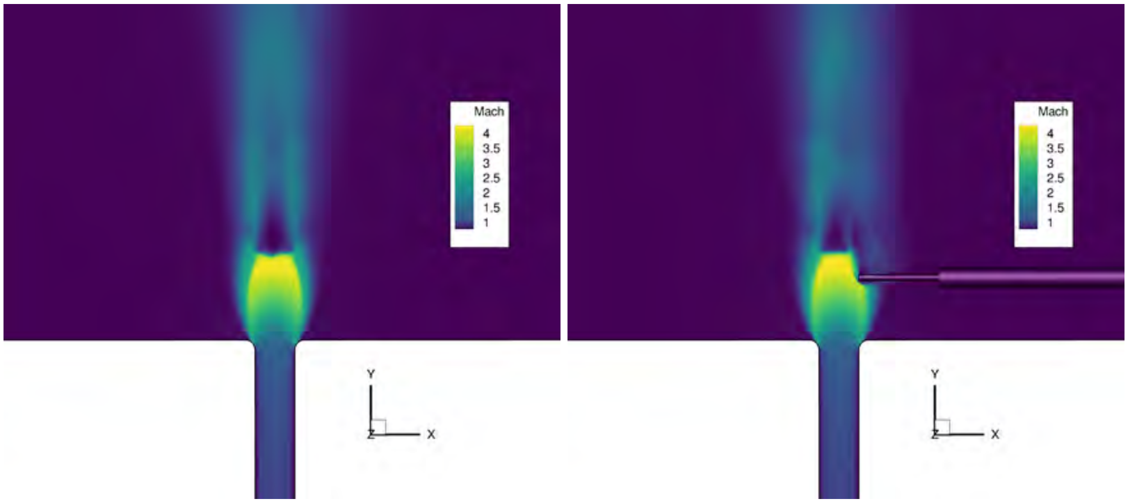

Figure 1. Mach number for an underexpanded jet expanding into a plenum without (left) and with (right) an injector positioned within the supersonic wake. Image is *x*-*y* plane at centerline.

THIS PAGE INTENTIONALLY LEFT BLANK

CCM

Computational Biology, Chemistry, and Materials Science

The Chemistry, Biology, and Materials Science (CCM) CTA focuses on advanced computational methods for predicting and understanding the fundamental properties of chemicals and materials, including nano- and biomaterials. These methods address a broad range of properties, such as molecular structure and energetics, spectroscopic signatures, intermolecular interactions, reaction pathways, and mechanical behavior across length and time scales. Under CCM, techniques including quantum chemistry, molecular dynamics, statistical mechanics, and multiscale modeling are applied to the design and optimization of chemical, polymeric, nanomolecular, and biomolecular systems.

These capabilities support defense-relevant applications in fuels and lubricants, laser protection, energetic materials, rocket propulsion, catalysis, structural materials, fuel cells, and chemical defense. Solid-state and materials modeling approaches further enable the development of high-performance materials for electronics, optical and neuromorphic computing, advanced sensors, aircraft engines and structures, semiconductor and solid-state lasers, next-generation rocket engine components, and select biomedical technologies. Emerging areas within the CCM CTA include bioinformatics, computational biology, and multiscale biological modeling, with growing emphasis on cellular- and systems-level simulations that integrate chemical, biological, and materials phenomena.

Title: Calculation of Materials Properties Via Density Functional Theory and Its Extensions
Author(s): J.L. Lyons
Affiliation(s): U.S Naval Research Laboratory, Washington, DC
CTA: CCM

Computer Resources: Penguin Open Compute Platform (OCP) [AFRL, OH]

Research Objectives: To determine the electronic structure, as well as the role of defects and dopants, for ultrawide-bandgap semiconductors (UWBGS) such as gallium oxide (Ga_2O_3) and lithium gallate ($LiGa_5O_8$), and novel materials such as cesium lead bromide ($CsPbBr_3$), using hybrid density functional theory (DFT).

Methodology: DFT has long been the workhorse for determining the electronic structure of semiconductor materials. In principle, DFT requires no experimental input, but when applied to UWBGS, the so-called "bandgap problem" makes quantitative prediction of defect properties difficult. To overcome this issue, we employ in this project so-called "hybrid DFT," which mixes in a fraction of screened Hartree-Fock exchange into the exchange-correlation functional. This provides accurate, quantitative prediction of bandgaps and defect transition levels, even for UWBGS. Using hybrid DFT, defect-related charge-state transition levels, formation energies, and optical transitions have been calculated. For the halide perovskites (e.g., $CsPbBr_3$), spin-orbit coupling is also required due to the presence of heavy atoms.

Results: In FY25, we studied a number of topics, including how the conductivity of tin-based perovskites could be reduced via donor doping. Our calculations showed that, like in the lead halide perovskites, yttrium and scandium could be effective donors. By compensating native vacancies that act as negatively charged acceptors, these donor dopants can reduce free hole concentrations by several orders of magnitude.

We also predicted the optical properties of bismuth dopants in $CsPbBr_3$, which we previously showed were deep donors in this system. Our calculations indicated that these donors should give rise to a 1.2 eV infrared emission when present in $CsPbBr_3$. Very similar deep signals were observed in Bi-doped, NRL-grown samples, confirming the validity of our approach.

Using hybrid functional calculations, we also explored the role of chalcogen dopants in aluminum nitride. Previously, these were thought to be superior donor dopants to silicon, which, despite being a *DX* center in aluminum nitride (AlN), is most effective at establishing *n*-type conductivity. Our calculations show that chalcogens (including elements S, Se, and Te), despite being non-*DX* donors, are in fact much deeper than silicon (see Fig. 1). Sulfur, which has the smallest ionization energy in AlN (0.45 eV), is still far less effective than silicon.

Defense Impact/Significance: Along with gallium nitride, GaN, UWBGS such as AlN can be deployed in power electronics that provide a crucial role in many Navy- and defense-relevant applications and afford significant SWaP-C savings while outperforming components based on traditional semiconductor materials. Newer materials such as the halide perovskites are attractive as potentially low-cost, highly efficient energy materials. Controlling electrical conductivity via impurity doping, understanding contaminant species, and characterizing unintentionally incorporated native defects are crucial steps for improving these materials and optimizing their device designs.

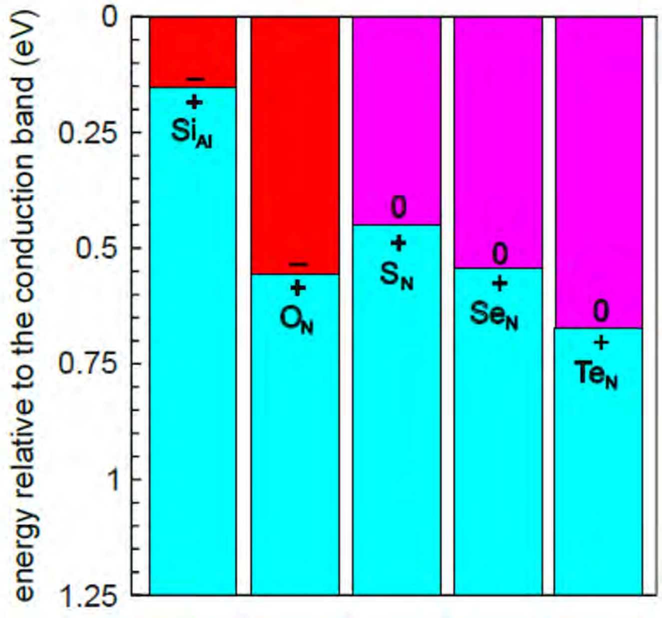

Figure 1. Donor transition levels for different dopants in AlN.

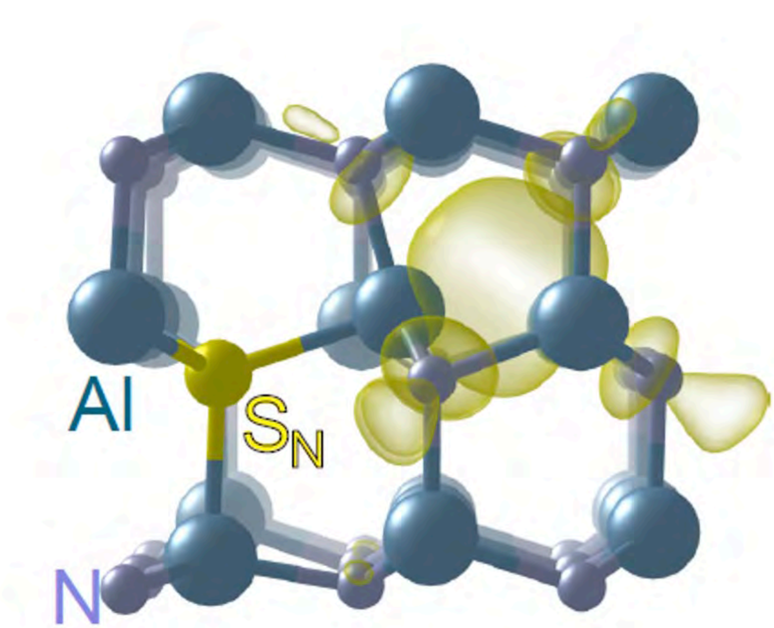

Figure 2. Spin isosurfaces of the sulfur donor in AlN.

Title: Machine-Learning Interatomic Potentials for Materials Science
Author(s): M.W. Swift
Affiliation(s): U.S Naval Research Laboratory, Washington, DC
CTA: CCM

Computer Resources: Liqid [ARL, MD]; HPE Cray EX [ERDC, MS]; Penguin Open Compute Platform (OCP) [AFRL, OH]

Research Objectives: To train machine learning interatomic potentials for predicting energies, forces, and stresses in Navy-relevant battery materials, specifically focusing on lithium-sulfur battery systems. The objectives include employing trained potentials to predict structure-property-performance relationships and developing models for organic liquid electrolytes, polymers, and ionic liquids used in advanced battery systems.

Methodology: We employed active learning to train machine learning potentials by fine-tuning the MACE-MP-0 model for specific battery material applications. The MACE potential relies on high-order equivariant message-passing neural networks and was initially trained on the Materials Project Trajectory database containing over 1.5 million structures. Our approach used molecular dynamics (MD) simulations with MACE-predicted forces, automatically identifying high-uncertainty configurations for density functional theory (DFT) calculation and training set expansion. Specifically, we performed MD simulations of lithium hexasulfide, Li_2S_6, and dimethylaminomethylsilane, DMAMS, in realistic solvent conditions (DOL:DME 1:1 by weight) to study polysulfide interactions in lithium-sulfur batteries. The methodology leveraged GPU acceleration for efficient calculations on large system sizes and extended simulation times.

Results: The active-learning-based training successfully yielded system-specific force fields with near-DFT accuracy, enabling simulations orders of magnitude larger and longer than accessible with conventional DFT-MD. Our computational studies revealed that the binding enthalpy of Li_2S_6 with DMAMS in the presence of solvent is 0.146 ± 0.038 eV — sufficiently large to trap polysulfides but small enough to maintain availability for further electrochemical reduction [1]. The simulations confirmed that Li_2S_n species remain as ion complexes rather than dissociating in solution (Fig. 1). These results directly supported experimental validation (Fig. 1) showing that polymer-coated separators effectively mitigate polysulfide crossover in lithium-sulfur batteries, with 40 nm coatings providing optimal performance balancing rate capability, cycling stability, and self-discharge protection [1].

Defense Impact/Significance: This research directly contributes to developing advanced battery technologies critical for defense applications. Improved lithium-sulfur batteries have the potential to dramatically increase energy density and safety compared to traditional lithium-ion batteries, enabling smaller and more efficient electrified UAVs, UUVs, and UGVs. The enhanced energy-storage capabilities improve the operational endurance of mobile electronics for the dismounted warfighter. Additionally, the computational framework developed for battery materials extends to sodium-ion batteries based on abundant elements, contributing to operational resiliency for grid-scale storage and backup systems. The machine learning potential methodology also supports development of improved thermal batteries for guided munitions, enabling increased hang time and greater guidance precision for hypersonic weapons systems.

References

[1] R. B. Nuwayhid, J. Yeom, H. O. Ford, Z. G. Neale, M. W. Swift, N. Bernstein, R. E. Carter, and J. W. Long, “Mitigating polysulfide crossover in lithium–sulfur batteries with polymer-coated separators,” *RSC Appl. Interfaces*, vol. 2, no. 2, pp. 472–483, 2025, doi: 10.1039/D4LF00369A.

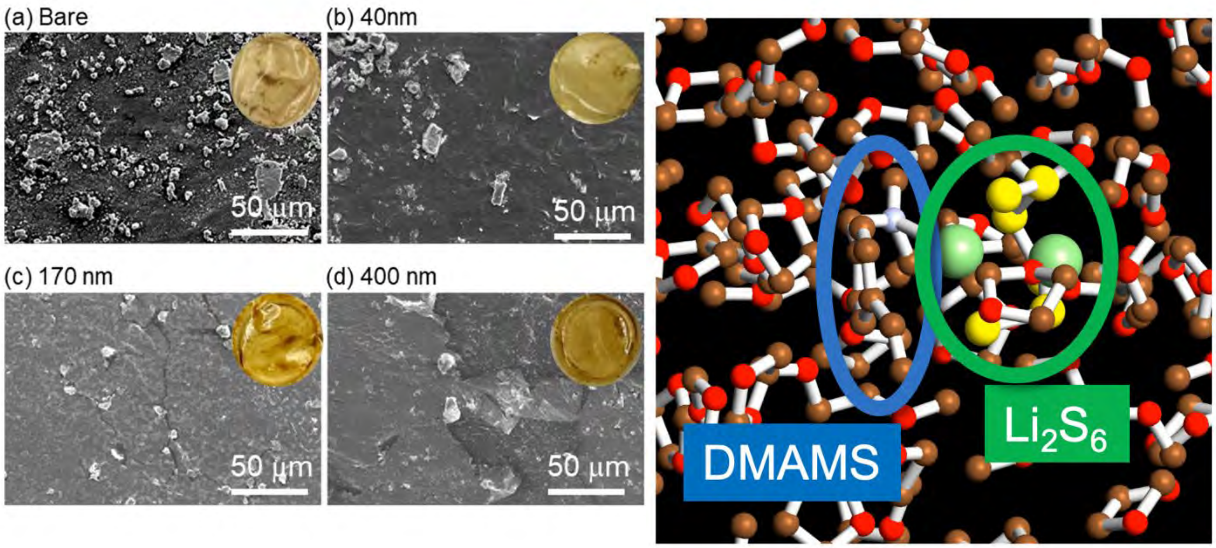

Figure 1. Left panel: Experimental results demonstrate that applying a DMAMS polymer coating to battery separators prevents the buildup of polysulfide deposits. Right panel: Computational simulations using machine learning force fields model how DMAMS interacts with polysulfide species in liquid electrolyte, validating that the separator coating can reversibly capture and release polysulfides.

Title: Materials for Energy Storage and Generation
Author(s): M.D. Johannes
Affiliation(s): U.S. Naval Research Laboratory, Washington, DC
CTA: CCM

Computer Resources: Penguin Open Compute Platform (OCP) [AFRL, OH]; Liqid Matrix XT-4 [ERDC, MS]

Research Objectives: The objectives of this program are to reproduce, analyze, and ultimately optimize materials properties relevant to energy storage and generation. Materials of particular interest include battery cathode materials of the family VFe_2O_x, anode and electrolyte materials, electrolytes for solid acid fuel cells (SAFC), and materials for catalysis based on ceria.

Methodology: Our primary methodology is density functional theory (DFT) because quantum mechanical accuracy is required for many electrochemical properties. However, to model larger systems, we develop a machine learned interatomic potential (MLIP) for structural and dynamic properties, obtaining accuracies as great as 2 meV/atom and 30 meV/angstrom for energies and forces, respectively. We have begun exploring incorporation of external fields by evaluating an Ewald sum and adding the resulting forces to the training set.

Results: In FY25, the project's focus work with solid acid fuel cell (SAFC) electrolytes continued, with rapid advances due to the ability to formulate and apply MLIPs and to run large time- and length-scale molecular dynamics simulations. Times as long as a nanosecond were simulated with cell sizes of several thousand atoms, giving solid statistics on proton diffusion as a function of temperature. Several previously undetected phase changes were observed in cesium dihydrogen phosphate, CsH_2PO_4, and analogue rubidium dihydrogen phosphate, RbH_2PO_4, each successively expanding the dimensionality of the proton transport.

We also calculated the effect of redox-inactive dopants on the performance of NRL-developed (and patented) VFe_2O_x. We showed that each dopant (Al, Zn) creates defect states in the intrinsic gap of the materials and that these states are preferentially filled during discharge, trapping electrons and decreasing the cycling efficiency as a function of time. However, the dopants simultaneously expand the physical structure of the material, increasing its ability to uptake Li ions and thereby increasing capacity.

We finished an analysis of the efficacy of Ni doping in ceria toward increased methane selectivity and catalytic activity by analyzing the valency of Ce and the clustering tendency of Ni at various levels of doping. This showed that Ni does not directly replace Ce but rather shifts dramatically to a new interstitial site and, at any concentration over ~ 5%, begins to cluster, drastically reducing its effectiveness in increasing reaction rates.

Defense Impact/Significance: Portable power is an obvious naval need. Currently, more than 150 different types of batteries are used for UUVs, UAVs, communications, and night-vision gear, and for general operational necessities. Each of these environments requires tailored storage and generation, and our work is providing understanding of new materials that can meet each of these specific needs.

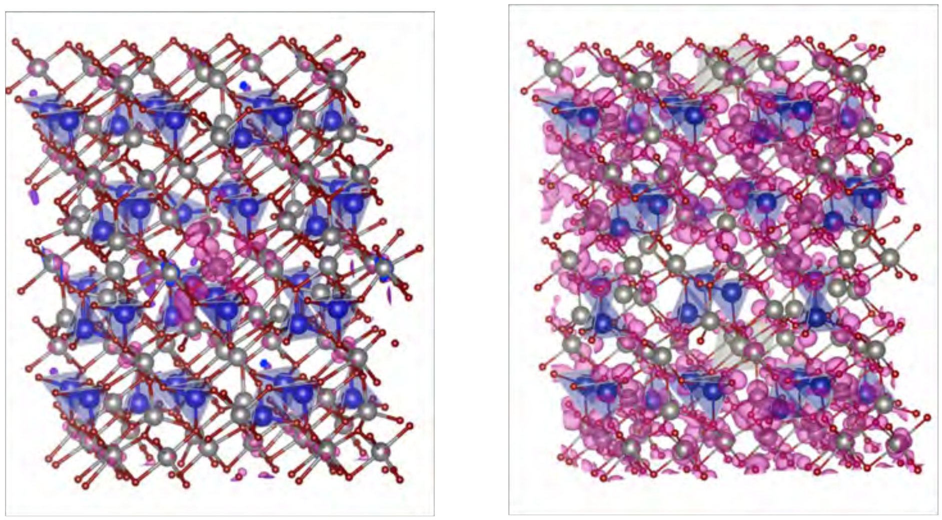

Figure 1. A comparison of the charge density of the lowest-energy unfilled electron state created by doping VFe_2O_x with aluminum to the charge density of the lowest-energy unfilled electron state in the same system without doping. The Al-derived defect state is localized and likely immobile compared to the band-like conductive state of the parent compound.

Title: Multiple Length and Time Scale Simulations of Material Properties
Author(s): N. Bernstein
Affiliation(s): U.S. Naval Research Laboratory, Washington, DC
CTA: CCM

Computer Resources: HPE Cray EX 4000 [ERDC, MS]; Penguin Open Compute Platform (OCP) [AFRL, OH]; Liqid [ARL, MD]

Research Objectives: To understand and predict mechanical, structural, and energetic material properties.

Methodology: Atomic energy, force, and stress are calculated using density functional theory (DFT) to generate reference fitting data for machine-learning interatomic potentials. The software implementing these methods includes VASP for DFT simulations, MACE for machine learning potential development, the ASE Python package for interfacing between various programs, the wfl Python package for job workflow management, wif for iteratively fitting potentials, and the LAMMPS software for molecular dynamics. The MACE neural network used GPGPUs via the PyTorch and Symmetrix libraries.

Results: We developed a model for the Cu-Al-Ni alloy system using VASP DFT calculations to evaluate reference data used to fit and test MACE machine learning interatomic potentials. These VASP calculations were set up and executed on HPC machines using the wif software package and the wfl Python library. We also used LAMMPS to evaluate the temperature-dependent structure of CsSnI, a halide perovskite. These simulations used a previously developed MACE model to carry out molecular-dynamics simulations at a range of temperatures that span the structural transitions that occur in this material. Because the time scales for transforming from one phase to another are very long, it is difficult to adequately sample the configuration space, and we therefore used the parallel tempering functionality of LAMMPS at different temperatures. The resulting structures revealed ferroelectric and anti-ferroelectric phases that have ordered localized distortions, either parallel or antiparallel, of the high-temperature cubic crystal structure.

Defense Impact/Significance: Machine learning interatomic potentials have revolutionized atomic resolution simulations of materials properties during the past few years by matching the accuracy of first-principles methods such as DFT, to which they are fit, with orders-of-magnitude lower computational cost. Materials with technological usefulness to the defense community, whether for structural applications such as armor or hypersonics, or for functional applications such as sensing, quantum information, or energy storage, usually involve several elements. The existence of a universal machine learning interatomic potential makes it possible to tackle new materials with arbitrary compositions without having to laboriously develop a new potential from scratch for each such application. The Cu-Al-Ni alloy family is an example of shape-memory materials, which can accommodate or induce large shape change as a function of temperature to absorb mechanical energy or can behave as a compact, stiff, and strong actuator. Halide perovskites have excellent optical-sensing and emission properties with applications to energy harvesting and quantum information. Their stability, electronic, and optical properties depend on their crystal structure, which must be controlled to achieve technological applications.

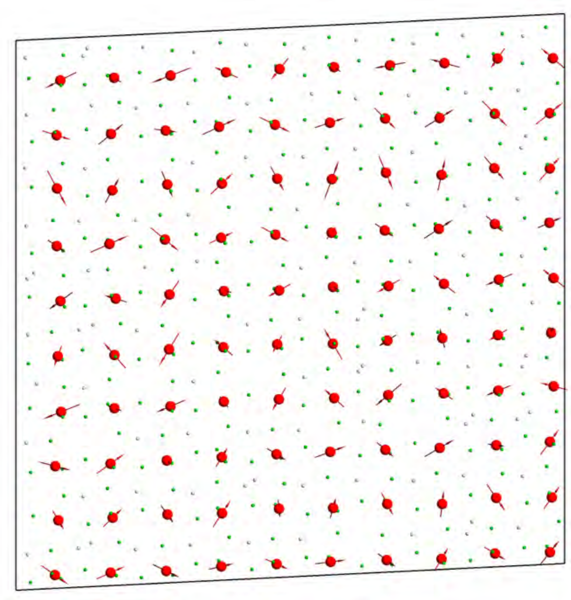

Figure 1. Visualization of a slice from a simulation of a 1000-unit-cell (5000-atom) system of cesium tin ionide, $CsSnI_3$, at T = 50 K using a MACE machine-learning interatomic potential. The arrows represent the direction of the electric dipole of each tin atom (red spheres), showing alternating y (vertical) component across columns, indicating anti-ferroelectric order at this low temperature.

Title: Materials Properties of Surfaces and Two-dimensional Systems
Author(s): M. Phillips
Affiliation(s): U.S. Naval Research Laboratory, Washington, DC
CTA: CCM

Computer Resources: Penguin Open Compute Platform (OCP) [AFRL, OH]

Research Objectives: Determine the appropriate orbital bases and real space potentials for analytic models of the flat electronic bands in near-60° twisted $MoSe_2/WSe_2$ bilayers.

Methodology: A bilayer material with a small interlayer twist exhibits a moiré pattern: a repeating pattern with a periodic unit many times the size of the periodic cell of the aligned bilayer material. The inverse is true in reciprocal space; i.e., the reciprocal cell of the aligned bilayer contains many of the "mini" reciprocal cells associated with the twisted system. The electronic band structure for the twisted bilayers can be modeled as the bands of the aligned bilayer "folded" into the mini reciprocal cell of the twisted bilayer and modified by a periodic potential with the length scale of the moiré pattern.

We perform density functional theory (DFT) calculations using the Vienna Ab initio Simulation Package (VASP) to compute the aligned bilayer electronic states that "fold" to form the twisted band structure. Then we determine the specific properties (orbital character, layer, spin) of the states at the band edges of the folded bands, which are the "parent states" of the flat bands in the twisted structures. This requires many small, relatively computationally cheap DFT calculations. To compute the periodic potential that modifies the folded bands, we compute the atomic relaxations of twisted structures at a series of angles and use the resulting displacement fields to compute the potential landscapes. The atomic relaxations of twisted structures are computationally expensive and require large amounts of memory. The energies at each reciprocal lattice point are computed in separate calculations.

Results: We determine the relationship between the aligned bilayer systems and the twisted systems in both real (Fig. 1a) and reciprocal spaces (Fig. 1c). The real space moiré supercell contains regions of aligned bilayer stacking, namely ABBA, AA, and BB stackings. The aligned bilayer reciprocal cell contains many mini reciprocal cells of the twisted bilayer. Figure 1d shows the aligned bilayer states that fold to the γ, q, k, and m points of the mini reciprocal space cell of the twisted system. The states at the valence band edge of the folded bands originate near the K′ (and K) points of the aligned system, as illustrated by the green dot in Figs. 1c, d. The conduction band edge states originate from the Q points of the aligned bilayer systems. Closer examination reveals that the valence band edge states are in-plane d-orbital states, while the conduction band edge states have both in-plane and out-of-plane d orbital components. This reveals that the appropriate bases for analytic models of the valence and conduction band states, while both d-orbital bases, will be different, with the conduction band model having a larger orbital basis.

The results of our potential calculations are shown in Fig. 1b, which shows a line cut of the potential landscape in the $MoSe_2$ layer along the dashed line in Fig. 1a, for a variety of twist angles. The potential landscape in the WSe_2 layer is qualitatively the same, but with slightly smaller-magnitude extrema. Given the sign convention in our calculations, this indicates that electrons will be localized around the AA stacked region of the moiré supercell, while holes are localized in the ABBA or BB regions (or both). We find that the same potential landscape, which arises from the atomic relaxations, can be used in both the conduction and valence band models. Potential landscape results were written up in a paper submitted for peer review in FY25. Work on the analytic model making use of the described results will continue in FY26.

Defense Impact/Significance: The work undertaken using the HPC machines in FY25 will allow us to construct analytic models of the flat bands in twisted $MoSe_2/WSe_2$ bilayers, which will enable us to simulate and understand the physics of these materials with much less computational cost and at angles that are still inaccessible using first-principles methods such as DFT. The physics of flat bands are of interest to the defense community because flat bands are associated with correlated electronic states, such as superconducting or Mott insulating states. In twisted-bilayer systems, one can switch between correlated and uncorrelated electron states by tuning a gate voltage, whereas in most systems, correlated states are accessed by less flexible means, such as chemical doping. Such flexible switching capabilities in the twisted-bilayer systems make these systems promising as elements of next-generation computing systems and low SWaP-C sensing devices that will be useful in a variety of defense scenarios.

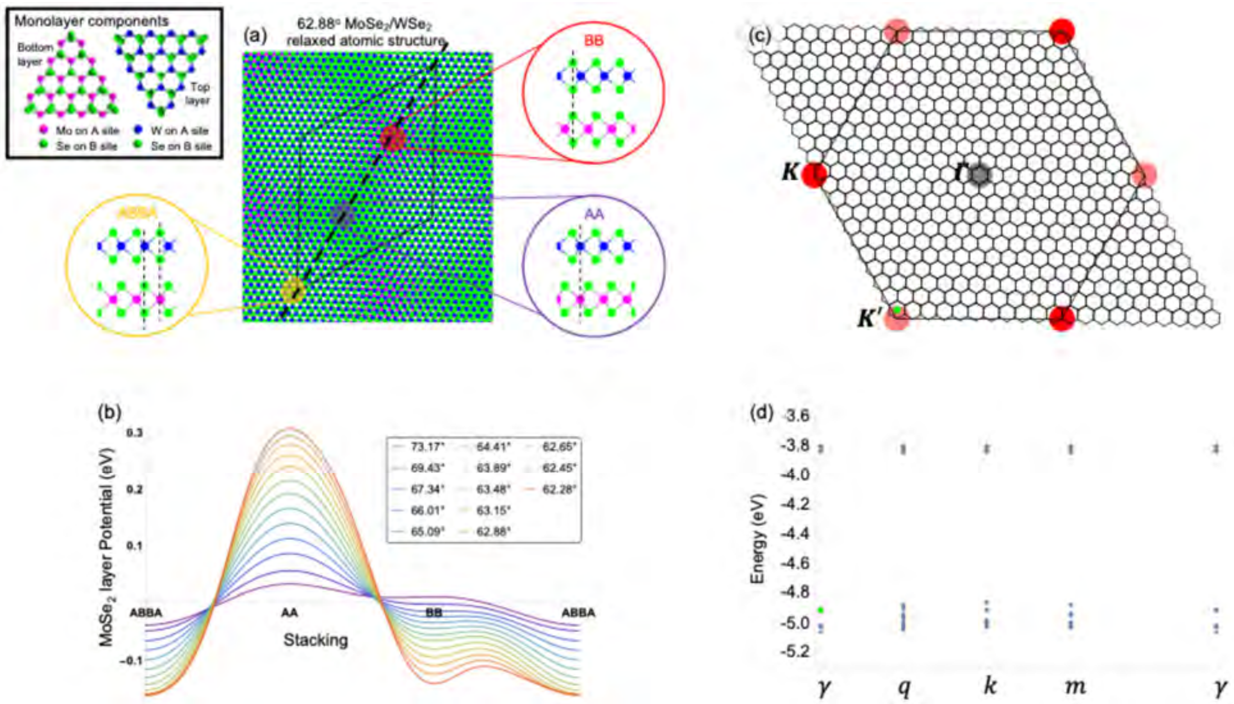

Figure 1. (a) Relaxed structure of 62.88° twisted $MoSe_2/WSe_2$ with the constituent monolayer structures and aligned-bilayer structures highlighted in the insets. The moiré supercell is defined by the black rhombus. (b) Line cuts of the potential landscape in the $MoSe_2$ layer of twisted $MoSe_2/WSe_2$ bilayers with various twist angles. Line cuts are along the dashed line shown in the moiré supercell in (a). (c) Relationship of the aligned-bilayer reciprocal space cell (large hexagon) to the tiled reciprocal cells (small hexagons) of the 63.15° twisted system. Specific reciprocal lattice points in the aligned-bilayer cell are identified by capital letters and are labeled with large, colored dots. (d) Electronic states in the aligned bilayer that fold to the given reciprocal cell points in the "mini" twisted reciprocal cell. The valence band edge at γ, highlighted by the green dot, originates from a state near the K′ point in the aligned-bilayer reciprocal cell. (See green dot in panel (c).)

Title: Surfaces and Interfaces in Oxides and Semiconductors
Author(s): C.S. Hellberg
Affiliation(s): U.S. Naval Research Laboratory, Washington, DC
CTA: CCM

Computer Resources: HPE Cray EX [NAVY, MS]; HPE Cray EX 4000 [ERDC, MS]; Liqid [ARL, MD]; Penguin Open Compute Platform (OCP) [AFRL, OH]

Research Objectives: To determine the atomic reconstruction in twisted moiré van der Waals heterostructures and the effects of the reconstruction on the electronic structure.

Methodology: Density functional theory (DFT) calculations of bilayers of two-dimensional semiconducting transition metal dichalcogenide heterostructures that are twisted relative to each other were performed. The constituent materials include $MoSe_2$, WSe_2, MoS_2, and WS_2. At certain twist angles, twisted bilayers form periodic structures that can be modeled with density functional codes; at all other angles, the twisted bilayer is incommensurate. The layers are bound to each other via the weak van der Waals interaction. We used the VASP DFT code at the AFRL, NAVY, ERDC, and ARL HPC centers. We focused on the dielectric properties of the heterostructures. Such calculations use density-functional-perturbation theory (DFPT).

Results: We relaxed the atomic structure of $MoSe_2/WSe_2$ at the following commensurate twist angles:

Twist angle (degrees)	**Number of atoms**
60	6
21.79	42
13.17	114
9.43	222
7.34	366
6.01	546
5.09	762
4.41	1014
3.89	1302
3.48	1626
3.15	1986
2.88	2382

As the twist angle gets smaller, the moiré length becomes longer and the number of atoms in the computational cell grows. The bilayers exhibit localized electronic states below critical twist angles. These calculations are particularly challenging because the spin-orbit coupling doubles the size of the Hamiltonian matrices. All relative lateral shifts between the layers are naturally included in the supercell due to the twist. For the larger twist angles, which have smaller numbers of atoms, density-functional-perturbation theory (DFPT) calculations are feasible for computation of the dielectric function. The imaginary part of the dielectric function for the 21.79-degree-twisted heterostructure is shown in the figure along with the sum of the dielectric functions of the two individual monolayers.

Defense Impact/Significance: Moiré dichalcogenide bilayers are candidates for hosting strongly correlated electrons because the dispersion of the electrons can be tuned by adjusting the angle of the twist. We are examining the feasibility of using these systems' low-SWAP-C optical gyroscopes.

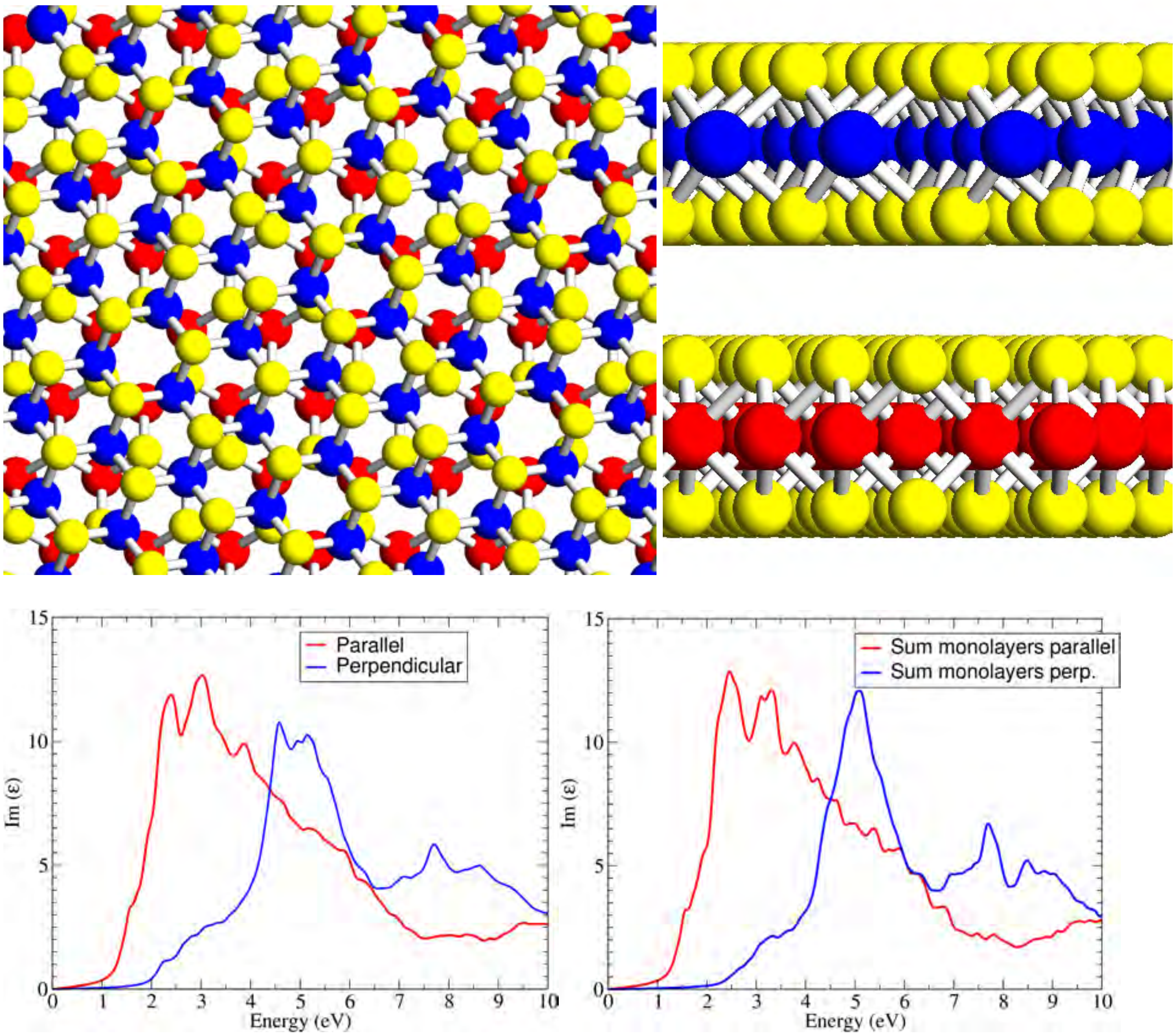

Figure 1. Relaxed atomic positions and computed imaginary dielectric function of $MoSe_2$/WSe_2 bilayers twisted at 21.79 degrees. The atomic structures are shown above in views from the top and the side. Mo atoms are blue, W atoms are red, and Se atoms are yellow. The structure has D_3 symmetry: notice each moiré cell has one Mo directly over a W and one pair of Se directly over the Se in the bottom layer. The imaginary part of the dielectric function of the heterostructure is shown in the bottom left, showing parallel absorption at lower energies than perpendicular absorption. The bottom right shows the sum of two isolated monolayers. Notice the differences, particularly in the perpendicular direction, show the importance of interlayer hybridization in the heterostructure.

Title: Atomistic Simulations of Navy-relevant Materials
Author(s): D. Fragiadakis
Affiliation(s): U.S. Naval Research Laboratory, Washington, DC
CTA: CCM

Computer Resources: HPE Cray EX [ARL, MD]; Penguin Open Compute Platform (OCP) [AFRL, OH]; Penguin True HPC [NAVY, MS]

Research Objectives: Photoacids are molecules that allow precise control of acidity using light. This allows noninvasive, accurate, and reversible control of chemical reactions, with numerous applications including advanced polymer materials, soft robotics, microfluidics, and drug delivery. Merocyanine photoacids are the most widely used due to their large acidity change upon illumination and their chemical versatility. Attaching functional groups to different parts of the molecule causes substantial changes to the acidity in the ground state (dark) and the excited state (illuminated), along with solubility, response times, and other molecular properties relevant to applications.

To design new molecular structures tailored to applications, computational support is critical because (a) the number of potential molecular structures is enormous, and (b) many merocyanine derivatives have very low solubility in water, making experimental determination of acidity challenging. Our objective is to develop a precise, efficient computational method to determine the acidity (quantified by the pKa) of merocyanine photoacids in aqueous solution from the molecular structure.

Methodology: We searched for all substituted merocyanine structures for which experimental pK_a values are published. For each merocyanine, we used density functional theory to calculate Gibbs free energies of the merocyanine forms observed under dark and light conditions, both protonated and deprotonated. For accurate results, we found it is necessary to consider multiple conformers for each form, Boltzmann-averaging their respective free energies, rather than using the lowest-energy structure only. Conformer searches were performed using CREST (parallelized with OpenMP), and DFT calculations using Gaussian 16. Analysis was done using in-house code in Python. The r^2SCAN(D3)/def2-TZVP model chemistry was used for structural optimization and vibrational frequency calculations, followed by single-point energy calculations using M06-2x/def2-QZVP. The implicit solvent model SMD was used to model interaction with the aqueous environment.

Results: The experimentally observed $pK_{a,dark}$ under dark conditions is an effective value with contributions from the open (merocyanine) and closed forms (spiropyran) of the molecule in equilibrium with each other. In some reported data, the amounts of the two forms are determined experimentally and the separate pK_a of the open-form merocyanine is calculated. With this subset of experimental data, together with the reported $pK_{a,h\nu}$ under illumination, we were able to calibrate a quadratic function relating the calculated free energy difference between protonated and deprotonated states of a merocyanine to the experimental pK_a. Using this relation, we can accurately predict the pK_a of a merocyanine, under both dark and illuminated conditions, with mean unsigned error of only 0.2 pK_a units.

To calculate the effective acidity in dark conditions, $pK_{a,dark}$, the relative concentrations of the open and closed forms of the molecule are needed. We found an approximate linear relation between the free energy difference of the two forms of the molecule and the log of the relative concentration determined experimentally; however, a separate linear function is needed for merocyanines with charges of +2, +1 and 0 (in the protonated state). Using these relations, we were able to calculate $pK_{a,dark}$ for the molecules for which pK_a was not measured (and therefore were not included in the calibration of the predictive model), and the resulting error in the prediction of $pK_{a,dark}$ is 0.32 pK_a units.

Defense Impact/Significance: Accurate prediction of the acidity of merocyanine-based photoacids, which so far has not been available, will enable the design of new photoacid molecular structures tailored to applications. The model's predictions are currently being used to design new, advanced polymers with dynamic covalent bonds, with mechanical properties that can be accurately controlled by light.

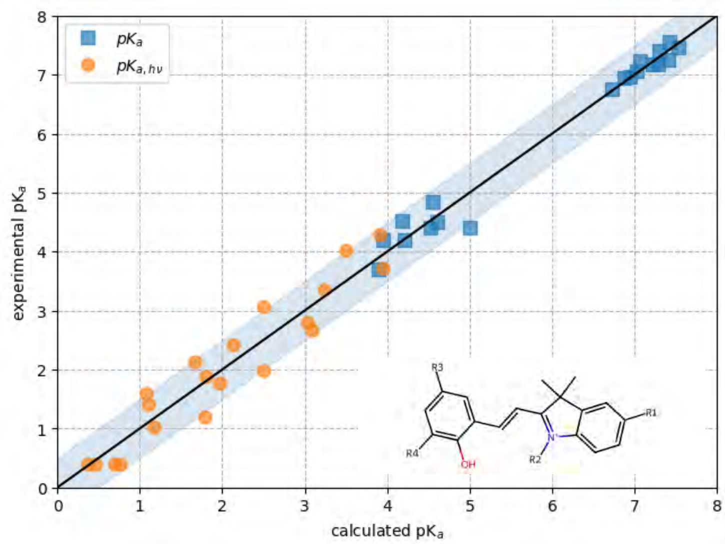

Figure 1. Calculated vs experimental values of pK$_a$ for substituted merocyanines (molecular structure in inset) under dark (blue squares) and illuminated (orange circles) conditions. The light-blue band indicates ±0.5 pKa units.

Title: Evaluating the Active Site of Metal-Zeolite Combinations for Selective Catalytic Reactions
Author(s): C.F. Holder and A.R. Shabaev
Affiliation(s): U.S. Naval Research Laboratory, Washington, DC
CTA: CCM

Computer Resources: HPE Cray EX [AFRL, OH], [NAVY, MS]; HPE Cray EX 4000 [ERDC, MS]

Research Objectives: To provide insights into the deposition of metal clusters, particularly Pt, into zeolitic pores. This program aims to provide foundational knowledge to investigate Pt clusters embedded into zeolites for carbon-utilization reactions including isomerization, aromatization, and up-conversion to value-added products.

Methodology: We used density functional theory (DFT) and the projector augmented-wave method as implemented in the Vienna Ab-initio Simulation Package (VASP) to investigate differences in the electronic properties of an LTL zeolite archetype due to changes in the elemental composition. Specifically, the substitution of Al atoms for Si atoms within the zeolite structure were investigated and how the presence of a charge-balancing cation affected the overall electronic signature.

Results: In FY25, our studies were focused on investigating the electronic effects within the LTL zeolite framework with the substitution of Al atoms for Si atoms. Additionally, efforts were focused on determining what the impact of the associated cation, in this case a proton, was on balancing the overall charge difference that arises due to the incorporation of an Al^{3+} ion compared to a Si^{4+} ion. These results were then correlated back to the deposition of Pt into the zeolite pores, which was reported on last year.

Figures 1a and 1b depict the converged geometries of the LTL zeolite with a substituted Al atom, without and with the presence of an H atom, respectively. Figures 1c and 1d depict the calculated electron density maps of these structures, with blue isosurfaces representing areas of decreased electron density and yellow isosurfaces representing areas of increased electron density. The substitution of the Al atom for a Si atom resulted in a significant loss of electron density around that atomic position, with the electron density being redistributed across the four oxygen bonds. This result was anticipated due to the decreased number of total electrons of Al^{3+} as well as the Al-O bond's being more ionic in character compared to the Si-O bond. The inclusion of a nearby H atom resulted in increased electron density within the neighboring pore, forming a pocket of increased electron density formed by the H-O-Al-O moiety. The increased, localized electron density is theorized to favorably promote the deposition of Pt onto the zeolitic surface, indicating that the inclusion of a cation within the framework is vitally important.

Defense Impact/Significance: Pt/zeolite catalysts are important materials for thermochemical CO_2 conversions toward value-added products. The activity of the Pt clusters, coupled with the inherently high surface areas provided by the zeolite support, offers significant advantages when compared to catalytic materials that are supported on metal oxide supports. Additionally, zeolites offer a large design space to enhance catalytic properties of interest. The theoretical studies conducted for this HPC program help to support ongoing experimental efforts in our group at NRL to develop and enhance the process of synthesizing additives for fuels such as JP-5 to enable drop-in replacements for the Navy and the Marine Corps.

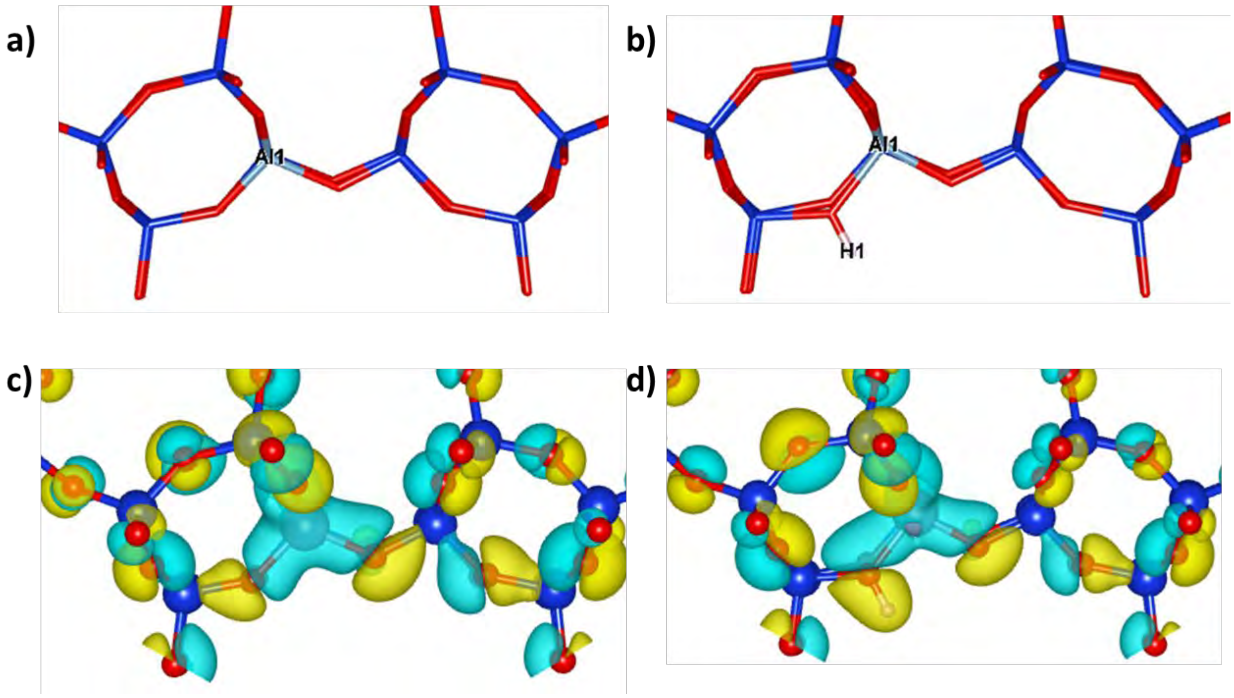

Figure 1. LTL zeolite framework that contains a substituted Al^{3+} atom at a Si^{4+} site (a) without and (b) with a nearby H atom. In (c) and (d), electron density maps are depicted for the structures without and with a nearby H atom, respectively. Blue isosurfaces indicate decreased electron density, while yellow isosurfaces indicate increased electron density. Si, O, Al, and H atoms are depicted as spheres or sticks of dark blue, red, light blue, and white, respectively.

Title: Target Material Detection by Comparison of Measured and DFT-calculated Absorbance Spectra
Author(s): A.R. Shabaev and C.F. Holder
Affiliation(s): U.S. Naval Research Laboratory, Washington, DC
CTA: CCM

Computer Resources: Cray XC40/50, HPE Cray EX4000 [ERDC, MS]; HPE SGI 8600, Penguin TrueHPC, HPE Cray EX [NAVY, MS]; HPE SGI 8600, HPE Cray EX [AFRL, OH]

Research Objectives: The objective of this research is to aid target-material detection by spectroscopy using density functional theory (DFT). Detection methodologies such as infrared (IR) spectroscopy are based on identification of unknown materials by comparison of measured spectra with reference spectra associated with known materials. DFT calculated IR absorption spectra corresponding to vibrational excitation states of molecular structures provide quantitative estimates of IR spectra that can be correlated with additional information obtained from laboratory measurements or spectra associated with detection in the field.

Methodology: The general methodology adopted for this task element involves DFT calculation of absorption spectra of various prototypical target materials of interest. These materials include, but are not limited to, microporous structures such as zeolites and adsorbate/support structures. Initial prototype materials included simple support structures and metal cluster deposition on zeolites for hydrogenation reactions. Correlation of DFT-calculated absorption with measured IR spectra will provide an interpretation of various spectral features for detection and will help to understand and control catalytic reactions.

Results: The DFT calculation of absorption spectra for prototypical target materials of interest, coupled with experimentally measured spectra, provide an understanding of signature features of various adsorbate/support models. For example, Figs. 1a and 1c shows two adsorption sites of CO and CO_2 molecules on the interface of a Mo_2C ribbon atop a MgO(001) slab and two adsorption sites of CO and CO_2 on the surface of Mo_2C. Metal carbides (Mo_2C) supported on transition metal oxide supports (MgO) have been studied as catalysts for the low-temperature RWGS reaction. The structures shown represent various geometries of molecules (including CO and CO_2) adsorbed onto the Mo_2C/MgO interface. The difference in molecular species resulted in unique IR signatures that are shown in Figs. 1b and 1d. These results will then be used to develop next-generation catalysts that leverage these findings to achieve improved catalytic activity and provide interpretation of signature features associated with experimentally measured spectra that are significant for realistic detection problems associated with detection of target materials.

Defense Impact/Significance: The proposed task, which provides a foundation for real-world deliverability of results, is that absorption spectra of major target molecules of interest are to be constructed using existing off-the-shelf software technology, including DFT software such as VASP and GAUSSIAN, as well as existing postprocessing software. Accordingly, it follows that a secondary deliverable of the proposed task element will offer more optimal procedures for calculation of response spectra using atomic orbitals basis functions and potential energy functions, which represent the basic information for modeling vibrational spectra using DFT.

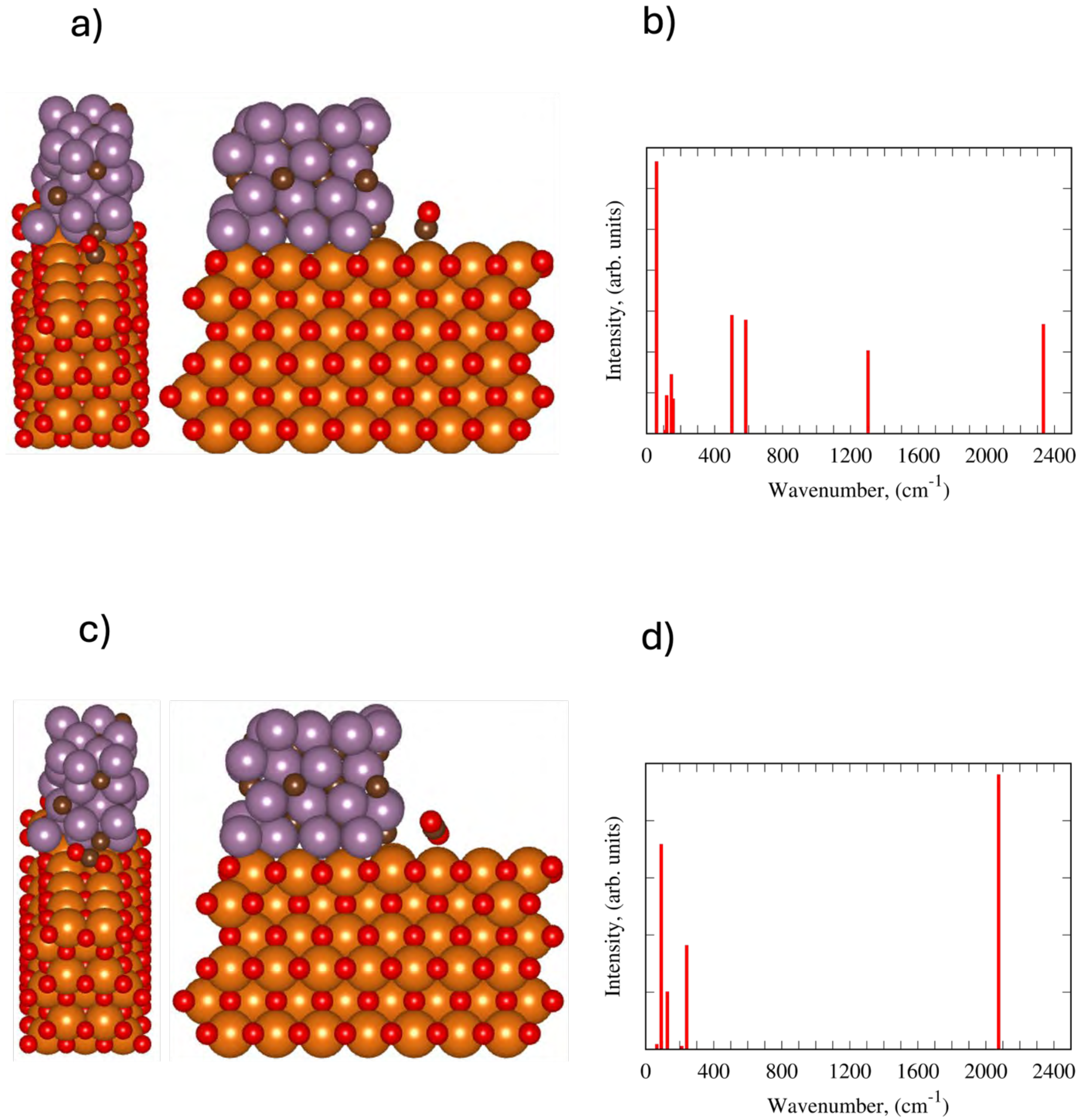

Figure 1. Relaxed geometries of CO (a) and CO_2 (c) at the interface of a Mo_2C ribbon atop a MgO substrate. The simulated IR spectra (b and d) of the relaxed geometries can then be used to verify and detect the presence of certain molecular species to determine the pathway of CO_2 adsorption on Mo_2C.

Title: First-principles Simulations of Condensed-Phase Decomposition of Energetic Materials
Author(s): I.V. Schweigert
Affiliation(s): U.S. Naval Research Laboratory, Washington, DC
CTA: CCM

Computer Resources: HPE Cray EX 4000 [ERDC, MS]; Penguin Open Compute Platform (OCP) [AFRL, OH]

Research Objectives: To predict thermal, chemical, and mechanical properties of crystals, polymers, nanoparticles, and molecules of interest to defense community.

Methodology: We use various methods of quantum chemistry to predict thermochemical properties and reactivity of target materials. Molecular graph enumeration (MGE) algorithms are being developed to generate model structures. Structure optimizations based on density functional theory (DFT) are used to determine atomic coordinates and crystal lattice parameters. DFT-derived electronic energies and vibrational frequencies are used to compute thermochemical properties such as enthalpies of formation and reaction. Ab initio electron-correlation methods are used to compute accurate electronic energies and to correct the DFT values. Quantum molecular dynamics (QMD) simulations are used to quantify effects of elevated temperatures and pressures on crystal structures as well as to identify possible reaction mechanisms. Infrared absorption (IR), nuclear magnetic resonance (NMR), and x-ray photoelectron spectra (XPS) are simulated to enable comparisons with experiments. To facilitate these simulations, we develop automated workflows for preparation of input files, job submission, detection and remediation of errors, and processing and analysis of the simulation results.

Results: This year, we focused on predicting atomistic structures of small, nonstoichiometric metal-chalcogenide M_nQ_m clusters. Because previous computational studies focused almost exclusively on stoichiometric chalcogenide clusters ($n = m$), the energetically favorable structures for nonstoichiometric clusters ($n \neq m$) are generally not known. We developed a molecular graph enumeration (MGE) algorithm to generate all possible atom-connectivity matrices for specific values of n and m. Our algorithm enforces specific coordination numbers (nearest-neighbor requirements) to reduce the number of possible connectivity matrices. A distance-geometry (DG) algorithm, implemented in the open-source cheminformatics library RDKit, is then used to generate atomic coordinates for the generated connectivity matrices. During initial testing, we found that the RDKit DG algorithm often produced unphysical cluster structures because of the hypervalent nature of chalcogen anions. To mitigate this issue, we implemented an alternative approach in which Si, SiH, SiH_2 moieties are used as placeholders for fourfold, threefold, and twofold coordinated metal cations and C, CH, CH_2 are used as placeholders for fourfold, threefold, and twofold chalcogen anions. The resulting organosilane structures are then generated using the MGE and DG algorithms, and the atomic coordinates for Si and C are used to specify the coordinates for metal cations and chalcogen anions. This approach is illustrated in the top panel of Fig. 1, which shows the three lowest-energy $Si_8C_8H_{16}$ isomers, wherein each Si atom is bonded to three C atoms, and the corresponding stoichiometric Zn_6S_6 clusters, wherein all Zn and S atoms are threefold coordinated. Our simulations predict that the lowest-energy structure is an asymmetric cluster consisting of two pairs of fused 6- and 4-atom rings, while the symmetric cluster consisting of two stacked 8-atom rings has higher energy. We then used this approach to generate nonstoichiometric, metal-rich clusters, Zn_6S_4, without ligands and ligated with water (as an example of hard electron-donating ligands) and phosphine (as an example of soft electron-donating ligands). These simulations are illustrated in the bottom panel of Fig. 1.

Defense Impact/Significance: Research completed this year focused on predicting atomistic structure of small metal-chalcogenide clusters. These simulations are currently being extended to study surface properties of metal-chalcogenide quantum dots (QDs) as part of a multidisciplinary project focused on QD-supported multienzymatic catalysts for biomanufacturing of defense-critical materials.

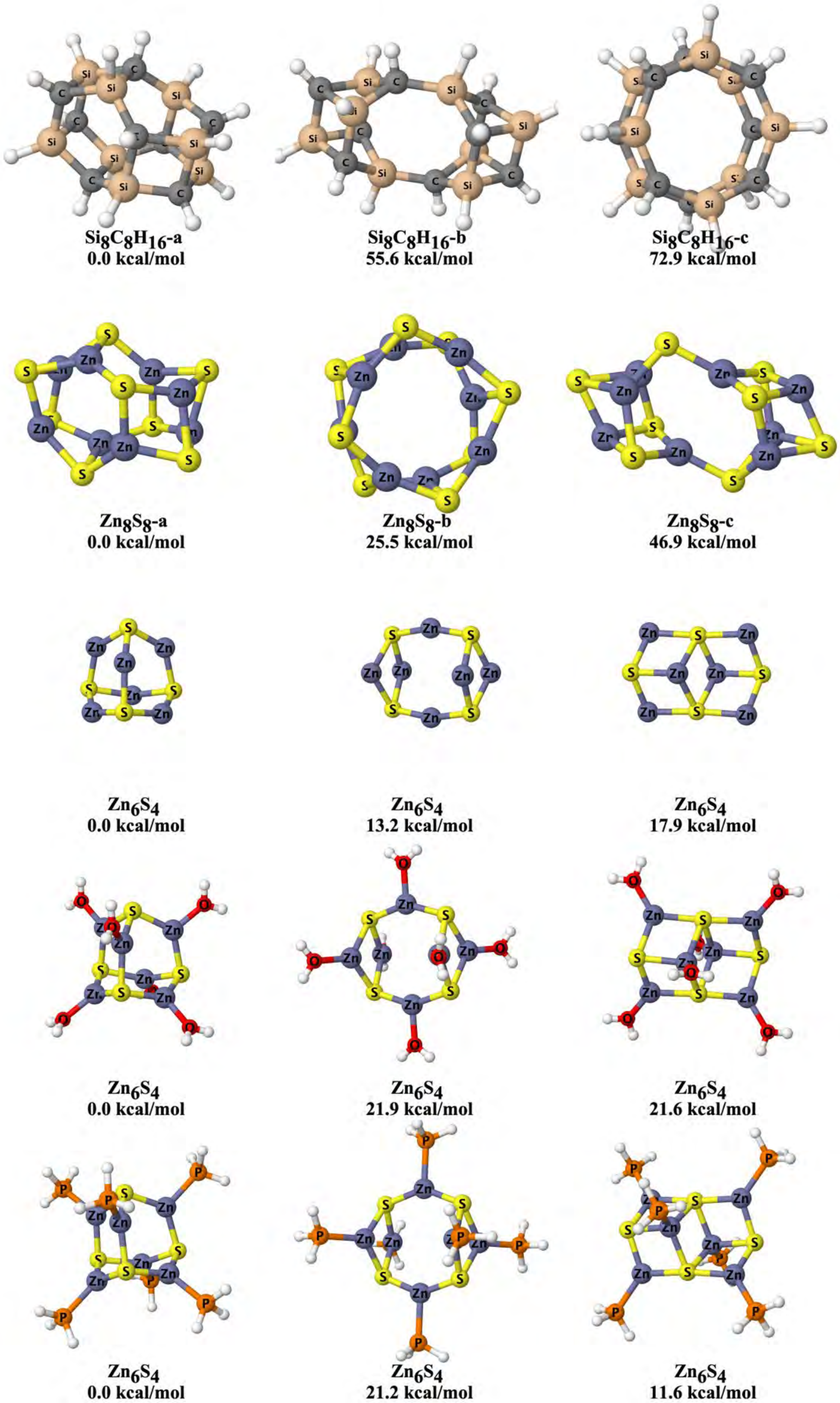

Figure 1. Organosilane molecules and zinc sulfide clusters simulated in this work.

Title: Computational Materials Design for Targeted Applications
Author(s): S. Mukhopadhyay
Affiliation(s): U.S. Naval Research Laboratory, Washington, DC
CTA: CCM

Computer Resources: HPE Cray EX 4000 [ERDC, MS]; Penguin Open Compute Platform (OCP), HPE Cray EX [AFRL, OH]; HPE Cray EX, Penguin TrueHPC [NAVY, MS]

Research Objectives: (i) Accurate characterization of HfO_2 growth at high temperature is critical for its use in neuromorphic computing. In this study, our objective was to understand the phase transition/phase nucleation process in HfO_2. (ii) To develop Cs-free GaN photocathodes with desired quantum efficiency (QE), it is important to understand the GaN surface chemistry so that air-stable operation of GaN-based photocathodes can be designed via polarization-band engineering. In this work, we aim at exploring various surface-passivation mechanisms of GaN surfaces.

Methodology: (i) Ab initio density functional methods using Quantum ATK were used to simulate the various phases in HfO_2 and its interfaces. We used moment tensor potentials (MTP) to optimize the structure and calculation of materials properties in various phases including the amorphous structure at various temperatures. (ii) We used density functional theory to explore various surface-passivation mechanisms of GaN surfaces using PBE functional forms as implemented in VASP.

Results: (i) We performed molecular dynamics (MD) simulation of thermal evolution and phase transformations of hafnia films. While the phase transformations of HfO_2 have been successfully calculated via a rapid-heating-and-cooling method, phase nucleation and phase separation could not be noted using moderately large cells with ~1400 atoms. Subsequently, we designed new calculations with larger cells consisting of ~6000 atoms with the help of machine trained potentials (MTP) that unlock the potential to observe phase nucleation/separation in the MD simulations. The accuracy of the MTP has been established by comparing the calculated forces and energies using MTP with those from standard DFT and, subsequently, by reproducing the XRD patterns from HfO_2 phases at various temperatures. These underscore the accuracy of the MTP used in the calculations and enable us to carry out large-scale simulations to unveil the possibility of HfO_2 phase mixing during its growth in the experiments. (ii) We considered H-passivation of N- and Ga-terminated GaN and passivation with two-dimensional (2D) materials such as graphene and h-BN. The calculations revealed that the H-passivation of N-terminated GaN shows better energy-band and vacuum-level alignment than Ga-terminated GaN. This explains why HCl surface treatment increases QE for N-terminated GaN and not for Ga-terminated GaN. Among all the passivation cases studied here, h-BN was found to offer the best energy-band and vacuum-level alignment with reduced effective work function.

Defense Impact/Significance: (i) These numerical simulations will provide critical understanding of crystallization mechanisms and will assist in optimizing laser annealing conditions to achieve the desired ferroelectric phase of HfO_2 required to enable neuromorphic devices for low size, weight, and power (SWaP) AI hardware for a variety of critical Navy/defense needs such as collaborative combat aircraft (CCA), counter-small unmanned aerial systems (UAS), and one-way attack/autonomous systems. (ii) The development of high-efficiency, stable photocathodes through this program will enable next-generation high-power microwave generation for applications in countering UAVs.

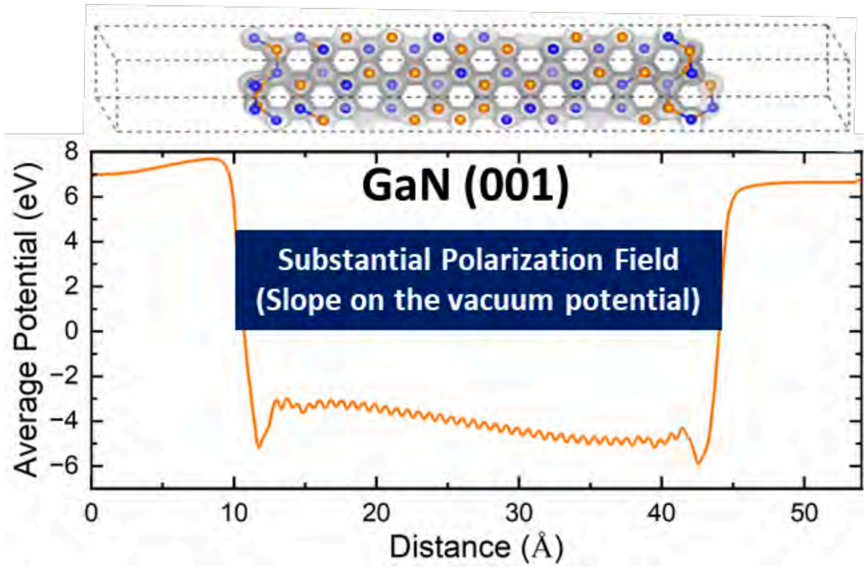

Figure 1. Average potential for GaN-001 surface calculated using density functional theory.

Title: Marine Biofilm Metaproteomics
Author(s): W.J. Hervey and G.J. Vora
Affiliation(s): U.S. Naval Research Laboratory, Washington, DC
CTA: CCM

Computer Resources: HPE Cray EX 4000 [ERDC, MS]; Penguin Open Compute Platform (OCP) [AFRL, OH]

Research Objectives: To maintain and update data-analysis workflows for large-scale multi-*omics* analytics, namely metagenomics and metaproteomics. Previous investments in distributed bioinformatics software development via the HPC Application Software Initiative (HASI) have enabled large-scale characterization of biological samples from complex environmental matrices, such as marine biofilms and other substrates of interest. In FY25, we planned to update resources and tools available for both metagenomic and metaproteomic analyses of complex environmental matrices.

Methodology: In FY25, updates were made to the available software tool sets applied to metagenomic and metaproteomic workflows. Metagenomic resources leveraged reproducible workflows to assemble raw sequence data, to annotate resulting assemblies, and to bin representative members of microbiomes. New tools deployed in FY25 were used to infer the composition of microbiomes distributed on marine substrates of interest. Existing software tools used for metaproteome analyses were benchmarked across a multilab proteomics study targeting ocean metaproteomic filter samples.

Results: Results of a multilaboratory ocean metaproteomic intercomparison study are shown in Fig. 1. The seven-way Venn diagram shows that a core set of 1,056 peptides was identified by peptide-spectrum matching (PSM) among labs participating in the study. NRL contributions to the study included metagenome sequencing and metaproteome informatics, as described in the peer-reviewed publication of the study [1].

Defense Impact/Significance: This HPC subproject has broad significance across both the Naval Research Enterprise (NRE) and the larger defense enterprise. Our subproject's general workflow for metagenomics and metaproteomics is applicable to the Navy Focus of "Sense and Sense-Making" from large data. In FY25, biotechnology was listed as a Seed Area of Emerging Opportunity by OUSD (R&E) and is a Reliance 21 Community of Interest.

References

[1] M. A. Saito et al., "Results from a multi-laboratory ocean metaproteomic intercomparison: effects of LC–MS acquisition and data analysis procedures," *Biogeosciences*, vol. 21, no. 21, pp. 4889–4908, Nov. 2024, doi: 10.5194/bg-21-4889-2024.

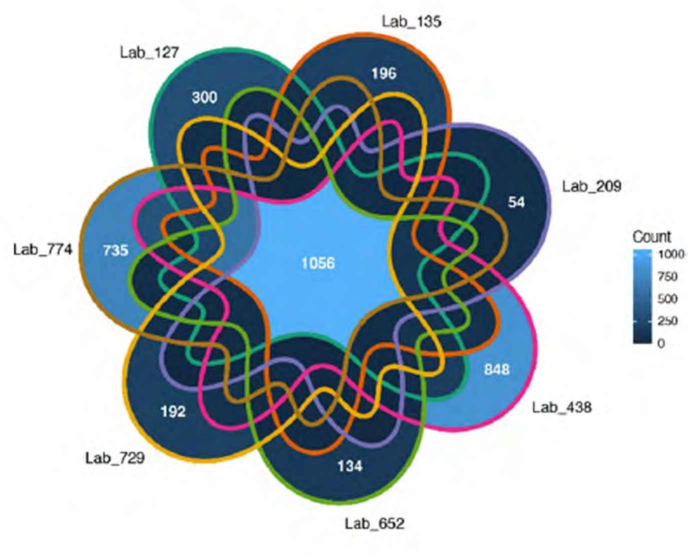

Figure 1. Peptide Identifications from seven-lab Ocean Metaproteome Intercomparison Study. Seven-way Venn diagram showing peptide identifications among laboratories participating in an intercomparison study. Participating labs processed portions of a filter according to their own sample-processing and data-acquisition methods (i.e., liquid chromatography-tandem mass spectrometry (LC-MS/MS)). Laboratory identification numbers were assigned to participants at random. This figure is adapted from Fig. 2c of [1].

Title: Synthetic Biology for Military Environments
Author(s): W.J. Hervey and G.J. Vora
Affiliation(s): U.S. Naval Research Laboratory, Washington, DC
CTA: CCM

Computer Resources: Penguin Open Compute Platform (OCP) [AFRL, OH]

Research Objectives: To engineer and deploy synthetic biology tools for biomaterials production. Routinely, biotechnology and synthetic biology research leverages knowledge of model genomic species, such as the bacteria *E. coli*, the yeast *S. cerevisiae*, and the fly *D. melanogaster*. Though tremendous amounts of knowledge have been accrued for each of these model genomic species, previous background may not be extensible to emerging synthetic biology chassis or targeted organisms. Here, we have applied the synthetic biology "design, build, test, learn" (DBTL) paradigm to measurements of species of interest for novel biological insight.

Methodology: In FY25, DBTL paradigm foci (Fig. 1) included proteome profiling in the test phase and resulting signal intensities in the learn phase. In the test phase, proteome profiling or other -omics-level measurement (e.g., genomics, transcriptomics, and/or metabolomics) can be performed on entire biological systems of interest. A high-level overview of the large-scale measurement's features, such as signal intensity, yields input that can drive the learn phase and iterative feedback into subsequent DBTL cycles.

Results: In FY25, large-scale genomic and proteomic measurements were performed on emerging species of interest in synthetic biology and biotechnology. FY25 allocations were leveraged to assist with genome sequencing of *Pseudomonas* sp. CBR-F from PFAS-impacted soil [1], among other dataset analyses.

Defense Impact/Significance: This HPC subproject has broad significance across both the Naval Research Enterprise (NRE) and the larger defense enterprise. Insights from actional biological data are applicable to the Navy Focus of "Sense and Sense-Making" from large data. In FY25, biotechnology is listed as a Seed Area of Emerging Opportunity by OUSD (R&E) and is a Reliance 21 Community of Interest.

References

[1] I. R. Baker, S. M. Colston, J. Hervey, B. J. Eddie, and L. J. Bird, "Complete genome of a fluorescent Pseudomonas sp. isolated from a PFAS groundwater treatment site," Microbiology Resource Announcements, vol. 14, no. 2, e00976-24, Jan. 2025. doi: 10.1128/mra.00976-24.

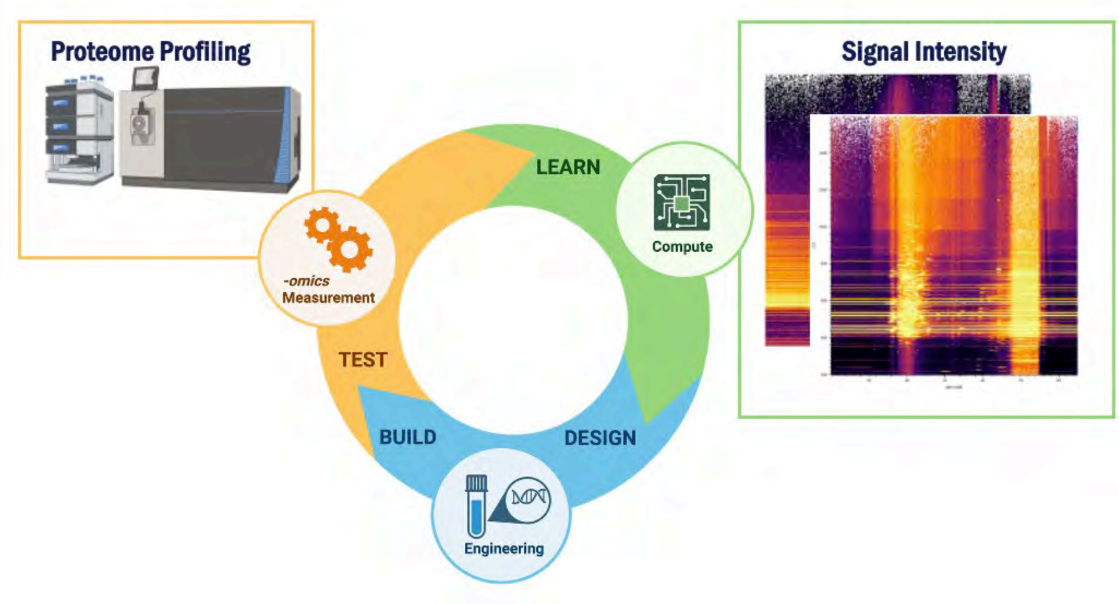

Figure 1. Synthetic biology DBTL paradigm. The test phase of the DBTL paradigm can be assessed by a number of -omics-level measurements. Here, proteome profiling is shown as the representative measurement to evaluate output of the design and build phases. In learn phase, representative data features from the -omics measurement, in this case signal intensity, provide primary feedback that may guide subsequent cycles or iterations of the DBTL paradigm.

THIS PAGE INTENTIONALLY LEFT BLANK

CEA

Computational Electromagnetics and Acoustics

The Computational Electromagnetics and Acoustics (CEA) CTA encompasses two complementary computational disciplines. Computational electromagnetics focuses on high-resolution, multidimensional solutions of Maxwell's equations to model complex electromagnetic phenomena. Defense-relevant applications include radio frequency (RF) sensor and antenna performance, radar scattering from ground, air, and maritime platforms, electromagnetic signatures of buried or obscured munitions, and high-power microwave systems. The discipline also supports interdisciplinary applications such as magnetohydrodynamics and laser-matter interactions, where tightly coupled electromagnetic and fluid or plasma processes are critical.

Computational acoustics addresses high-resolution, multidimensional solutions of acoustic wave equations in both solids and fluids. These capabilities support modeling of acoustic fields for surveillance, sensing, and communication, seismic wave propagation for mine and buried-object detection, and blast-induced acoustic and shock waves associated with explosive events and weapon effects. Together, these approaches enable predictive analysis of complex wave phenomena across a wide range of operational environments.

Title: Low Grazing Angle Radar Backscatter
Author(s): J.V. Toporkov, J.D. Ouellette, and M.A. Sletten
Affiliation(s): U.S. Naval Research Laboratory, Washington, DC
CTA: CEA

Computer Resources: HPE Cray EX, Penguin Open Compute Platform (OCP) [AFRL, OH]; HPE Cray EX 4000 [EDRC, MS]; HPE Cray EX, Penguin HPCTrue [NAVY, MS]

Research Objectives: Reflections from sea surfaces are routinely observed by many radar systems operating in the ocean environment, often under low-grazing-angle (LGA) conditions. Such surface signatures can act as clutter that masks a target echo. On the other hand, they are a source of information about local ocean states. Understanding the properties of sea scatter, their dependence on wind speed and other factors, and how they differ from those of man-made target echoes is key to improving or even enabling performance of such radar systems and applications. This project studies detailed characteristics of radar returns from ocean surfaces under both monostatic and bistatic observation geometries. The task is accomplished through simulations that involve both direct numerical solution of the scattering problem and, where suitable, numerical implementations of approximate scattering models.

Methodology: The approach combines a physics-based model for evolving ocean surfaces with computationally efficient evaluation of the scattered electromagnetic field. The most rigorous implementation is limited to the two-dimensional (2D) space but is relevant for commonly occurring three-dimensional (3D) geometries (e.g., oncoming or receding waves). A wind-driven surface is represented by realizations of a Gaussian random process defined by a certain wave spectrum. Inherent hydrodynamic nonlinearities (that affect shape and motion of smaller, scattering ripples) are commonly introduced with approximate, computationally manageable techniques such as Creamer or “choppy wave” models. Those do not describe wave breaking, so their utility is limited to sea states up to 3, perhaps somewhat higher for longer electromagnetic wavelengths (S band and below) that are less sensitive to whitecaps. The field scattered by a “time-frozen” scene at a particular frequency is found by iteratively solving a boundary integral equation (BIE) for the induced surface current. This first-principles formulation accounts for many phenomena (multiple scattering, shadowing) that could be problematic for analytical treatment. The procedure is repeated for every surface profile in the sequence to capture the temporal evolution. OpenMP parallelism is used.

Results: Including interharmonic interactions when modeling surface evolution is an important aspect of the Doppler scattering simulations. However, the two most-often-used approximate techniques to introduce such surface nonlinearities, the Creamer and choppy wave models, yield notably different Doppler shifts (spectral centroids), cf. Fig. 1. At the same time, the widths of the spectra resulting from the two approaches are rather similar. (For reference, Fig. 1 displays “linear” curves corresponding to the surface evolution according to the linear wave theory that does not include any interharmonic interaction — leading to abnormal behavior of the spectral moments, especially the width, at large incidence/low grazing angles.) A modulation transfer function (MTF)-based theory suggests that such a behavior of the Creamer and choppy wave-related spectral moments could be explained if the models induced different levels of modulation of short ripple amplitudes by longer waves. The latter seems to be the case, as the example with the two-harmonic surface in Fig. 2 suggests. For a rigorous, conclusive assessment, we proceeded with measuring the so-called “hydrodynamic modulation transfer function” (HMTF) for both nonlinear models through the Monte Carlo-based numerical experiment. The HMTF quantifies the local modification of the short-scale wave spectrum along the underlying large wave field. It is a function of two variables: the wavenumber, K_x, of the large-scale surface and its counterpart, k_x, for the short ripples. The dependencies on the two parameters are examined in Fig. 3. The results testify that the HMTF values for the Creamer model are substantially larger than those for its choppy wave counterpart. Per the MTF-based Doppler theory, these larger values would indeed translate into higher Doppler shifts, as observed in Fig. 1a for the Creamer results. This study therefore directly measured essential characteristics of the two surface models while providing an explanation to the discrepancies in the Doppler moments that have been confounding the researchers. The investigation also flags the more heuristic choppy wave model as clearly deficient in describing ripple modulations.

Defense Impact/Significance: The efforts under this project contribute to improving the Navy's ability to assess and predict fleet sensor performance through the development and integration of advanced model physics.

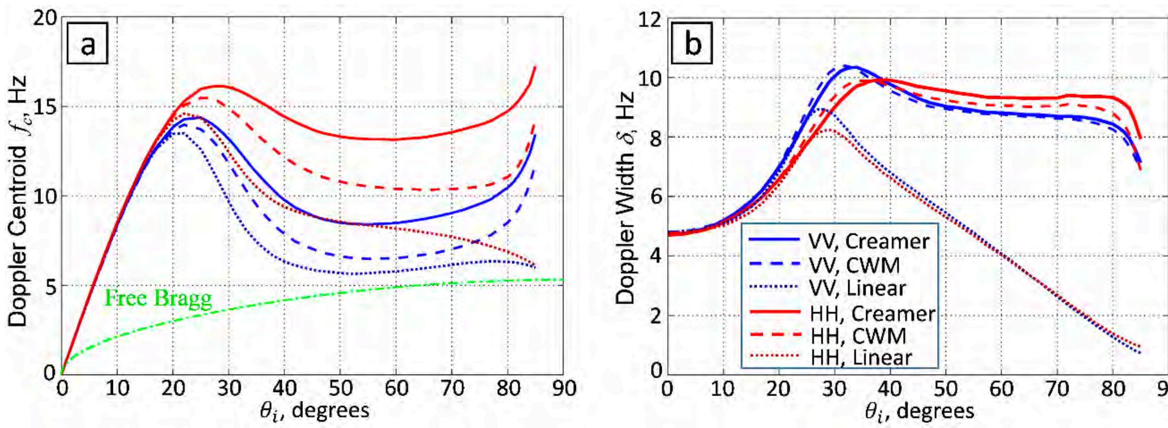

Figure 1. (a) First and (b) second moments of the sea backscatter Doppler spectrum simulated with different models for surface harmonic interactions (electromagnetic wavelength is 12 cm and wind speed is 7 m/s.)

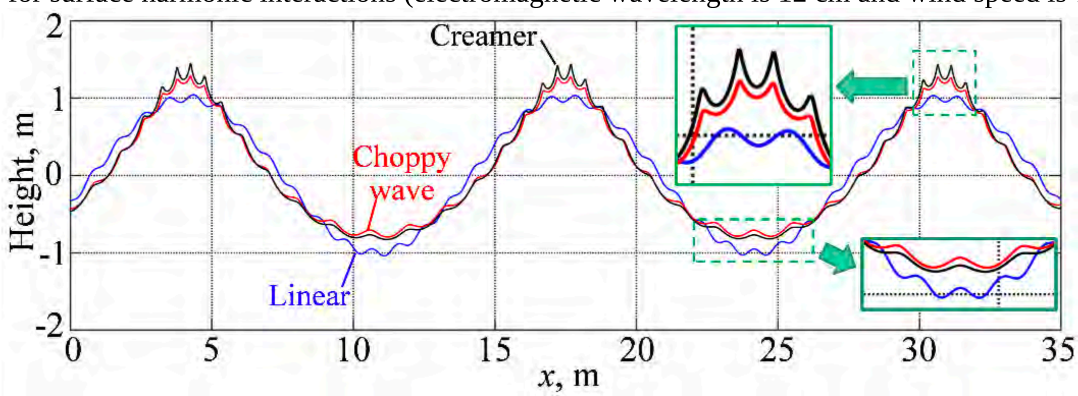

Figure 2. Sample profiles resulting from applying the nonlinear transformations to the prototype two-harmonic sinusoidal surface (labeled as "linear"). The Creamer formulation apparently produces greater enhancement of ripples at the crests of the large wave, indicating stronger hydrodynamic modulation effects inherent to the model.

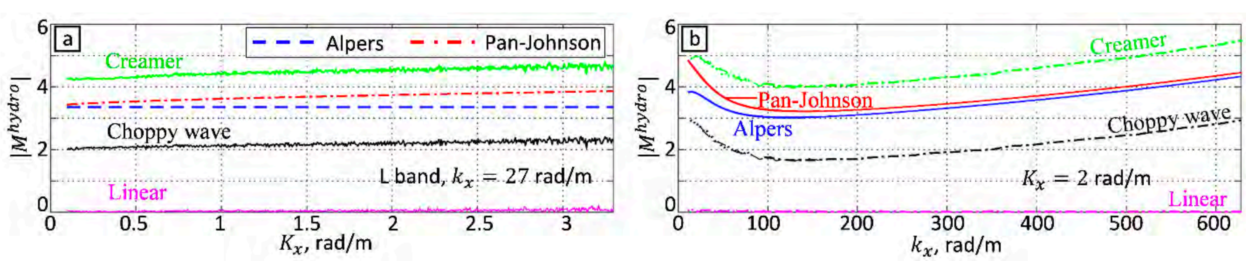

Figure 3. Hydrodynamic modulation transfer functions (HMTFs) for the surface models evaluated through a numerical experiment using Monte Carlo simulations (solid lines). The panels (a) and (b) highlight dependencies on the large-scale and short-scale wavenumbers, respectively, with the other argument fixed. Theoretical curves (named after researchers who proposed the corresponding formulas) are provided for reference as dashed and dash-dotted lines. The HMTF for noninteracting "linear" surface is near zero, as expected.

Title: Interactive Scenario Builder
Author(s): B.W. Dowd,[1] Z. Liebowitz,[1] and D. Richie[2]
Affiliation(s): [1]U.S. Naval Research Laboratory, Washington, DC; [2]Brown Deer Scientific, Forest Hill, MD
CTA: CEA

Computer Resources: Penguin Open Compute Platform (OCP) [AFRL, OH]; Penguin TrueHPC [NAVY, MS]

Research Objectives: The overall technical objective is to enable NRL's Interactive Scenario Builder (Builder) — a three-dimensional, interactive radio frequency (RF) tactical decision aid (TDA) — to seamlessly execute on HPC resources. As a mission planning tool, Builder aids warfighters in the tactical decision-making process by providing insight into and visualization of the RF capabilities of platforms in addition to providing geospatial and temporal situational awareness (SA). Builder models communication and radar systems by calculating one- and two-way RF propagation loss. Computations incorporate complex antenna and radar cross section (RCS) pattern data as well as the effects of meteorology, terrain, and countermeasures. Builder enhances the warfighter's geospatial SA by visualizing NGA map products, including CADRG and CIB imagery and DTED elevation data. Builder can be used for premission planning, near-real-time SA, and after-action debriefing.

Methodology: A preponderance of workloads executed by the Builder software are embarrassingly parallel and can be distributed across an HPC system for significant performance gains. The back end employs a conventional synchronous data parallel MPI model using a rank-0 manager process and (N-1) worker processes to perform computationally intensive calculations. The work queue manager receives work through callbacks and schedules the work across MPI processes in a round-robin distribution. Each worker process picks up the work, performs calculations, and returns the results to the queue. The results are requested by follow-up callbacks to the manager, which then returns the completed results.

Results: The primary focus in FY25 was the functionality and robustness of the work scheduler. The strong scaling and weak scaling were assessed for representative use cases of the Builder software. A typical RF propagation-loss calculation in Builder is performed along a line of bearing originating from a transmitter (site) and extending a defined range — referred to as a "propagation radial." For the scaling results shown here, there are multiple radials associated with each "site" and the computations for each radial are assigned to one CPU core at one time.

Figure 1 shows the parallel efficiency and expected performance scaling based on a weak scaling workload. The CPU core count ranged from 1,024 up to 18,432, with efficiency and scaling relative to the 1,024-core case. The parallel efficiency and expected scaling show exponential trends with no indications of nearing a hard limit on scaling. The weak-scaling case indicates that an 18-fold increase in core count is expected to yield a 7.4× performance increase. Figure 2 shows that the strong scaling case, like the weak scaling case, shows no indication of hitting a parallelization wall. The 48-site case yields an 8.8× improvement from a 16× increase in core count — going from 384 to 6,144 cores. Comparing 1,536 and 6,144 cores yields a 2.82× improvement from a 4× increase in core count. This supports the assertion that typical RF propagation loss calculations qualify as an embarrassingly parallel workload. While appreciable scaling has been demonstrated, significant scheduler improvements remain on the table and will be pursued in future work.

Defense Impact/Significance: MPI-capable Builder leverages HPC resources to deliver previously untenably large RF data sets, exponentially larger-scale electromagnetic products, and expanded capabilities for users across the defense community.

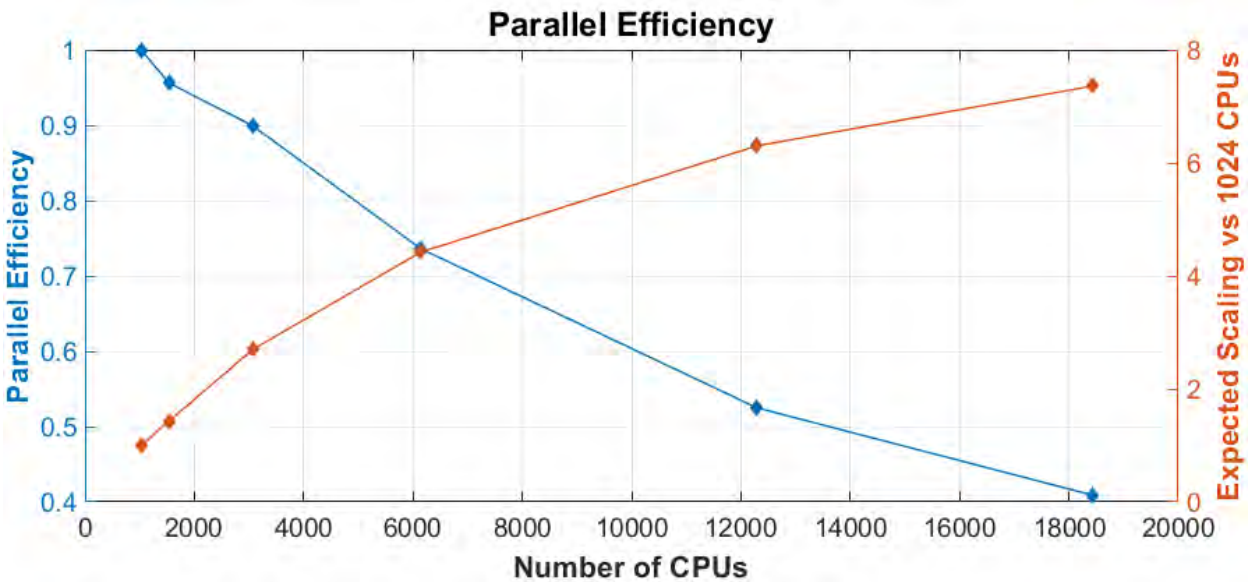

Figure 1. Parallel efficiency (blue) and the expected strong scaling performance (orange) for increasing CPU core count relative to 1,024 cores.

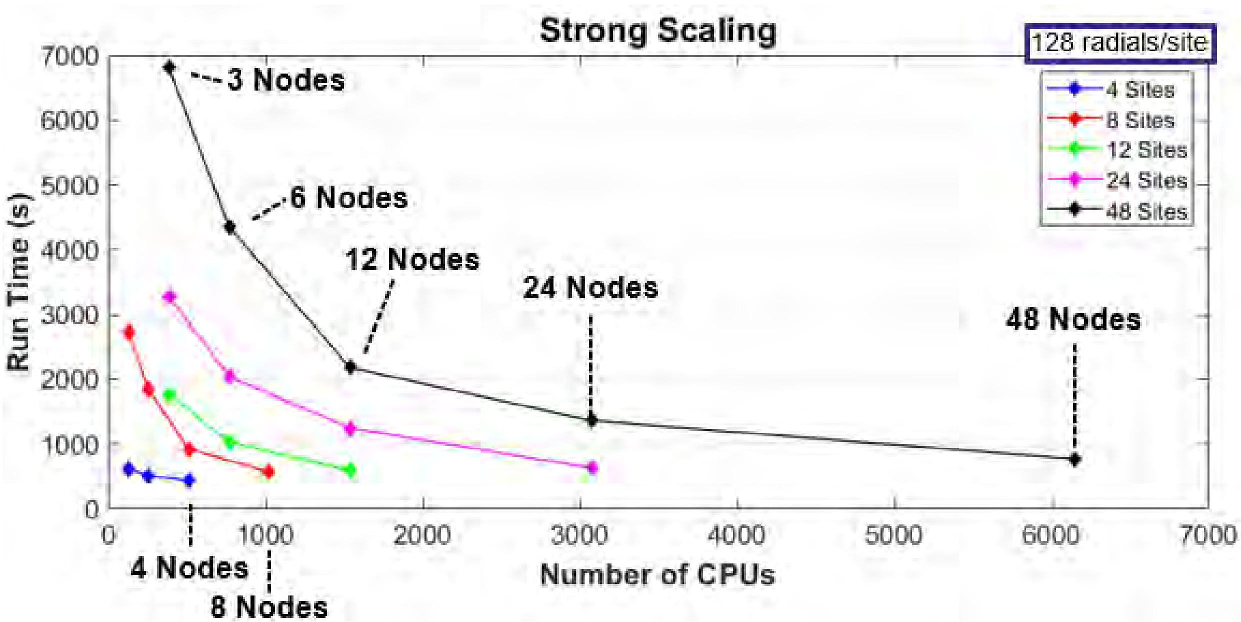

Figure 2. Strong scaling performance on up to 6,144 cores for several test scenarios, each with varied numbers of transmitter sites (4, 8, 12, 24, and 48 sites). Each site consists of 128 radials, each of which runs on one core at a time.

Title: Infrared Scattering by Micro-particles
Author(s): R. Furstenberg and A.R. Shabaev
Affiliation(s): U.S. Naval Research Laboratory, Washington, DC
CTA: CEA

Computer Resources: HPE Cray EX [AFRL, OH], [NAVY, MS]; HPE Cray EX 4000 [ERDC, MS]

Research Objectives: The objective of this research is to provide insights into spectral features of microparticles, especially those with irregular shapes (i.e., nonspherical), commonly found in solid aerosols and surface contaminants. As the sizes and shapes of these particles vary, the observed signatures differ from their bulk values. This change is most pronounced in the Mie regime, where the wavelength of light is comparable to the size of the particles. Mie theory provides exact solutions for perfect spheres, but those results cannot be widely applied to irregularly shaped particles, often found in solid aerosols and other trace contamination on surfaces. Accurate description of infrared scattering spectra is of importance for the development of detection instrumentation and in other fields, such as atmospheric research. The main goal of this research is to develop a predictive tool for spectral signatures of liquid and solid aerosols as a function of size and shape.

Methodology: Our approach to modeling irregularly shaped particles will involve using established electromagnetic codes that are suitable for solving the scattered electromagnetic field. In addition, we have developed a code that generates random particles. For these particles, we calculate the angle-dependent scattering cross sections for a range of optical constants (n and k). Each particle is characterized by the three-dimensional (3D) shape parameters (aspect ratios, convexity, sphericity, etc.). Large datasets are analyzed statistically to ascertain which shape parameters influence the scattering cross sections the most. These parameters can be used to construct a multidimensional lookup table, or a trained neural network will be constructed to rapidly predict the scattering response (with confidence bands) of an arbitrary ensemble of microparticles. This analysis provides the basis for predictive models.

Results: The modeling of scattering response provides foundation for the analysis of a small number of shape parameters that are responsible for the majority of the observed scattering cross section. This characterization is needed to limit the required dimensionality of the lookup table and, therefore, to allow for the formulation of a reasonably accurate predictive model that can be used both by detection instruments (in the field) or for research purposes (in the lab) in various scientific fields, such as atmospheric and environmental science, and for detection of hazardous materials. In FY25, we developed scripts to numerically calculate the scattering efficiencies (and other related properties) of random particles. Figure 1(a) shows a particle of random shape and size generated by drawing a convex hull around random points and (b) its equivalent volume sphere. To validate the numerical methods, in Fig. 1(c)we compare the Mie theory (gray line) to the scattering efficiency numerically calculated for three spectral bands (blue, red, and green lines). Finally, in Fig. 1(d), we show the difference in the scattering efficiency of the random particle (blue, red, and green lines) and the sphere with equivalent volume (gray line).

Defense Impact/Significance: Better understanding of spectral signatures from microparticles is of great interest to the defense community in general and to the Navy in particular. Protecting the warfighter in contested and hazardous environments as well as the homeland from attacks by monitoring the environment is greatly enhanced from higher sensitivity and low false-alarm rates possible when the exact spectral signatures of the hazardous materials are known. An immediate use of our predictive model will be to support relevant defense agencies that are tasked with mitigation and detection of hazardous aerosols (both liquid and solid) as well as trace contaminants on surfaces. Our predictive models will be used to train the algorithms — particularly in the early stages of the program, when sufficient data is not yet available — and later, to supplement experimental results with synthetic data.

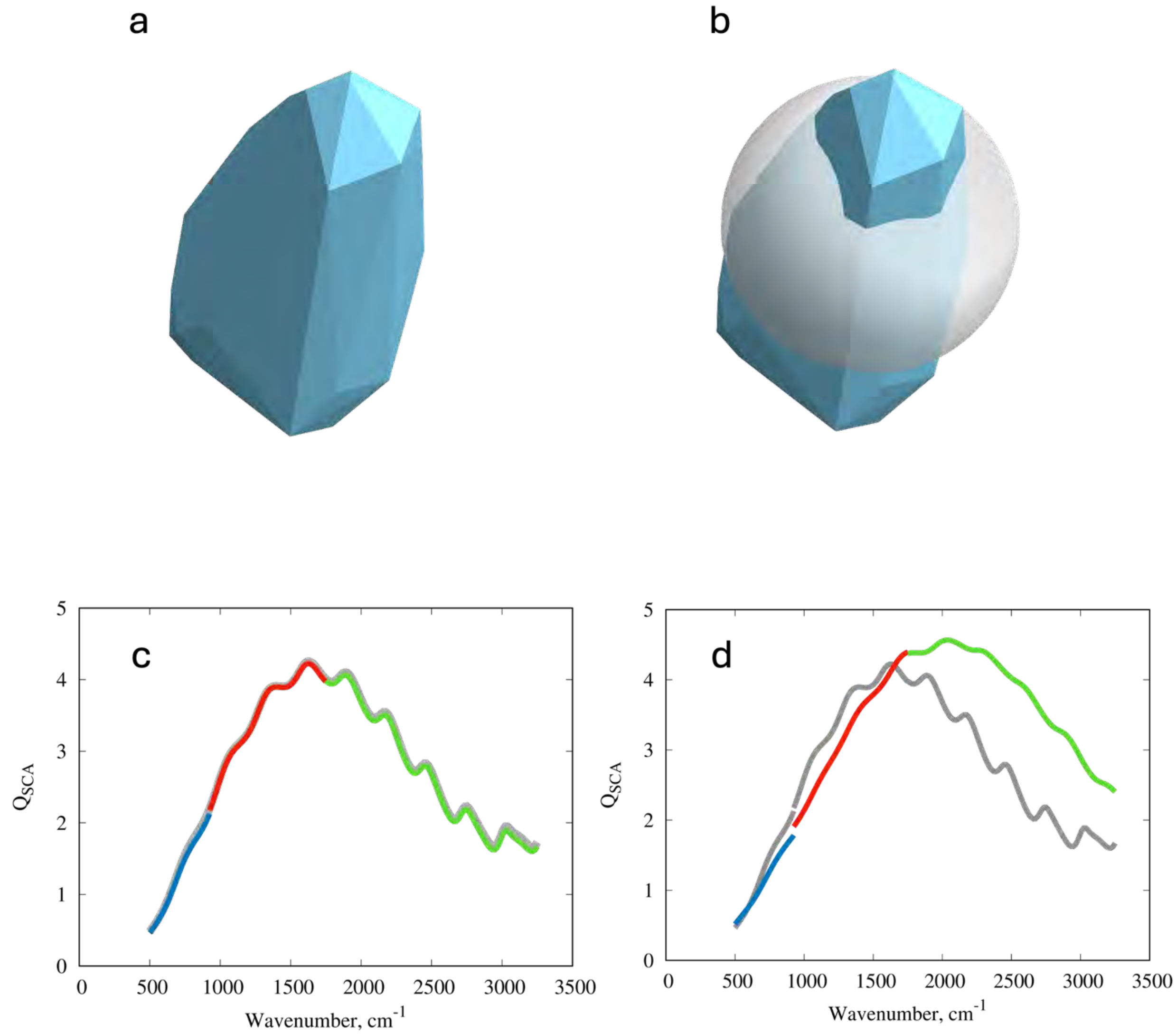

Figure 1. (a) Random-shape and -size particle generated by drawing a convex hull around random points. (b) Random particle and its equivalent volume sphere. (c) Scattering efficiency of the equivalent sphere numerically calculated for three bands (blue, red, and green lines) and evaluated using Mie theory (gray line). (d) Scattering efficiency of the random particle (blue, red, and green lines) and its equivalent sphere (gray line).

Title: Acoustic Parameter Variability over an Ocean Reanalysis (AVORA)
Author(s): B.A. Melzer and J. Fabre
Affiliation(s): U.S. Naval Research Laboratory, Stennis Space Center, MS
CTA: CEA

Computer Resources: HPE Cray EX, Penguin HPCTrue [NAVY, MS]

Research Objectives: Translating ocean fields to acoustically significant parameters is important in the development of products to support Navy operations. Likewise, the advancement of geophysical products to characterize the environment along the seafloor requires extensive data processing and testing. The objectives of this effort are to analyze these environments and to develop tools and prototypes to increase the capabilities of acoustic modeling in the ocean and seabed environments. Focus has been placed on data assimilation and identifying acoustically sensitive environments in which to direct sampling platforms (e.g., floats, gliders) in the ocean.

Methodology: We developed techniques to identify acoustically sensitive environments from ocean reanalyses and global seabed models that can inform a user of the optimal acoustic simulations to compute for real-world applications and scenarios. We investigated differences in acoustic simulations initialized with various model configurations and observational datasets. Specifically, many HPC hours were spent spinning up a regional ocean model from its initial conditions to get to a steady state. Synthetic observations were pulled from this model to simulate the impact of their assimilation on acoustic propagation loss in the area. In addition, decades of ocean reanalysis files have been pulled from the archives to aid in the development of products that quantify the variability of acoustic properties on different time scales across multiple regions and areas of interest within each region. Acoustically significant feature extraction was explored.

Results: We moved subsets of global HYCOM reanalysis output to local machines through the transfer queue for use in several projects, including model evaluation, data assimilation, and acoustic parameter characterization. Using these HYCOM subsets, we analyzed the spatial/temporal scales on which HYCOM sound speed profiles change over multiple geographic study areas. We ran acoustic simulations with both forecast and assimilated ocean model outputs, where the assimilated fields employed targeted observational profiles based on an acoustic sensitivity field. Certain features can have large impacts on acoustic sensitivity, such as secondary sound channels, which create a direct pathway for sound through the ocean between a source and a receiver for distances as far as tens or hundreds of kilometers. Figure 1 shows profiles of such secondary sound channels, visible as local sound speed minimums in the water column. The presence, absence, or positions of these channels can be incorrect in model forecasts (Fig. 1), indicating the need for supplemental observations in order to correct the model toward the true state of the ocean for exploitation in acoustic undersea warfare applications.

Defense Impact/Significance: "In Joint Vision 2020, the Department of Defense's strategic plan to ensure battlespace dominance in the 21st century, a key element is information superiority enabled by emerging technologies ..." "An important aspect of information superiority is situational awareness. This implies knowing where you are, where allied and coalition forces are and where enemy forces are. It means understanding the environment, from the sea floor to the top of the atmosphere." [Heart of ForceNet: Sensor Grid, Advanced Command and Control by RADM Steven J. Tomaszeski]. Our efforts directly inform environmental variability as it applies to acoustics.

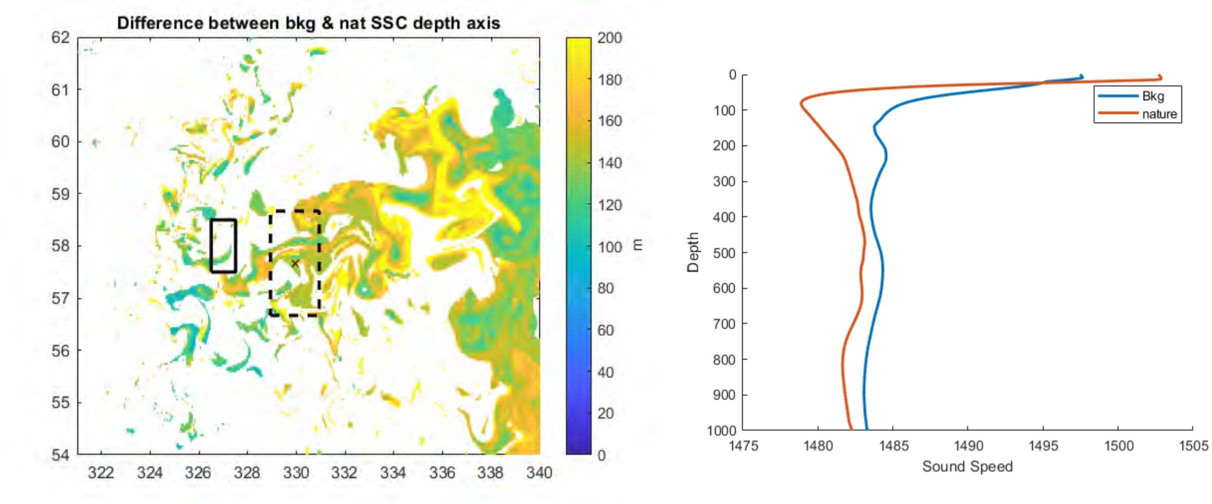

Figure 1. (left) Magnitude of the difference in sound speed channel depth when comparing the truth (nature) to the forecast (Bkg) fields. The X at location 329.932E, 57.668N in the northeast Atlantic Ocean. This marks the location of the profiles in the right plot. (right) Sound speed profiles of the nature and background field at location X, truncated to 1000 m.

Title: Simulation of Passively Mode-locked and Frequency Modulated Interband Cascade Laser Frequency Combs
Author(s): M. Povolotskyi,[1] I. Vurgaftman,[2] and J.R. Meyer[2]
Affiliation(s): [1]Amentum, Hanover MD; [2]U.S. Naval Research Laboratory, Washington DC
CTA: CEA

Computer Resources: HPE Cray EX [AFRL, OH]

Research Objectives: 1) Use the HPC cluster to extend the numerical modeling software for interband cascade laser (ICL) frequency combs to take into account electron and hole injectors. 2) Explain the absence of AM combs in conventional ICL designs. 3) Propose a new ICL design for AM combs.

Methodology: Light propagation inside the cavity is modeled in the slowly varying-envelope approximation with a single-transverse-mode cavity being considered. The group velocity dispersion (GVD) of the mode without the active layer effect as well as the band structure of active well and the electron/hole injector are obtained using external simulators. A stable algorithm based on the Fast Fourier Transform for the pulse-propagation simulation allows us to treat the GVD effects up to an arbitrary order.

The active-layer effect is included in the light propagation equation via a dipole polarization term. The polarization is computed by solving the semiconductor Bloch equations for the coupled electric-field/electron/hole system. The major difference between interband and intraband systems is that in the interband system, the transition energy depends on the electron wave vector. Therefore, the laser's performance depends on the distribution of electrons and holes over the Brillouin zone. Modeling a nonequilibrium electron gas distribution over energy is a challenging task. In this research, it is assumed that the electron and hole relaxation times are constant, so the electrons and holes gradually thermalize to the local Fermi distributions. It was found that the ICL performance strongly depends on the ability of electron and hole injectors to accumulate carriers. The injector model has been improved to consider an energy-dependent density of states, computed by an external $k \cdot p$ band structure solver. The transfer of electrons between the injector and the active well is modeled assuming elastic scattering with an energy-independent scattering time. The injector is doped by donors to improve the ICL performance. The process of dopant ionization and recombination is modeled using the mass action law.

Results: Two ICL designs have been studied. First, the simulations predict that the conventional design [1] ICL cannot produce AM combs mostly because of the slow recovery of the saturable absorber (Fig. 1). The effective recovery time exceeds the round-trip time because holes are transferred to the injector well from the active well. Since electrons and holes are spatially separated, they cannot effectively recombine even if recombination centers are present. Second, it was found that by modifying the band structure, it is possible to make the process of hole accumulation in the injector less favorable. A new design has been suggested for which AM combs have been predicted, provided the electron injector doping lies within an optimal range (Fig. 2).

Use of the HPC resources is critical for this work because the ICL typically needs to be simulated for 200 ns operation time until the AM comb stabilizes. A single simulation requires 2 hours of wall time on 128 CPU cores.

Defense Impact/Significance: AM combs in type-II ICLs have not yet been realized experimentally. The simulations reveal that in the conventional design, the SA is not restored during the round-trip time because of the hole accumulation in the injector, which prevents AM comb phase locking. Simulations of the modified design with an optimized band structure predict the generation of AM combs. The proposed design is being fabricated for characterization.

References

[1] I. Vurgaftman, W. W. Bewley, C. L. Canedy, C. S. Kim, M. Kim, C. D. Merritt, J. Abell, J. R. Lindle, and J. R. Meyer, “Rebalancing of internally generated carriers for mid-infrared interband cascade lasers with very low power consumption,” Nat. Commun., vol. 2, Article no. 1595, 2011. doi: 10.1038/ncomms1595.

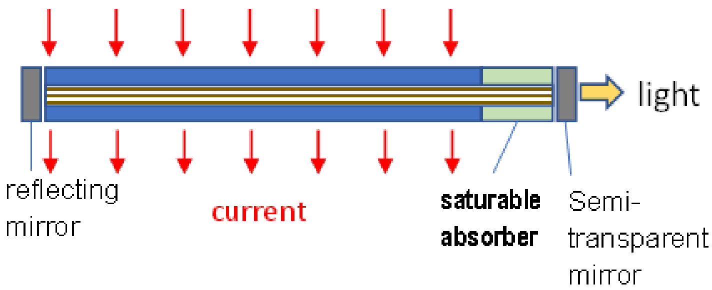

Figure 1. Schematic layout of the ICL structure with a saturable absorber and two different mirrors: fully reflecting and semitransparent (cleaved facet).

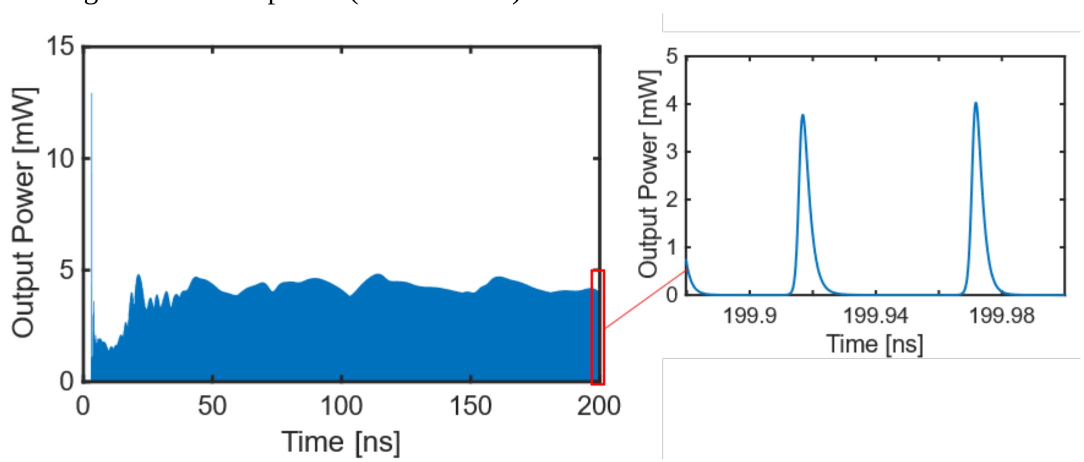

Figure 2. Power output computed for the conventional ICL structure. The output consists of individual pulses, but the amplitude is not stable.

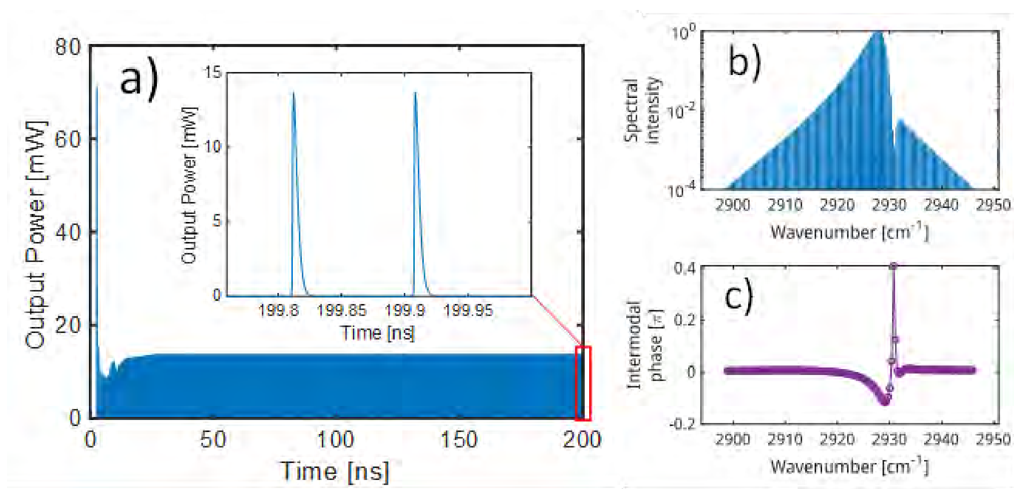

Figure 3. ICL output computed for the proposed ICL structure in the AM comb regime. a) Output power consists of pulses of the same amplitude and shape. b) Spectral intensity of the output field. c) Intermodal phase difference of the output field.

Title: Three-Dimensional Acousto-Elastic Modeling
Author(s): S. Dey and D. Raudales
Affiliation(s): U.S. Naval Research Laboratory, Washington, DC
CTA: CEA

Computer Resources: HPE Cray EX, Penguin HPCTrue [NAVY, MS]

Research Objectives: Generate high-fidelity structural acoustic response ensemble for canonical problems to verify and improve accuracy of fast-running reduced-order models (ROM) for structural-defect detection.

Methodology: We utilized a high-order hp-finite and infinite element-based solver (STARS3D) developed at NRL for solving the coupled elastoacoustics problem [1]. This enables high-accuracy solution of the scattering response up to the mid-frequency regime. The use of high-order heirarchic basis combined with infinite elements that automatically satisfy the farfield radiation condition and the perfectly matched-layer approximations ensure accurate first-principles-based solution of the acoustic field near the elastic structure and far away from it.

The high-fidelity solutions are used for verification of the solution obtained by fast-running reduced-order models utilizing facet-based coherent sum of Helmholtz-Kirchoff approximations. The verified reduced-order model is used in the design and optimization of structural-acoustics-based scanners to detect structural defects in fluid-loaded elastic structures.

Results: Figures 1(a) and (b) depict the canonical domain used in the study and a representative mesh of the domain generated using the Capstone meshing and geometry platform [2], respectively. Figure 2 shows the time-dependent pressure field obtained using an inverse Fourier transform of a wideband frequency-domain response. One can see the excellent performance of the reduced-order model with significantly less computational cost compared to a first-principles-based model. This enables rapid evaluation and optimization of various operational and design scenarios.

Defense Impact/Significance: Fast-running and sufficiently accurate digital surrogates for structural acoustics provide timely data for use in the design, operation and maintenance of complex undersea systems.

References

[1] S. Dey and D. K. Datta, “A parallel hp-FEM infrastructure for three-dimensional structural acoustics,” Int. J. Numer. Meth. Eng., vol. 68, no. 6, pp. 583–603, 2006.
[2] S. Dey, R. M. Aubry, B. K. Karamete, and E. L. Mestreau, “Capstone: A Geometry-Centric Platform to Enable Physics-Based Simulation and System Design,” *Computing in Science & Engineering*, vol. 18, no. 1, pp. 32–39, Jan./Feb. 2016, doi: 10.1109/MCSE.2015.108.

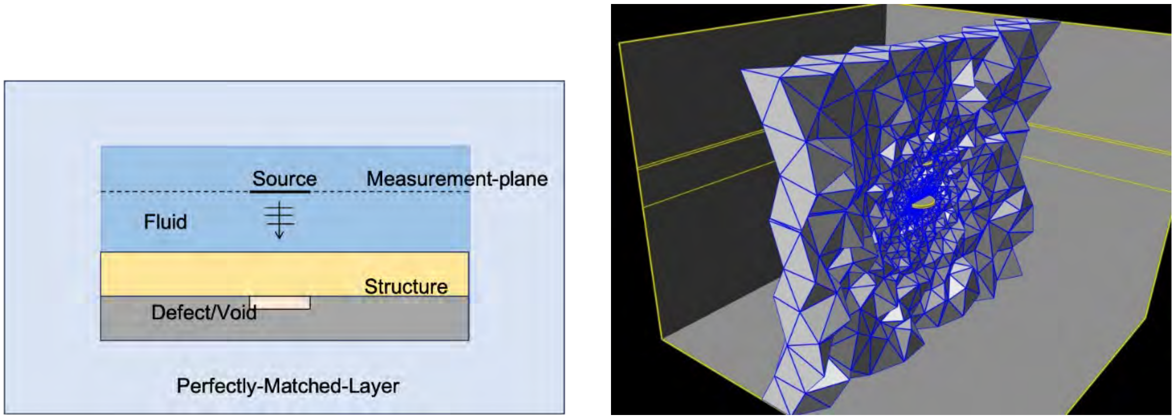

(a) (b)

Figure 1. (a) Canonical computational model for defect detection and (b) slice through volume mesh.

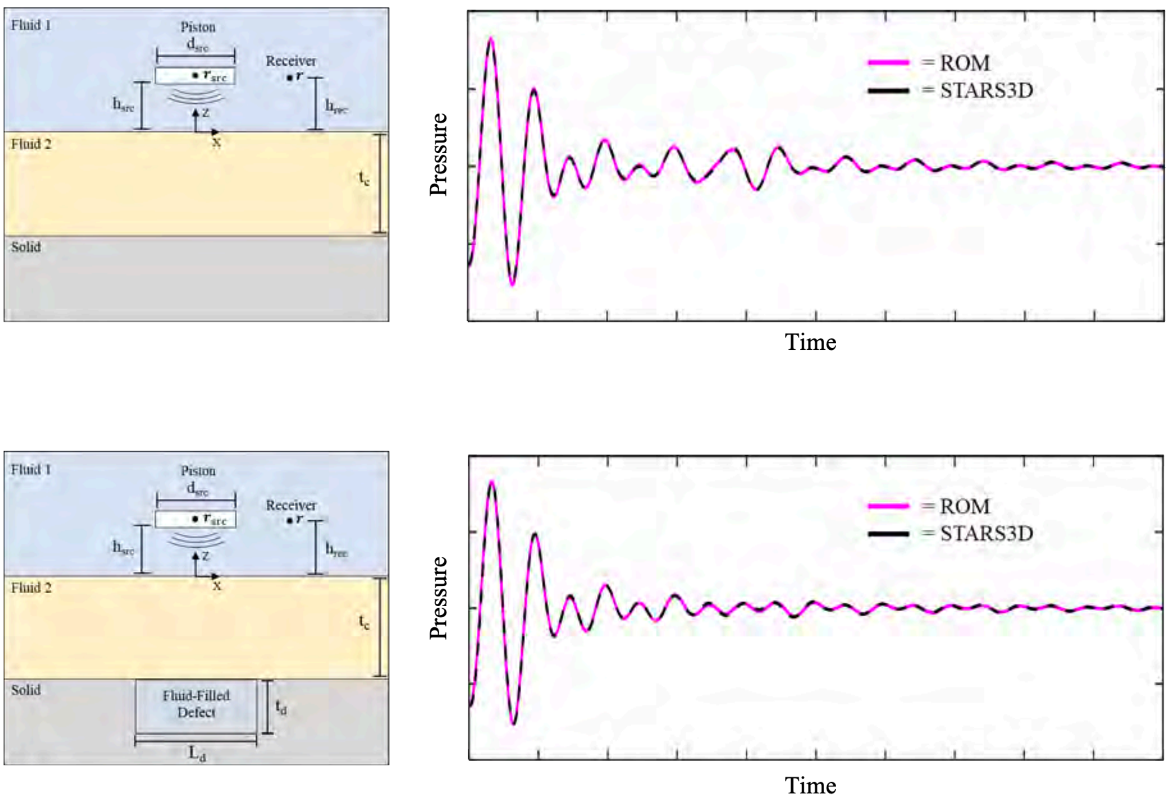

Figure 2. Verification of the reduced-order model (ROM) against first-principles-based (STARS3D) results for configurations with and without a fluid-filled defect.

Title: Advanced Modeling of Anode Plasma Dynamics
Author(s): I.M. Rittersdorf and A.R. Vazsonyi
Affiliation(s): U.S. Naval Research Laboratory, Washington, DC
CTA: CEA

Computer Resources: Penguin Open Compute Platform (OCP) [AFRL, OH]; Penguin TrueHPC [NAVY, MS]

Research Objectives: A high-power electron or ion beam can be used to simulate the effects of nuclear weapons. However, there is evidence that the ion beams generated from high-power diodes are nonuniform, making their use as surrogates for the effects of warm and cold x-rays from a nuclear weapon less attractive. The purpose of this project is to examine the role that electrode plasmas might play in the overall quality of electron and ion beams generated by a pulsed-power-driven electron/ion beam diode. For example, instabilities in the electrode plasma might influence the uniformity of the charged particle beams that can be extracted from high-power diodes. Furthermore, this project will address whether there exist techniques to mitigate such nonuniformities and to produce higher-quality nuclear weapon effect surrogates.

Methodology: The thermal-resistive instability in electrode plasmas can cause the electron beam to break up into filaments as it leaves the cathode. A filamented electron beam born at the cathode would be accelerated across the anode-cathode gap and would deposit its energy nonuniformly on the anode, ultimately producing a spotty, nonuniform ion beam. Furthermore, the more recent theory of the electrothermal instability was assessed to determine its relevance to high-power diode electrode plasmas. Armed with this understanding, particle-in-cell simulations were set up to simulate pulsed-power diodes with electrode plasmas, applying modern computing methods and cross-section data.

Results: Plasma dynamics have been included in particle-in-cell simulations of high-power diodes using the Chicago code. The focus has been on including an anode plasma in simulations of rod pinch diodes, which are used as flash x-ray sources. This modeling effort involves including neutral contaminant desorption off the rod/anode, which is subsequently ionized to form a surface plasma. These simulations are significantly more computationally expensive than diode simulations without the plasma due to more stringent grid size requirements and increased particle counts necessary to resolve the plasma. Available high-performance computing resources make the simulations tractable, although we have found they take on the order of days to weeks when running on hundreds of processors.

Initial results from inclusion of the anode plasma in PIC simulations are promising. Diode impedance collapse has been observed, an effect previously only seen in experiments, that is due to the plasma expansion that closes the A-K gap. Furthermore, observations of plasma forming a filamentary structure as it expands have been made, attributable to some form of instability. It is yet unclear what instability is the culprit of this behavior. Previous simulations have shown that the cathode plasma can expand much more rapidly due to anomalous diffusion caused by an instability that results from the strong coupling of a transverse magnetic mode in the electron sheath with the expanding resistive plasma layer. In the coming year, the physics intuition gained from this work will be applied to simulations of a vacuum rod pinch field on NRL’s Mercury pulsed-power generator and the results will be compared to experimental evidence.

Defense Impact/Significance: This model represents a first step toward predictive modeling capabilities of advanced radiation sources. Such a tool allows for the design and refinement of such radiation sources, which are critical technologies for nuclear weapons effects testing, which contributes to hardening and survivability of Navy assets in the nuclear threat environment.

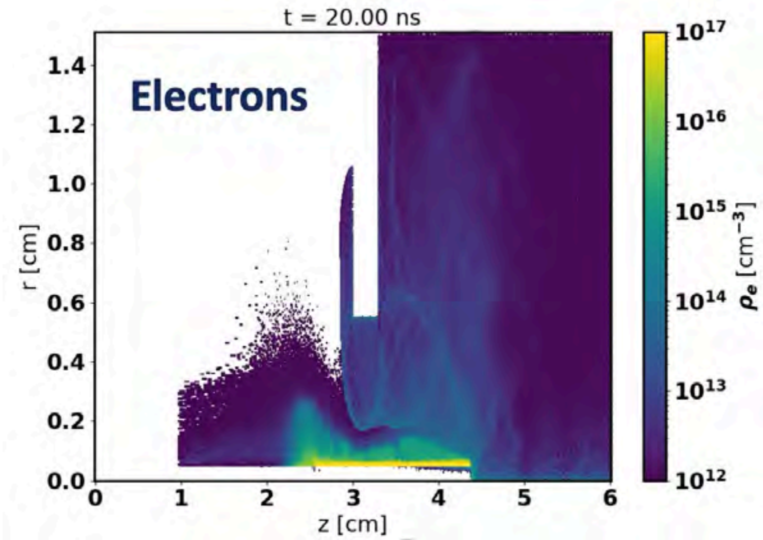

Figure 1. Three-dimensional geometries of the vacuum diode (left) and gas cell (right) used in the particle-in-cell simulations. In the diode, the blue is the cathode boundary and red is the anode boundary driven with an idealized pulse. In the gas cell, the beam is injected into the beam region and current is monitored at various points in the region.

Title: Empire PIC Simulations of an Intense Electron Beam in N_2

Author(s): N.D. Isner,[3] E.R. Kaiser,[1] S.L. Jackson,[1] S.B. Swanekamp,[4] C.H. Moore,[2] and K.L. Cartwright[2]
Affiliation(s): [1]U.S. Naval Research Laboratory, Washington, DC; [2]Sandia National Laboratories, Albuquerque, NM; [3]Commonwealth Technology, Inc., Alexandria, VA; [4]Syntek Technologies, Inc., Fairfax, VA
CTA: CEA

Computer Resources: HPE Cray EX, Penguin HPCTrue [NAVY, MS]

Research Objectives: Intense electron beams are effective in generating nonequilibrium plasmas in low- and high-pressure environments. These plasmas have complex kinetic and chemical processes that warrant the need for improved models and are of particular importance when studying radiation sources and effects. The primary objectives of this research are to develop and improve capability to perform particle-in-cell (PIC) simulations of the electron beam plasma system, to study the macroscopic quantities of interest, and to track various plasma component (dissociation, charge state, electronic state, vibrational state, and rotational state) populations.

Methodology: PIC simulations are preformed to model NRL's Febetron experiment, a small, pulsed-power device that injects an electron beam into a low-pressure gas cell. Figure 1 shows 3D models of the vacuum diode, the vacuum region, and the gas cell all coupled that are developed and used in EMPIRE simulations. Figure 2 shows the idealized pulse used for the simulations. These parameters are all critically dependent on the electron-beam current density and the gas pressure and are inputs that we will vary in the next simulation study. A coarse grid was used to achieve fast results, and we are improving the grid resolution as a next step.

Results: We analyzed key plasma quantities such as the electric field, the current-enclosed contours ($2\pi r B_\theta/\mu_0$), and the density populations. Results are shown at the peak of the pulse, t = 50 ns. Figure 3 shows the linear electric field and the current-enclosed contour at 50 ns. A large induced electric field is shown accelerating into the gas cell and the highest amount of current is shown on the return current rod while some current cancellation occurs in the beam region. In Figs. 4 and 5, the key density populations are compared for total electrons, total ions, beam electrons, and plasma electrons. The total electron and ion densities have similar distributions and magnitudes, while the plasma electrons surpass the beam electrons in density. Additionally, the plasma electrons oppose the charge of the beam electrons, creating the magnetic null that is seen in the beam region of the current enclosed contour.

Defense Impact/Significance: The simulations performed show improved 3D modeling capability and improved physics development with the quantities of interest. This model will be further improved through direct comparison with NRL's experiments and will help guide future developments of electromagnetic interactions of low-temperature plasma models. The objective of these validation experiments is to have predictive capability to improve the hardening design of military systems in extreme environments.

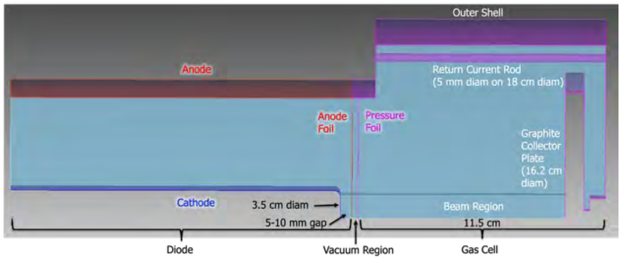

Figure 1. Three-dimensional geometries of the vacuum diode (left) and gas cell (right) used in the particle-in-cell simulations. In the diode, the blue is the cathode boundary and red is the anode boundary driven with an idealized pulse. In the gas cell, the beam is injected into the beam region and current is monitored at various points in the region.

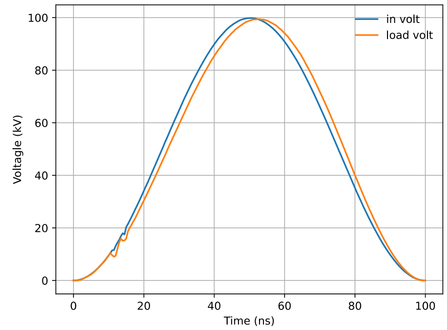

Figure 2. Simplified voltage trace that is input and measured by probes in the simulation. The probes are set at two measurement points: at the start of the transmission line (inlet) and at the A-K gap (load).

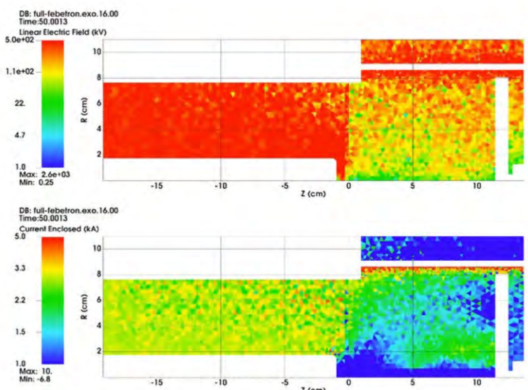

Figure 3. Shows the linear electric field (above) and the current-enclosed contours (below) in the diode and the gas cell at the peak of the pulse t = 50 ns. The diodes' increased electric field strength causes cathode emission. The highest magnitude of current is shown on the return current rod, and current cancellation is shown in the beam region of the current-enclosed contour.

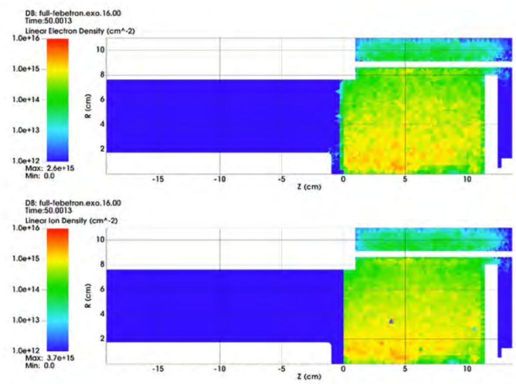

Figure 4. The electron density (above) and the ion density (below). At the peak of the pulse, t = 50 ns, the electron and ion densities are comparable and are reaching a higher value than what is seen in the experiment.

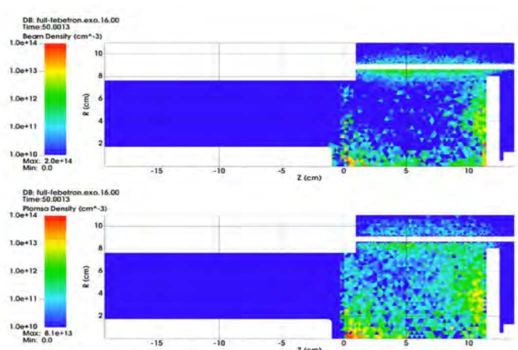

Figure 5. The beam electrons (above) the plasma electrons (below). The beam electrons have traversed the gas cell at t = 50 ns and have started to generate the plasma electrons. At 50 ns, the plasma's electron density has surpassed the beam's electron density and has started to fill the gas cell. A large buildup of density occurs on the collector plate.

THIS PAGE INTENTIONALLY LEFT BLANK

CWO

Climate/Weather/ Ocean Modeling

The Climate/Weather/Ocean Modeling and Simulation (CWO) CTA focuses on high-fidelity numerical simulation of the Earth's atmosphere and oceans across the spatial and temporal scales critical to both scientific understanding and defense operations. The field encompasses simulation and prediction of atmospheric variability — including temperature, winds, pressure, humidity, cloud processes, precipitation, storms, aerosols, trace constituents, and surface fluxes — as well as oceanic variability, such as temperature, salinity, currents, tides, waves, sea ice dynamics, sediment transport, and optical properties. These capabilities span the full coupled system, from the upper atmosphere to the deep ocean, and rely on advanced numerical methods and data-assimilation techniques that integrate in situ and remotely sensed observations into operational prediction systems.

CWO supports a broad range of defense applications on daily basis, including mission planning and execution across air, land, sea, and space domains. It is essential for flight and maritime safety, search-and-rescue operations, optimal routing of aircraft and vessels, and the design and evaluation of weapon and sensor systems. By delivering real-time, high-resolution environmental forecasts, CWO enables timely, informed decision-making and enhances operational effectiveness under challenging weather and ocean conditions. In addition, realistic simulations of dynamic atmospheric and oceanic environments support mission rehearsal, training, and materiel development across the defense enterprise.

Title: COAMPS-TC® Tropical Cyclone Rapid Intensification Prediction
Author(s): J.D. Doyle
Affiliation(s): U.S. Naval Research Laboratory, Monterey, CA
CTA: CWO

Computer Resources: HPE Cray EX, Penguin TrueHPC [NAVY, MS]

Research Objectives: While the prediction of tropical cyclone (TC) tracks has improved significantly over the past few decades, intensity prediction lags behind, particularly for TCs undergoing rapid intensification (a 30 kt-or-greater wind increase in 24 hours). This disparity can be attributed to our limited ability to accurately model the physical processes governing TCs and the inherent sensitivity of forecasts to the initial conditions. The primary aim of this project is to advance and evaluate the COAMPS-TC® numerical weather prediction system, which supports Navy, defense community, and civilian operations. The COAMPS-TC® system is operational at the Fleet Numerical Meteorology and Oceanography Center (FNMOC), and our objective is to improve its predictions of TC track, intensity, and surface wind field by enhancing both its deterministic and ensemble prediction systems.

Methodology: In the past year, we have tested advanced versions of the COAMPS-TC® deterministic and ensemble systems using two main types of experiments. The first involves rapid development and prototyping. Rigorous testing for a sample of hundreds of individual cases is essential to assess system performance in a statistically significant manner. This approach is indispensable for analyzing the impact of specific advancements, such as increased resolution or improved parameterizations, and is critical for the evaluation and transition of upgrades to the operational COAMPS-TC® version at FNMOC. The second focus is the near-real-time execution of an experimental version of COAMPS-TC® that contains advanced capabilities relative to the operational system. This prototyping of the experimental system is conducted for numerous TCs across the globe. A key goal is to improve forecast confidence and to capture a wider range of possible forecast outcomes by experimenting with larger ensemble sizes.

Results: Important COAMPS-TC® advances, including a new cloud microphysics scheme, were tested over numerous TCs worldwide, leading to the transition of advanced deterministic and ensemble systems to FNMOC operations in 2024. Figure 1 compares 21- and 100-member COAMPS-TC® ensemble forecasts for Super Typhoon Mawar (1200 UTC 21 May 2023), which caused considerable damage on Guam, including to defense bases. Both ensembles capture the rapid intensification of Mawar; however, the 100-member ensemble depicts impacts on Guam more accurately. The COAMPS-TC® is a top-flight TC prediction model worldwide for track, intensity, and storm size. The new, advanced version of COAMPS-TC®, developed on the Navy DSRC's HPE Cray EX and Penguin TrueHPC, indicates even greater accuracy for improved operational tropical cyclone applications.

Defense Impact/Significance: Improving tropical cyclone forecast accuracy offers considerable cost benefits to the U.S. Navy by mitigating the substantial hazards TCs pose to missions. The latest version of the COAMPS-TC® deterministic and ensemble systems will enable new decision-making capabilities for fleet sorties and will reduce exposure to hazardous weather. Real-time testing and development on HPC DSRC platforms have resulted in major enhancements to the predictive skill of COAMPS-TC®. These advancements also facilitate a quicker transition of new capabilities into Navy operations at FNMOC. The improvements demonstrated in this project will play a crucial role in shaping the future of TC model development for the Navy, the defense community, and civilian sectors, particularly as increasing computational power enables higher-resolution forecasts, more accurate representations of physical processes, and more ensemble members.

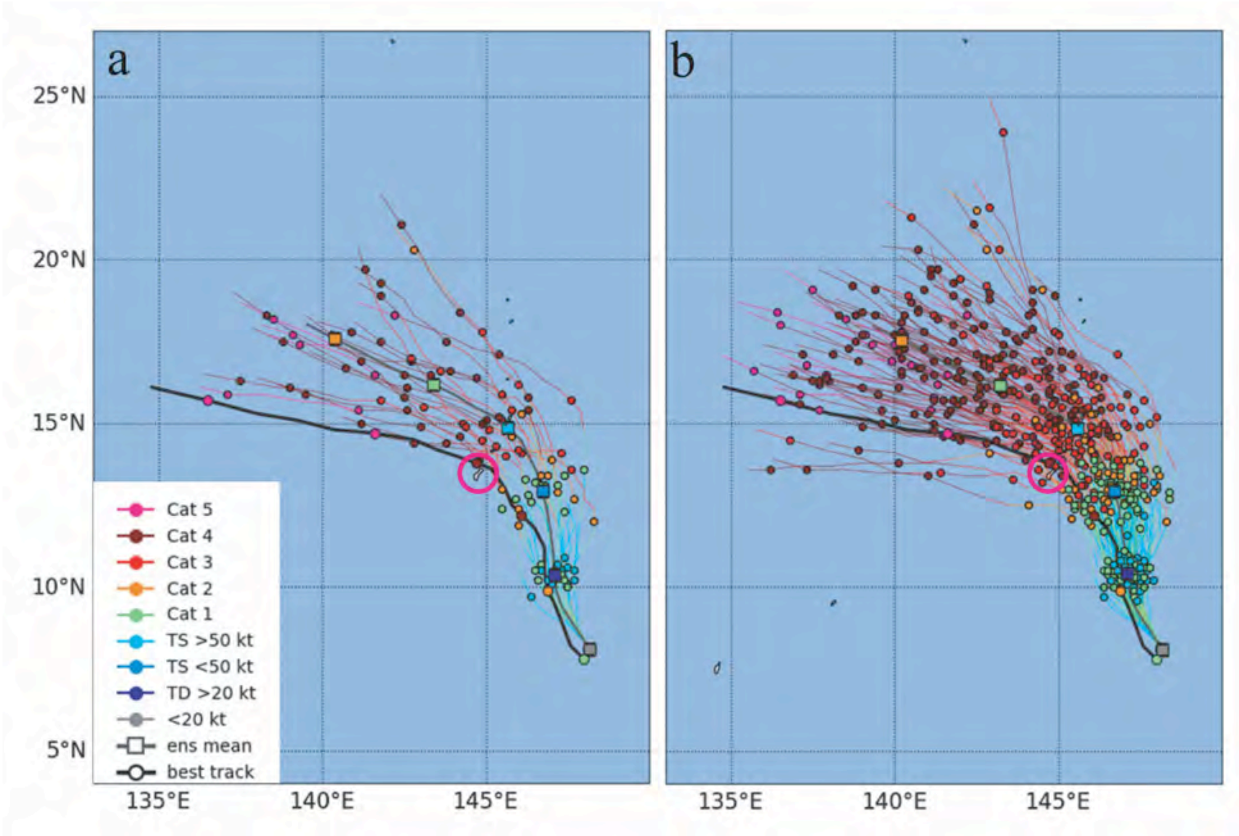

Figure 2. Track and intensity forecasts comparing NRL COAMPS-TC® ensemble forecasts with (a) 21 members and (b) 100 members for Super Typhoon Mawar initialized at 1200 UTC 21 May 2023. The forecasts show the best (observed) track (black line) and ensemble members colored by the intensity category according to the legend in the lower left of (a). The location of Guam is shown by the magenta circle.

Title: Improved Mixed Layer Depth and Upper Ocean Structures via Turbulent Mixing Advancements
Author(s): Y. Fan
Affiliation(s): U.S. Naval Research Laboratory, Stennis Space Center, MS
CTA: CWO

Computer Resources: HPE Cray EX [NAVY, MS]

Research Objective: Improve upper ocean predictions in the Navy's operational ocean models by developing a new mixing parameterization that builds on new theories and improves on the shortcomings of each.

Methodology: This project utilized extensive numerical studies using Hybrid Coordinate Ocean Model (HYCOM) and the NCAR large eddy simulation (LES) model. Two new K-Profile parameterizations with Langmuir circulation-enhanced turbulence [1,2] were implemented in HYCOM and were evaluated against the original KPP parameterization by Large et al. [3], which had been previously implemented in HYCOM, as well as against observations and LES simulations. Carefully designed numerical experiments were conducted at Ocean Station Papa (OSP) for model evaluations. Hourly meteorological (10 m wind, net surface heat flux) and oceanographic (temperature, salinity) data for the HYCOM runs are obtained for year 2011 from the moorings at OSP operated by the Ocean Climate Stations (OCS) group at Pacific Marine Environmental Laboratory of the National Oceanic and Atmospheric Administration (NOAA/PMEL) [4]. Time-varying wind stress were calculated from these data using the vectorized COARE 3.5 algorithm modified from Fairall et al. [5] by Woods Hole Oceanographic Institution (WHOI). New capability was developed in HYCOM to read in vertical profiles of global Stokes drift time series from data files. Global WAVEWATCH III is used to calculate the vertical Stokes drift profiles on the HYCOM grid. Two global HYCOM simulations were conducted using the KPP and Solano and Fan [1] mixing parameterizations, respectively, for January 2017 to look at the impact of the new parameterization.

Results: The new mixing parameterizations are implemented in HYCOM and are evaluated at OSP against observations for sea surface temperature (SST) and mixed layer depth (MLD) during the entire year of 2011 in Fig. 1. The Solano and Fan [1] is shown to significantly improve SST (Figure 1a) and MLD (Figure 1b) simulations over the original K-Profile parameterization (KPP), especially in the summer and fall months, when our new parameterization is able to capture the rapid deepening and shoaling of the mixed layer depth, closely following the observations. The mean error (ME) of modeled MLD is improved by 63%, and the root-mean-square error (RMSE) is improved by 26%. Despite the significant improvements, there is still large shallow bias during the spring period. Through the analysis of the dynamical and turbulent responses in the LES model (not shown), we found two main mechanisms missing in our mixing parameterizations that lead to the shallow biases. The first one is the penetration of fresh water due to rainfall that leads to the generation of salt fingers, and the second one is the penetration of inertial oscillation beyond the base of the mixed layer and the generated shear instability in the ocean interior. We are working to better represent these physics in our model. Li and Fox-Kemper [2] is the second parameterization we implemented in HYCOM. It improves entrainment buoyancy flux at the base of the mixed layer. Similarly to the Solano and Fan [1] parameterization, it shows good improvements during the summer and fall, and still large, shallow bias in the spring (Fig.1c and d). But this parameterization has generated large, deep bias in the wintertime (Fig. 1d). Analysis of mixing coefficients in our model and the wind-wave conditions during the winter months suggested that the mixing generated by Li and Fox-Kemper [2] is too strong and penetrated too deeply and beyond the actual depth the mixed layer (not shown). The reason is this parameterization assumes perfect alignment between the wind and the wave. Since the waves at OSP are strong and are dominated by remote swells during the wintertime, the wind-wave angle is very large and can often reach 180 degrees. By assuming perfect alignment between wind and wave, the Li and Fox-Kemper [2] parameterization significantly overestimated wave enhanced mixing during this period.

Defense Impact/Significance: This study will improve the battlespace environment forecasting accuracy for ocean models with more accurate vertical thermal profiles and better prediction of acoustic and optic properties in the upper ocean to support the Navy's search, sanitize, and avoid operations.

References

[1] M. Solano and Y. Fan, “A new K-profile parameterization for the ocean surface boundary layer under realistic forcing conditions,” *Ocean Modelling*, vol. 171, p. 101958, 2022, doi:10.1016/j.ocemod.2022.101958.

[2] Q. Li and B. Fox-Kemper, “Assessing the effects of Langmuir turbulence on the entrainment buoyancy flux in the ocean surface boundary layer,” *Journal of Physical Oceanography*, vol. 47, no. 12, pp. 2863–2886, Oct. 2017, doi:10.1175/JPO-D-17-0085.1.

[3] W. G. Large, J. C. McWilliams, and S. C. Doney, “Oceanic vertical mixing: A review and a model with a nonlocal boundary layer parameterization,” *Reviews of Geophysics*, vol. 32, no. 4, pp. 363–403, Nov. 1994, doi:10.1029/94RG01872.

[4] U. Send *et al.*, “A global boundary current circulation observing network,” in *Proceedings of OceanObs’09: Sustained Ocean Observations and Information for Society*, Venice, Italy, 2010, pp. 21–25.

[5] C. W. Fairall, E. F. Bradley, J. E. Hare, A. A. Grachev, and J. B. Edson, “Bulk parameterization of air–sea fluxes: Updates and verification for the COARE algorithm,” *Journal of Climate*, vol. 16, no. 4, pp. 571–591, Feb. 2003, doi:10.1175/1520-0442(2003)016<0571:BPOASF>2.0.CO;2.

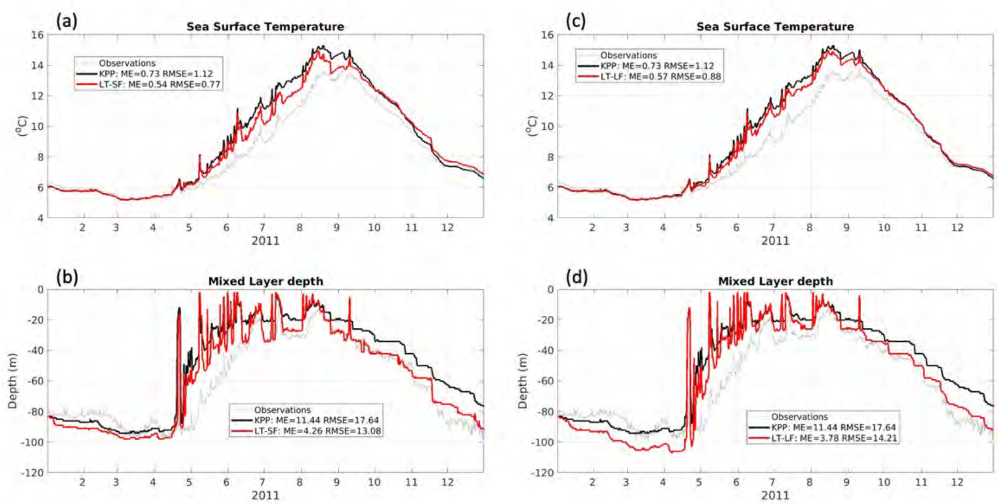

Figure 1. Comparisons of HYCOM simulations at OSP for (a)/(c) sea surface temperature and (b)/(d) mixed layer depth using the original KPP mixing scheme (black) and the new Langmuir turbulence-enhanced KPP by Solano and Fan [1] LT-SF/Li and Fox-Kemper [2] LT-LF. Observations are given by the gray lines for reference. The MLD comparison between the two global simulations has shown quite a bit of deepening of the mixed layer in the high latitude of North Atlantic using the Solano and Fan [1] parameterization, especially in the Labrador Sea region and the Denmark Strait. There are also pronounced shoaling of the summer mixed layer depth in the Southern Ocean. More in-depth analysis is underway.

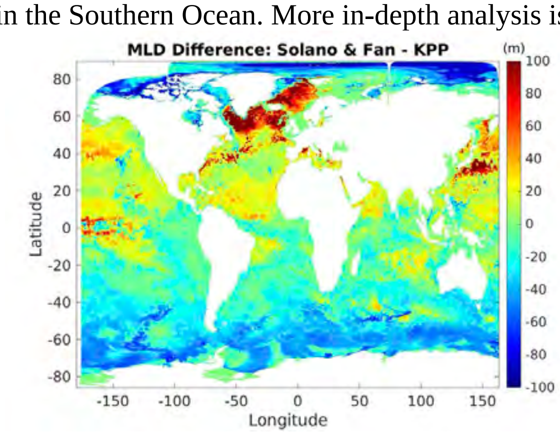

Figure 2. Mixed layer depth difference between the global HYCOM runs using the Solano and Fan [1] mixing parameterization and the original KPP scheme on January 27, 2017.

Title: Atmospheric Process Studies
Author(s): H.W. Christophersen, S.S. Rushley, and C.A. Reynolds
Affiliation(s): U.S. Naval Research Laboratory, Monterey, CA
CTA: CWO

Computer Resources: HPE Cray EX, Penguin Open Compute Platform (OCP) [AFRL, OH]; HPE Cray EX, Penguin TrueHPC [NAVY, MS]

Research Objectives: The objectives of this project are to improve the Navy's global weather-prediction capability and, from a basic research perspective, to improve our understanding of the dynamical and physical mechanisms that operate in the atmosphere, including its interactions with land and ocean. Basic research helps to inform forecast system development, so this component complements our more direct efforts to enhance Navy battlespace awareness.

Methodology: The project this year focused largely on the development, application, and validation of the NAVGEM global atmospheric forecast system, both as a stand-alone model and as a component of the coupled Navy Earth System Prediction Capability (ESPC). The work involved several key efforts:

- Model physics development: To improve the Navy ESPC v2.1 prototype, updates were made to the model's treatment of turbulence mixing, cloud physics, precipitation, and convection. Development was supported by a combination of uncoupled data-assimilation cycling runs and hindcast tests within the coupled ESPC. Additionally, a flaw in the treatment of imported sea ice albedos from CICE was identified, and a corrective fix was developed and was merged into the NAVGEM repository.
- Stochastic physics implementation: To account for model uncertainty arising from deep convection, particularly the unphysical dissipative processes associated with deep convection, a stochastic kinetic energy backscatter (SKEB) scheme was implemented in NAVGEM.
- Land-atmosphere interaction study: To understand the impact of land surface uncertainties on maritime forecasts, three 20-member ensemble experiments were run for a case of offshore flow over the U.S. East Coast during August 2020. The ensembles were configured with different initial condition perturbations: (1) atmospheric-only, (2) land-surface-only, and (3) both atmospheric and land surface.
- NAVGEM v2.2 validation: To validate the new model version, an eight-month parallel run was conducted comparing NAVGEM v2.2 directly against the previous version, v2.1. Performance was evaluated by comparing forecasts for geopotential height, temperature, and wind against independent data.

Results: The methodological efforts produced significant improvements and new insights into the NAVGEM model's performance.

- Improved model physics: The updated physics in the Navy ESPC tests led to improved wind and cloud forecasts, which, in turn, resulted in more accurate sea surface temperature (SST) forecasts. The fix for the sea ice albedo flaw corrects an issue that could cause excessive surface downwelling solar radiation in areas with partial ice cover. This fix is active by default in the CV3.2 physics.
- Benefits of stochastic physics: The implementation of the SKEB scheme improved not only atmospheric forecasts of winds and clouds, but also forecasts for ocean sea surface temperature (SST). This work is scheduled for submission to a peer-reviewed journal [1].
- Impact of land surface uncertainty: The ensemble experiments demonstrated that accounting for land surface uncertainties is important for maritime forecasts. By the end of a two-week forecast, the ensemble spread growth from land-only perturbations was similar in magnitude to that from atmosphere-only perturbations. The land surface was also shown to have a significant impact on spread growth in the upper troposphere, highlighting the need to represent land surface processes in oceanic as well as continental forecasts. This work is also scheduled for journal submission [2].
- Successful NAVGEM v2.2 validation: The eight-month evaluation showed that NAVGEM v2.2 represents a net improvement over v2.1 (Table 1), with strong gains in the tropics and in polar regions. The updated model produced more accurate forecasts, demonstrated by reduced long-range wind speed errors and better predictions when compared to radiosonde data. Verification also confirmed a more accurate

representation of outgoing longwave radiation (OLR), a reduced amplitude bias in the Madden-Julian Oscillation (MJO), and enhanced accuracy in the newly expanded upper atmosphere [3].

Defense Impact/Significance: Advances in forecast skill and in our understanding of atmospheric processes and forecast uncertainty targeted through this project enable delivery to decision makers of more accurate weather information for environmentally sensitive risk assessment. HPCMP resources are essential to this work, whose downstream impacts extend to other closely related Navy efforts that are also supported by HPCMP. An example is the deployment to Navy operations this year of the first deterministic high-altitude version (ESPC-D v2.0) of the Navy ESPC system, the culmination of a multiyear development cycle.

References

[1] H. W. Christophersen, C. Hartman, D. Tyndall, and M. Janiga, "Navy Global Environmental Model (NAVGEM) v2.2 System Validation Test Report," NRL formal report, submitted to information release.
[2] M. Ulate, C. A. Reynolds, W. Crawford, M. Janiga, and J. McLay, "Impact of stochastic kinetic energy backscatter scheme on the Navy Earth System Prediction Capability," submitted to *Weather and Forecasting*, 2025.
[3] S. Rushley, C. A. Reynolds, P. Finocchio, and W. Crawford, "Impact of land surface uncertainty on coastal maritime weather prediction," submitted to *Weather and Forecasting*, 2025.

Reference	Level	Region	Lead time	Variable	Level type	Metric	Weight	Score
Fixed Buoy	None	N.H.	96	Wind Speed	surface	Mean Error	2	0
Fixed Buoy	None	Tropics	96	Wind Speed	surface	Mean Error	2	0
Manual Sfc Land	None	N.H.	96	Air Temp.	surface	Mean Error	1	0
Radiosondes	100	Global	96	Geopotential H.	pressure	RMS Error	1	+1
Radiosondes	250	Global	96	Air Temp.	pressure	RMS Error	1	0
Radiosondes	250	Global	96	Wind	pressure	Vector RMS Error	1	0
Radiosondes	500	Global	96	Geopotential H.	pressure	RMS Error	1	0
Radiosondes	700	Global	96	Relative Humidity	pressure	Mean Error	1	0
Radiosondes	850	Global	96	Air Temp.	pressure	Mean Error	1	0
Radiosondes	850	Global	96	Air Temp.	pressure	RMS Error	1	0
Radiosondes	850	Global	96	Wind	pressure	Vector RMS Error	1	0
Self Analysis	200	N.H.	96	Wind	pressure	Vector RMS Error	1	0
Self Analysis	200	S.H.	96	Wind	pressure	Vector RMS Error	1	0
Self Analysis	200	Tropics	96	Wind	pressure	Vector RMS Error	1	0
Self Analysis	500	N.H.	120	Geopotential H.	pressure	Anomaly Corr.	2	0
Self Analysis	500	S.H.	120	Geopotential H.	pressure	Anomaly Corr.	1	0
Self Analysis	500	N.H.	120	Geopotential H.	pressure	RMS Error	2	0
Self Analysis	500	S.H.	120	Geopotential H.	pressure	RMS Error	1	0
Self Analysis	850	N.H.	96	Wind	pressure	Vector RMS Error	1	0
Self Analysis	850	S.H.	96	Wind	pressure	Vector RMS Error	1	0
Self Analysis	850	Tropics	96	Wind	pressure	Vector RMS Error	2	0
Self Analysis	1000	N.H.	120	Geopotential H.	pressure	Anomaly Corr.	1	0
Self Analysis	1000	S.H.	120	Geopotential H.	pressure	Anomaly Corr.	1	0
Total								+1

Table 1. NAVGEM scorecard comparison of the NAVGEM v2.2 and v2.1 runs from June 2021 to January 2022. Positive scores denote improvement for NAVGEM v2.2, and negative scores denote skill degradation. "Northern Hemisphere" corresponds to latitudes between 20° and 80°N, "Southern Hemisphere" corresponds to latitudes between 20° and 80°S, and "Tropics" to latitudes between 20°S and 20°N. Adapted from Christophersen et al. [3].

Title: Dynamics of Coupled Models
Author(s): I.G. Shulman and S. Cayula
Affiliation(s): U.S. Naval Research Laboratory, Stennis Space Center, MS
CTA: CWO

Computer Resources: HPE Cray EX [NAVY, MS]

Research Objective: Improve our understanding of coupled bio-optical and physical processes in the coastal zone and the variability and predictability of the coastal ocean's optical properties on time scales of 1–5 days. Investigate the coupled dynamics of ocean bio-optical, physical, and atmospheric models.

Methodology: The approach is based on using nested, coupled physical-bio-optical models of the coastal region together with bio-optical and physical in situ and remotely sensed observations. Data-assimilation techniques for both physical and bio-optical fields are being used to examine project research issues and objectives. The approach is also based on joint studies of the bioluminescence (BL) potential and inherent optical properties (IOPs) over relevant time and space scales. Dynamical, biochemical, physical, and BL potential models are combined into a methodology for estimating BL potential and nighttime water-leaving radiance (BLw).

Results: We have developed a statistical model simulating ensembles of time series of intensity of mechanically stimulated bioluminescence potential (BL) measured in situ by a bathyphotometer. The model simulates BL time series by accounting for advection of a collection of individual specimens through the bathyphotometer with prescribed physical parameters. The characteristics of mechanically stimulated bioluminescent emissions (flash kinetics parameters) of individual specimens are taxon-specific and are randomized to account for natural variability within a given taxon. We have tested the model with observations from the Svalbard area of Norway. The results of the model runs demonstrated the ability of the statistical model to simulate BL time series recorded by UBAT bathyphotometer (Fig. 1). This model will be used to estimate transfer functions between bathyphotometers. It uses ensembles of possible bioluminescent plankton abundances as input to generate corresponding ensembles of bioluminescence potential time series for various bathyphotometers. This simulates multiple joint deployments of bathyphotometers within bioluminescent biological structures defined by plankton abundances. Calibrated and tuned using available observations, these ensembles can serve as training data sets for AI models. These AI models can then predict bioluminescence potential time series for a specific bathyphotometer based on input from one or more other bathyphotometers. Results are documented in the paper, which is under peer review in the Journal of Atmospheric and Oceanic Technology.

Defense Impact/Significance: Emerging Navy electro-optical (EO) systems under development and special operations missions require an improved understanding of the ocean optical environment. This is critical for operations and weapon deployment, especially in the coastal and littoral zones. Improved basin-scale-to-mesoscale forecast skill is critical to both military and civilian use of the oceans, particularly on the continental margins.

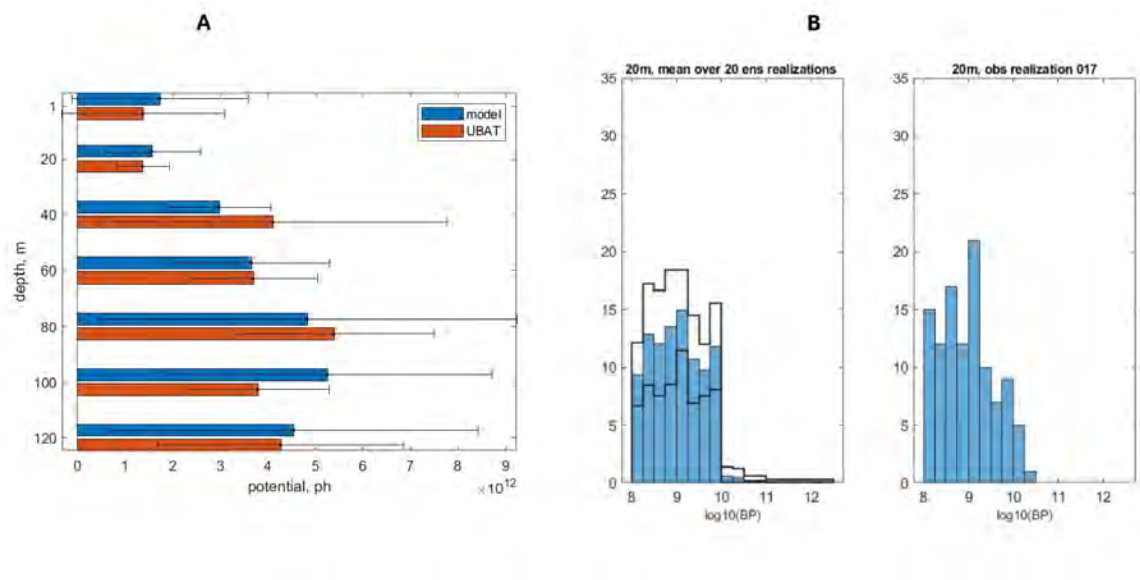

Figure 1. (A) Modeled (blue) and observed (red) mean bulk bioluminescent potential (ph/s) and its standard deviation for different sampling depths. (B) Distributions of the number of emissions over amplitude for modeled (left) and observed (right) times series. For modeled distributions, blue bars show ensemble mean bin counts, black staircase lines present mean ± STD counts.

Title: Coastal Mesoscale Modeling
Author(s): P.M. Finocchio
Affiliation(s): U.S. Naval Research Laboratory, Monterey, CA
CTA: CWO

Computer Resources: Penguin Open Compute Platform (OCP) [AFRL, OH]; HPE Cray EX, Penguin TrueHPC [NAVY, MS]

Research Objectives: The coastal zone is characterized by mesoscale weather phenomena that adversely affect Navy operations. Sharp gradients of wind, temperature, moisture, aerosols, refractivity, and visibility exist in the lowest kilometer of the atmosphere in the coastal zone. Such mesoscale variability also exists in the ocean. Accurate prediction of coastal mesoscale meteorological phenomena requires coupled land-ocean-atmosphere numerical forecast systems that represent dynamics from the synoptic scales to the scales of the largest eddies. The objective of this project is to develop and validate a coastal/littoral modeling system that provided high-resolution (< 5 km) analysis, nowcast, and short-term (0–120 h) coupled forecast guidance for tactical-sized areas of the world. This system can also be used for basic and applied research leading to an improved understanding of atmospheric and oceanic processes.

Methodology: The primary tool being developed, tested, and utilized for research in this project is the Coupled Ocean/Atmosphere Mesoscale Prediction System (COAMPS®). The atmospheric component of COAMPS® is made up of a data-assimilation system, an initialization procedure, and a multinested, nonhydrostatic numerical model. The numerical model includes parameterizations for cloud, precipitation, and radiation processes, as well as for surface and boundary-layer effects. The NRL Coastal Ocean Model (NCOM) is currently used for the simulation of the mesoscale ocean circulation response to the atmospheric forcing in one-way and two-way interactive modes. The Noah Land Surface model is currently used to simulate land surface processes and exchanges with the atmosphere. COAMPS® has also been modified to predict electro-optical quantities of interest for directed-energy applications.

Results: In FY25, a new capability was added to COAMPS® that allows forecast output from a global aerosol model to be passed into the COAMPS® domain boundary. Figure 1b shows an example from a COAMPS® simulation of smoke being transported into the high-resolution COAMPS®, where the sharp visibility gradients associated with the smoke plume are better resolved. Previously, this smoke would have been missing altogether from the COAMPS® forecast because it originated outside of the model domain. Other aerosol-related improvements to COAMPS® in 2025 included adding four new aerosol species (dust, sea salt, smoke, and sulfates) and fixing issues related to soil moisture, dust lofting, and near-surface aerosols. Applied research projects using COAMPS® on DSRC resources in FY25 led to new discoveries and insight on coastal fog, the marine atmospheric boundary layer, polar lows and tropical cyclones, and the influence of soil moisture on coastal mesoscale circulations. DSRC resources were also used in FY25 for training machine learning models for tactical-scale weather forecasts and for developing the Navy’s next-generation global numerical weather prediction system, NEPTUNE.

Defense Impact/Significance: COAMPS® continues to play a significant role in providing atmospheric forecasts in support of the warfighter. These critical forecasts aid in weapons-system deployment, strike warfare, radar propagation, and search-and-rescue operations. Research and development performed at HPC DSRCs has led to significant improvements in the predictive skill of COAMPS® that will greatly benefit its operational performance. For example, the new aerosol forecasting capabilities introduced in FY25 enable regional, high-resolution visibility forecasts allowing the warfighter to maintain tactical advantage. The HPC DSRCs have also been instrumental for the development of the fully coupled COAMPS® system, including the emerging electromagnetic and electro-optical (EM/EO) and ensemble capabilities, as well as for training new artificial intelligence/machine learning weather-prediction models (based in part on COAMPS®) that can be forward deployed.

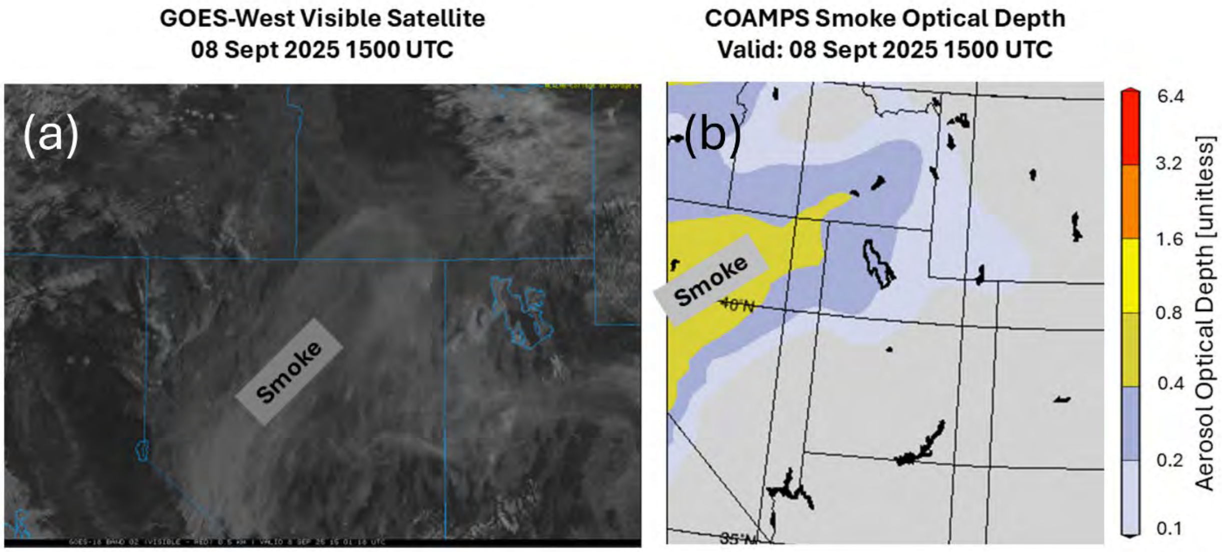

Figure 1. (a) Visible satellite imagery from the GOES-West satellite showing smoke from the Garnet Fire in central California in the local morning (1500 UTC) of 08 September 2025. The lightning-caused fire sent smoke into Nevada and southern Idaho (labeled off-white cloud feature). (b) COAMPS® forecast valid at 1500 UTC on 08 September 2025 of aerosol optical depth, a derived value representing the extent of aerosol coverage through the column of the atmosphere (higher values denoted by warmer colors signify smokier skies). The Garnet Fire was located outside of the COAMPS® outer domain and relatively few fires were actively emitting smoke within the domain; therefore, almost all the smoke in the COAMPS® forecast originated from the global aerosol input data. This demonstrates a new capability added to COAMPS® in FY25, allowing communication of aerosol output from a global aerosol model through the COAMPS® outer domain boundaries.

Title: Retrieving Surface Soil Moisture from CyGNSS Reflectivity Measurements
Author(s): J.D. Ouellette
Affiliation(s): U.S. Naval Research Laboratory, Washington, DC
CTA: CWO

Computer Resources: HPE Cray EX [NAVY, MS]

Research Objective: Measuring terrestrial surface soil moisture (SSM) content at global scale is an important component in operational weather forecast models. SSM serves to regulate the separation of incident solar radiation into sensible and latent heat flux and thus helps to determine the flow of water between the Earth's surface and the atmospheric boundary layer. The Cyclone Global Navigation Satellite System (CyGNSS) is a NASA-funded constellation, presently comprising seven operational microsatellites, each of which receives Global Positioning System (GPS) signals reflected from the Earth's surface. The primary science goal of CyGNSS is to characterize ocean surface wind speed during tropical cyclone conditions but, given the properties of land surface reflections measured by CyGNSS, investigations have been launched with the goal of producing SSM and inundation products from CyGNSS observations.

Methodology: The SSM algorithm developed under this project employs a matrix-based change detection algorithm to derive SSM estimates from CyGNSS reflectivity data. An NRL Karles Fellowship supported development of the original version of this SSM retrieval algorithm, referred to as the time-series-ratio (TSR) method. The algorithm relies on ratios between consecutive radar backscatter or reflectivity values within a time series of observations. These ratios, which populate the off-diagonal terms of the sparse TSR matrix equation, theoretically change only with changes in SSM, given that changes in surface roughness and/or vegetation are negligibly small between each repeat pass. The TSR method was originally conceived for use with L-band radar and radiometer data from NASA's Soil Moisture Active/Passive (SMAP) mission. TSR method-error performance with SMAP data has since been assessed using in situ data; the TSR method outperformed the official SMAP algorithm and furthermore required no training data and minimal ancillary information. The same algorithm has since been applied to CyGNSS under this project, with significant modifications being necessary for application to this sensor suite, including reflectivity ratio denoising and preconditioning.

Results: Building upon work from the previous reporting period, the SMAP and CyGNSS-TSR SSM products were both used to cross-validate the SSM deliverable from USSF's Weather System Follow-on Microwave (WSF-M) satellite, which launched in April 2024 and reached its initial operating characteristic (IOC) period during Q3 FY25. The time-series history of CyGNSS-TSR SSM estimates proved to be particularly valuable during this endeavor, given its very high temporal revisit time and the resulting ease of colocation with other data sources. This SSM cross-validation procedure helped to identify several anomalies in the prerelease version of the WSF-M data product, which have since been mitigated. Error analyses from cross-validation between the CyGNSS-TSR algorithm and the WSF-M SSM product have since been included in the WSF-M IOC report.

Defense Impact/Significance: Navy forecasting tools use models of soil moisture, derived from precipitation measurements, to constrain storm likelihood and intensity forecasts. This project addresses the following science and technology areas identified by the Navy: Assure Access to Maritime Battlespace, Information Dominance, and Platform Design and Survivability.

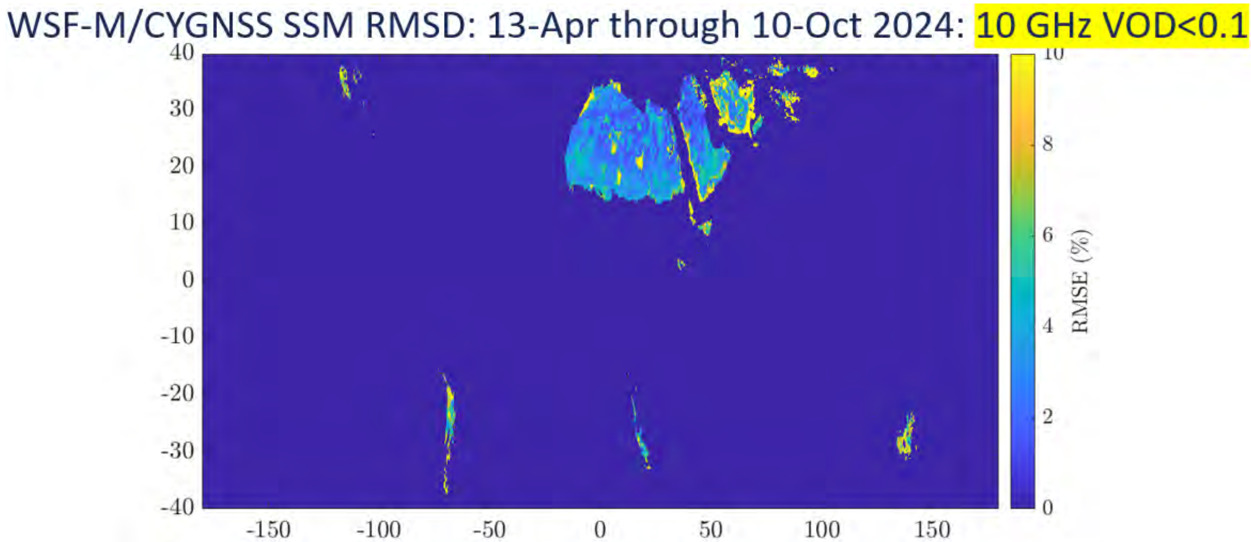

RMSE (%)	Bias (%)	ubRMSE (%)	Correlation coef
4.78	-0.39	4.77	0.02

Figure 1. Root-mean-square difference/error (RMSD/RMSE) between WSF-M and CyGNSS SSM products, for WSF-M 10.7 GHz vegetation optical depth (VOD) less than 0.1. Global error statistics for the analysis period are shown in the lower portion of the figure.

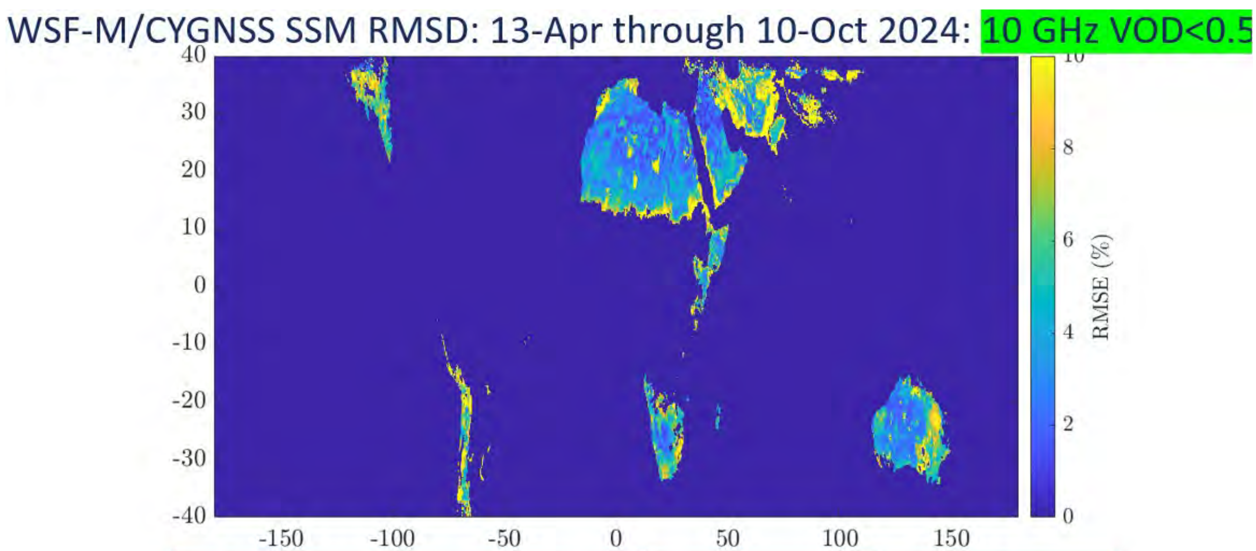

RMSE (%)	Bias (%)	ubRMSE (%)	Correlation coef
5.63	-1.02	5.53	0.42

Figure 2. Root-mean-square difference/error (RMSD/RMSE) between WSF-M and CyGNSS SSM products, for WSF-M 10.7 GHz vegetation optical depth (VOD) less than 0.5. Global error statistics for the analysis period are shown in the lower portion of the figure.

Title: Multiscale Characterization and Prediction of the Global Atmosphere from Ground to the Edge of Space using Next-Generation Navy Modeling Systems

Author(s): C.A. Barton, S.D. Eckermann, J.F. Kelly, J. Ma, D.D. Kuhl, M.A. Herrera, K.W. Hoppel, and D.R. Allen
Affiliation(s): U.S. Naval Research Laboratory, Washington, DC

CTA: CWO

Computer Resources: HPE Cray EX, Penguin TrueHPC [NAVY, MS]

Research Objectives: Develop and test new, seamless, atmospheric specification-and-prediction capabilities from 0 to 500 km of altitude for future Navy Earth System Prediction Capability (ESPC) and ground-to-space numerical weather prediction systems, linking prediction of the ocean, the atmosphere, and space over time scales from hours to decades.

Methodology: This project develops and tests key components of state-of-the-art systems required for improved modeling, prediction, and analysis of the extended operational environment for Navy applications, focusing on the atmosphere, the near space, and the geospace. Several model prototypes and operational systems are under development, including: (a) two high-altitude versions of the Navy Global Environmental Model (NAVGEM), based on upward extensions of the Navy's operational global numerical weather prediction (NWP) system into 1) the middle atmosphere for seasonal prediction (NAVGEM-MA) and 2) the upper atmosphere for thermospheric prediction and data assimilation (NAVGEM-HA), and (b) two high-altitude extensions of the next-generation Navy NWP model NEPTUNE (Navy Environmental Prediction system Utilizing a Nonhydrostatic Engine) comprising 1) a "middle atmosphere" extension (NEPTUNE-MA) for seasonal prediction and 2) a ground-to-space prototype extended into the thermosphere (NEPTUNE-HA).

Results: Major results directly facilitated by HPC resources during FY25 include: (a) production of multiple years of atmospheric reanalysis from data-assimilation runs of NAVGEM-MA for initialization of NEPTUNE-MA and -HA forecasts and background specifications for gravity wave models, (b) validation of MA physics in long forecasts for new tagged releases of deterministic NAVGEM and the coupled ESPC system (Fig. 1), (c) continued validation of new wind measurements from meteor radar and satellite observations to improve the NAVGEM-MA reanalysis of the mesosphere and the lower thermosphere, (d) reanalysis of 0–500 km atmosphere in NAVGEM-HA for validation of prototype NEPTUNE-HA forecast configurations (Fig. 2), and (e) continued development and testing of ground-to-space NAVGEM and NEPTUNE modeling capabilities using advanced numerical algorithms that enable the dynamical cores to operate at high altitudes, including off-line testers for new eddy and viscous diffusion parameterizations.

Defense Impact/Significance: This research addresses Navy and defense community requirements to develop and test new high-altitude atmospheric specification and prediction capabilities leading to 1) a planned Navy Earth System Prediction Capability (ESPC), and 2) a Navy space weather-prediction capability. This project performs the research and development needed to install high-altitude (both middle- and upper-atmosphere) specification and forecast capability in next-generation Navy NWP systems, ultimately providing improved near-space specification and prediction to the warfighter over both tactical and strategic time frames. HPC resources for this project provide critical support for the development of novel ground-to-thermosphere NWP models fully coupled to ionospheric models and data assimilation to address key space-environment prediction goals of the Defense Advanced Research Projects Agency's Space Environment Exploitation (DARPA SEE) program.

Acknowledgement: Support for this research was provided by the ONR Base Research program.

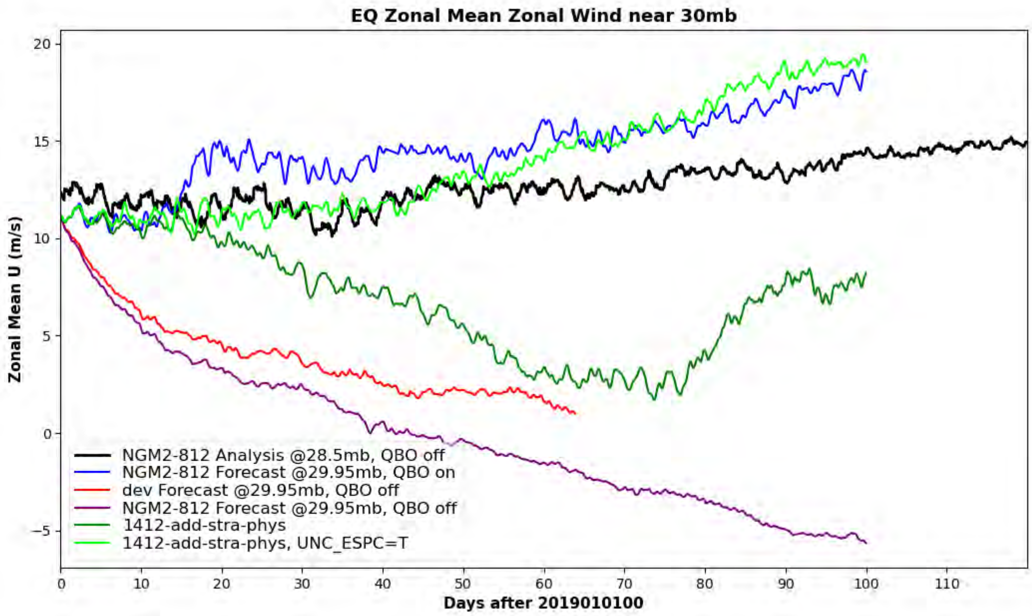

Figure 1. Comparison of equatorial zonal-mean zonal wind at 30 hPa altitude for NAVGEM-MA and the NAVGEM development build and long (100-day), free-running forecasts from each system. Various configurations are presented to demonstrate the impact of improved middle atmosphere physics ("QBO on" vs. "off").

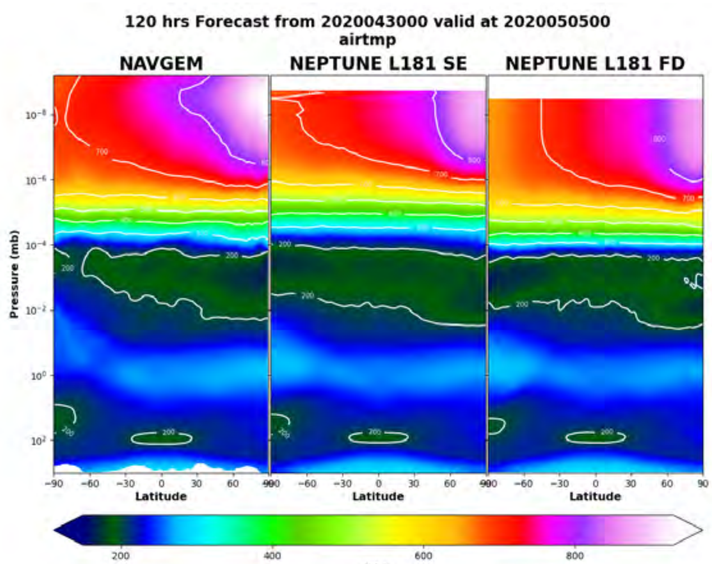

Figure 2. Comparison of five-day forecast zonal-mean temperatures over 0–425 km altitude from NAVGEM-HA (left) and NEPTUNE-HA with spectral element (middle) and finite difference (right) vertical discretization.

Title: Ocean Data Assimilation – ODYSEA Velocity Data Assimilation
Author(s): S.R. Smith, J. May, J.M. D'Addezio, and R.W. Helber
Affiliation(s): U.S. Naval Research Laboratory, Stennis Space Center, MS
CTA: CWO

Computer Resources: HPE Cray EX [AFRL, OH], [NAVY, MS]; Penguin TrueHPC [NAVY, MS]

Research Objectives: The velocity data-assimilation capability within the Navy Coupled Ocean Data Assimilation (NCODA) system version 4.4 was validated in the Gulf of America and the western Atlantic Ocean by assimilating velocities inferred from the movement of large deployments of surface drifters. In this project, we further tested the velocity data-assimilation capability by performing an observing system simulation experiment (OSSE) in the Gulf of America, assimilating simulated velocity observations collected from a proposed wide-swath satellite called Ocean Dynamics and Surface Exchange with the Atmosphere (ODYSEA).

Methodology: An OSSE is a modeling experiment used to evaluate the potential impact and effectiveness of a proposed observing system. The first component that is needed for an OSSE is a nature run that is considered as the true ocean environment. For this, we used an assimilated solution that was created in the Gulf of America for validation from July 15 to December 31, 2020, using the Coupled Ocean and Atmosphere Mesoscale Prediction System (COAMPS®). The second model run is a nonassimilative free run that has some type of error introduced to it. For this OSSE, we used an incorrect initial condition by initiating the experiment on July 1 using an initial condition extracted from the nature run on September 1, 2020. Starting with an initial condition that is 2 months in the future and not assimilating data guarantees that the free run will be different from the nature run for the entire experiment. The third and fourth model runs were the assimilation experiments spun off from the incorrect free run on Aug 1, 2020. The only difference between these experiments is that one included the additional assimilation of velocity observations to gauge the impact that adding the potential ODYSEA satellite has on the predictability of COAMPS®. Since this is an OSSE, the real observation values were not used. Instead, a process was performed to replace the values of all the observations with data from the nature run interpolated in time and space to the observation. Since the nature run is considered as the true environment, random error was added to each observation to mimic the instrument and representation error for each observation type.

Results: The results of this experiment show that the new velocity-assimilation capability in NCODA can improve the predictability of COAMPS® if this potential satellite were to launch. Figure 1 shows that the overall RMS analysis error (panels b and d) are smaller than the overall innovation error (panels a and c) for the u-component (panels a and c) and v-component (panels b and d) of velocity. The reduction in error can be deduced by examining and comparing how close the overall slope of the scatter plot (green line) is to 1.0 (black line). Panel e shows the locations of the assimilated velocity data, where the color represents the innovations. Figure 1 presents the results for Oct 21, 2020, and the results for the remaining analysis days are similar in that the slopes of the analysis scatterplots are closer to unity than the innovations. The number of assimilated observations does change significantly from day to day, depending on the positions of the ODYSEA ground tracks. Figure 2 shows the time series of overall RMS error between the three runs and the nature run for the u-component (panel a) and v-component (panel b) of velocity. These results show that the ODYSEA assimilating experiment had errors significantly less than the other assimilation and free-run experiments.

Defense Impact/Significance: The assimilation experiments tested under this project went toward improving the Navy's capability of forecasting the ocean environment and directly addresses Navy priorities as outlined in the following documents: OPNAVN2N6E FY 2021 RDT&E Priorities Letter 3062, Ser N2N6E/20U119707 (March 26, 2020), and the NRL ocean modeling roadmap developed in consultation with the Navy operational modeling centers, NAVOCEANO and FNMOC.

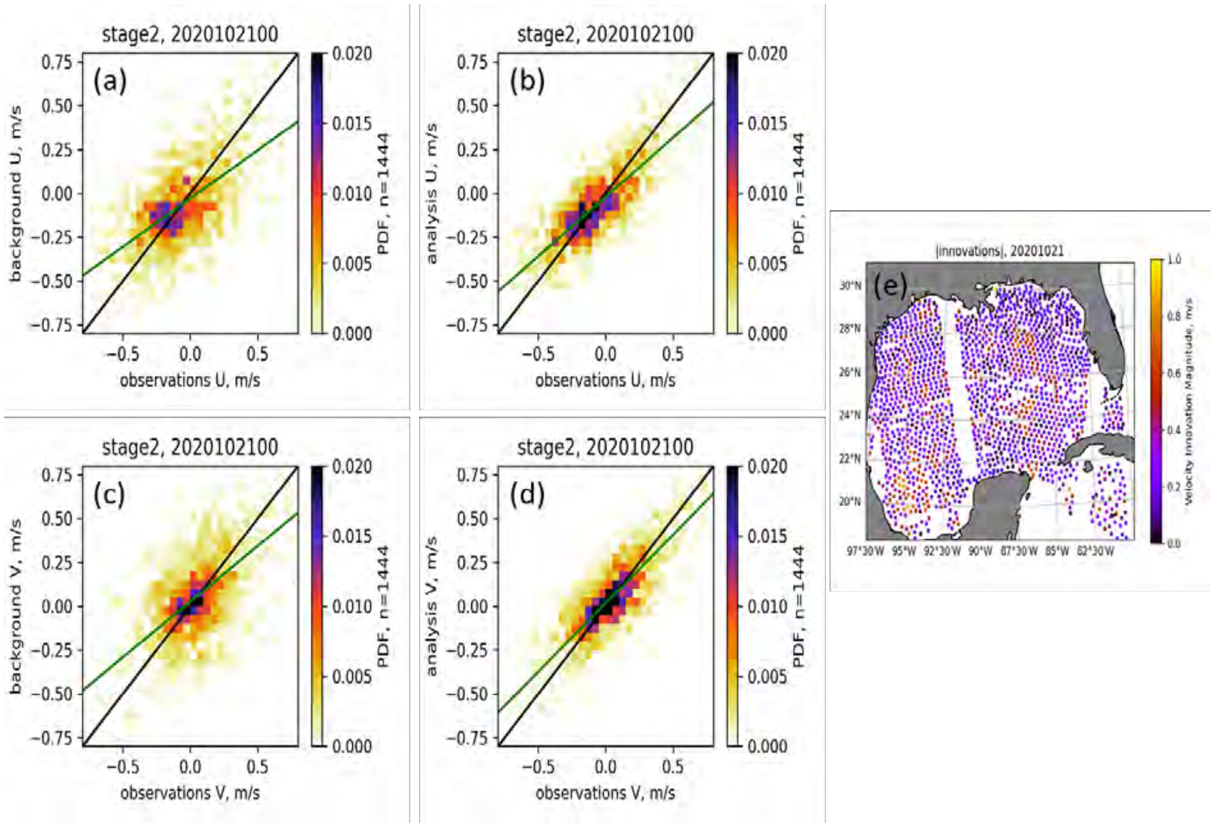

Figure 1. Scatter plots of velocity values on Oct 21, 2020. The first column compares observations versus background for the u-component (a) and the v-component (c) of velocity. The second column compares the observations versus analysis (b and d). The colors in panels (a)–(d) are the observation error and the green line is the overall slope of the data. The number of assimilated observations, n, is indicated in the color bar label. Panel (e) displays the locations and innovation magnitudes of the velocities being assimilated on Oct 21, 2020.

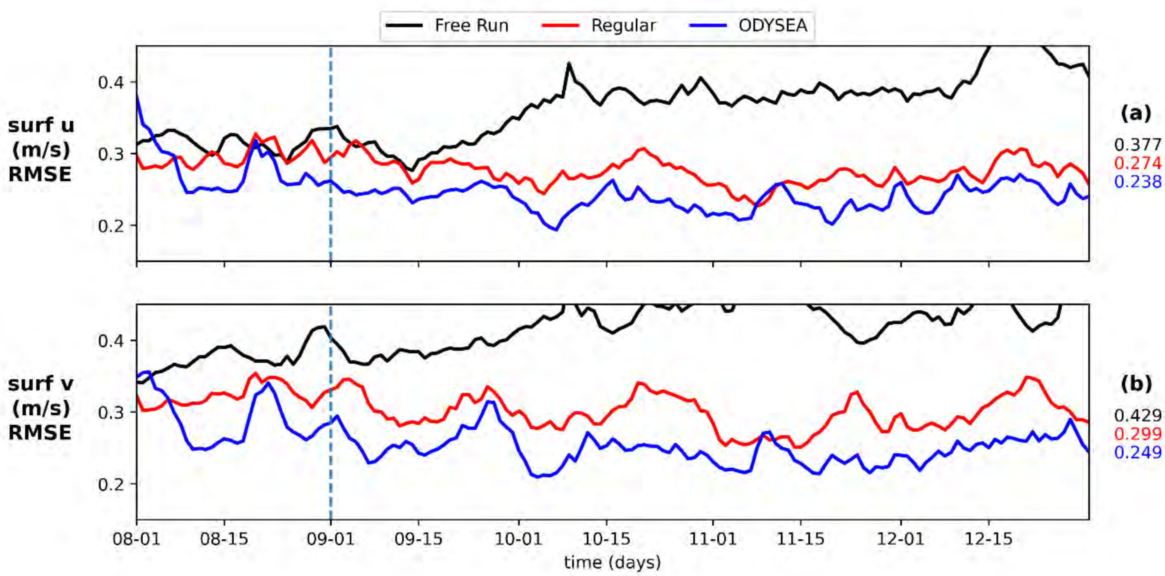

Figure 2. RMS error of the free (black line), regular assimilation (red line), and ODYSEA assimilation (blue line) runs relative to the nature run for the u-component (a) and v-component (b) of velocity. Errors were computed every day at the analysis time for the time period of the experiment (Aug 1–Dec 31, 2020).

Title: Ocean Data Assimilation – Ocean Surface Velocity Physics
Author(s): J.M. D'Addezio,[1] A.J. Iversen,[2] Y. Fan,[1] and J. May[1]
Affiliation(s): [1]U.S. Naval Research Laboratory, Stennis Space Center, MS; [2]Peraton, Inc., Stennis Space Center, MS
CTA: CWO

Computer Resources: HPE Cray EX, Penguin TrueHPC [NAVY, MS]

Research Objectives: In the 2030s, NASA expects to launch the Ocean DYnamics and Surface Exchange with the Atmosphere (ODYSEA) satellite into near-Earth orbit. The satellite is novel in that it is proposed to concurrently measure surface atmospheric winds and surface ocean currents on a global scale once per day. Currently, ocean surface measurements are extremely rare, yet incredibly important to Navy operations: surface currents predict mine drift and search-and-rescue efforts, and through Navy technology, can also inform undersea warfare. This Navy technology is a new surface velocity-assimilation methodology, whereby ocean model trajectories are corrected daily using such observations. Therefore, we expect that ODYSEA observations will have a significant impact on near-future Navy warfighting.

However, current Navy velocity-assimilation technology assumes that ocean velocity measurements provide estimates of velocities many meters below the surface. ODYSEA will measure the very surface velocity, which contains several physical mechanisms that are not actively present in measurements taken meters below the surface. Therefore, this project sets out to quantify ocean-velocity dynamics at the very surface of the ocean and how those basic research findings can help tune future velocity-assimilation methodologies for ODYSEA observations.

Methodology: Current operational and research Navy ocean models use vertical grids with 50–100 layers, with only a few layers within the top 0–10 m of the water column. This limits the ability of these simulations to properly resolve velocity dynamics at the very surface of the ocean (< 2 m). Using HPC resources in FY25, we created a first-of-its-kind ocean simulation with 200 vertical layers, 100 of them being placed in the top 10 m of the water column (Fig. 1). This vertical density has never been tested before, and we have demonstrated its possibility and utility for the first time. Very high vertical resolutions require a very small model time step, and in this case, we had to use a 2-second time step. This makes the simulation incredibly computationally expensive, and therefore only possible on Navy DSRC resources. Two other experiments were created, one with 50 vertical layers (operational configuration) and one with 100 vertical layers (research configuration), allowing us to directly intercompare results from each.

Results: Figure 2 shows a daily composite of temperature, mixed layer depth, and vertical velocity shear in the top 10 m of our simulation. There is a clear daily cycle, with temperatures peaking very close to the surface around hour 15. This significantly shoals the mixed layer, trapping momentum in the very-near-surface environment. This momentum trapping is demonstrated by the strong vertical shear that sets up shortly afterward. Using these simulations, we can quantify this highly dynamic, daily cycle in a region that is extremely difficult to probe using currently available observations. Therefore, the ocean model provides significant scientific utility for quantifying physics in this underobserved region of the ocean.

Defense Impact/Significance: The dynamics we observe in Fig. 2 are not currently taken into account in the operational version of the Navy's velocity-assimilation technology. By performing basic research in this underquantified region of the ocean, we can provide recommendations for how the future velocity-assimilation technology needs to be tuned for forthcoming ODYSEA observations. The combination of ODYSEA and this updated assimilation technology is expected to significantly increase modeling capabilities of the ocean physical battlespace environment, which directly leads to warfighter impact and overall U.S. Navy lethality.

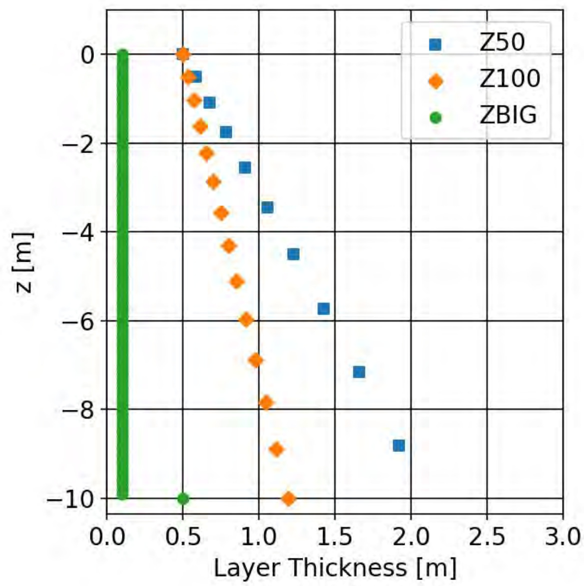

Figure 1. Comparison of model vertical layering from three simulations, highlighting the significant increase in model fidelity in the top 0–10 m of the water column provided by our 200-layer ocean simulation.

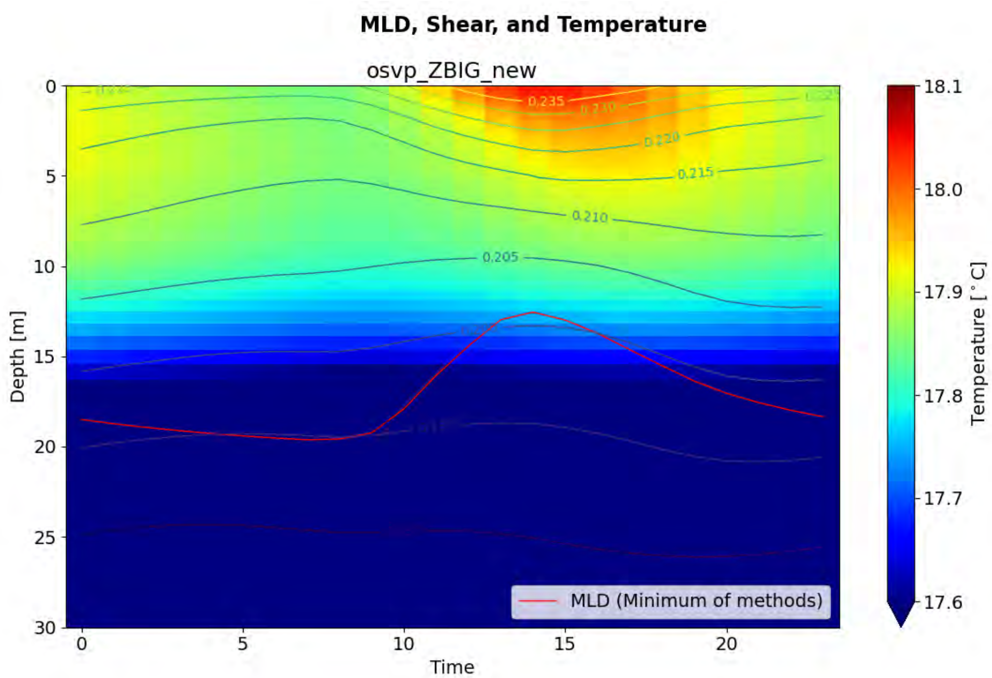

Figure 2. Daily composite of temperature (color), mixed layer depth (red contour), and vertical shear (gray contours) in the top 0–10 meters of the simulated ocean water column.

Title: Coupled Ocean-Wave-Air-Ice Prediction System
Author(s): J. Veeramony,[1] T. Campbell,[1] E. Douglass,[1] K. Edwards,[1] D. Hebert,[1] T. Jensen,[1] G. Panteleev,[1] T.A. Smith,[1] J. Yu,[1] and M. Phelps[2]
Affiliation(s): [1]U.S. Naval Research Laboratory, Stennis Space Center, MS; [2]Peraton, Inc., Stennis Space Center, MS
CTA: CWO

Computer Resources: HPE Cray EX, Penguin TrueHPC [NAVY, MS]

Research Objectives: The weather and oceanic surface and subsurface conditions are affecting Navy operations and understanding how the atmosphere and ocean interact is crucial for developing better environmental forecast models. At NRL, state-of-the-art numerical models are under constant development for the atmosphere, the ocean, surface waves, and sea ice. In recent years, these models have been coupled to form a comprehensive prediction system. The coupled modeling system, Coupled Ocean/Atmosphere Mesoscale Prediction System (COAMPS®) is six-way coupled with the Navy Coastal Ocean Model (NCOM), WaveWatch-III (WW3), and SWAN wave models and is now being used and validated in many regional areas around the globe. Additionally, the sea ice model, Community Ice CodE (CICE), is a valuable research tool in the prediction of sea ice thickness. The Office of Naval Research (ONR) has several ongoing field experiments in many areas around the world, and an important task is to apply uniquely designed COAMPS® and CICE modeling systems for each of those areas and to run real-time forecasts as well as hindcasts. Forecasts are used to assist research ships and autonomous platforms such as gliders to provide guidance on where to deploy vessels to get optimal measurements, while hindcasts can assimilate observations and can help the quality of model simulations.

Methodology: For accurate simulation and prediction on regional scales in mid-latitudes, we have used new configurations of NRL's state-of-the-art, fully coupled atmosphere-ocean-wave model system COAMPS® with very high spatial and temporal resolution. For the Atlantis Seamounts area in the North Atlantic, a two-nest simulation with very high vertical resolution used 100 vertical layers and up to 600 m horizontal resolution in the ocean and two nests in the atmosphere (18 km and 6 km). The coupling interval for data exchange between the model atmosphere and ocean was 6 min. Additionally, the CICE model was used to compare observed ice motion during the Beaufort Gyre Exploration Project (BGEP). Sea ice thickness is an important factor in sea ice strength, motion, and heat flux between the ocean and the atmosphere. Typically, ice models use 2–5 ice categories, but here, CICE was used to analyze the impact of multiple (22) sea ice categories ranging from 1 to 6 meters, with highest resolution (15 categories) for ice less than 2 meters thick to compare to the BGEP observations.

Results: The 2-month-long coupled COAMPS® simulation in the Atlantis II Seamounts area produced real-time sections of temperature, salinity, currents, and sound speed that demonstrated high intermittency of subsurface acoustic ducts due to internal wave activity. The high-resolution GEBCO topography data set was used and a new general vertical coordinate grid was also implemented and tested. For the CICE project, an overall comparison of the behavior of the CICE model during the period of strong ice divergence/convergence does not agree well with the observations, with some similarity of the probability density functions (pdfs) of ice thickness being observed only when ice is deformed solely by the shear. In particular, the modeled results show that (a) the peak of the modeled pdf does not shift with increasing divergence/convergence, whereas observed ice pdf peaks shift by as much as 0.5 m. A shift in ice thickness has important impacts on ice strength and ridging. This suggests that processes related to ice divergence and convergence need further investigation.

Defense Impact/Significance: The development of the relocatable coupled air-ocean-wave prediction system can have a pronounced effect on Navy forecasting by improving anti-submarine warfare (ASW) performance, tropical cyclone prediction, and search-and-rescue and mission planning. Also, Arctic ice modeling and prediction has become a Navy priority.

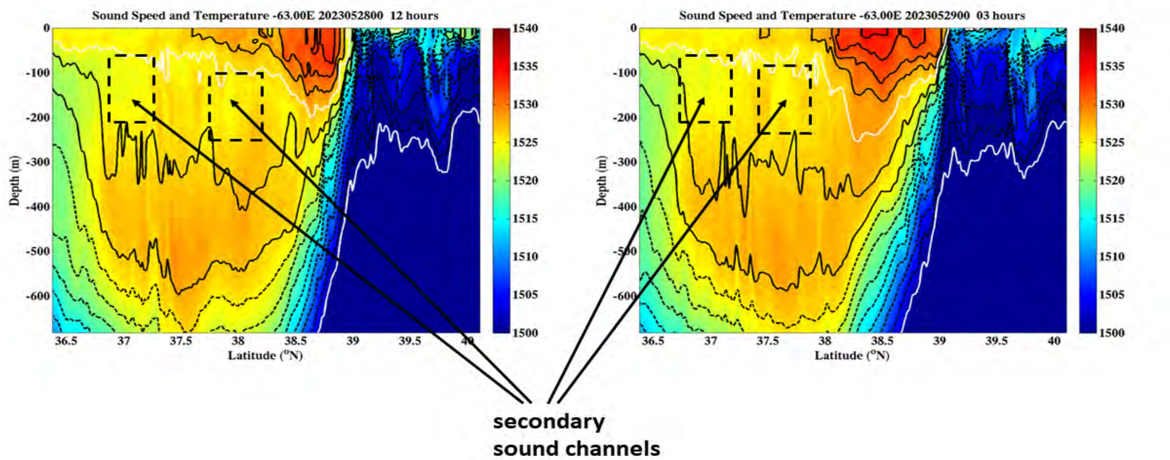

Figure 1. COAMPS® modeling of the Atlantic Seamount area in the North Atlantic. Instantaneous sound speed on 600 m grid 28 May 12 UTC and 29 May 03 UTC show high intermittent variability in the sound channel in the Atlantis Seamount observational area. Contour interval is 1 °C. Dash line is 17 °C or colder. White lines are 10 °C and 20 °C. Rectangles show areas of secondary sound channels. The steep gradient near 38.5N is the position of the North Wall of the Gulf Stream.

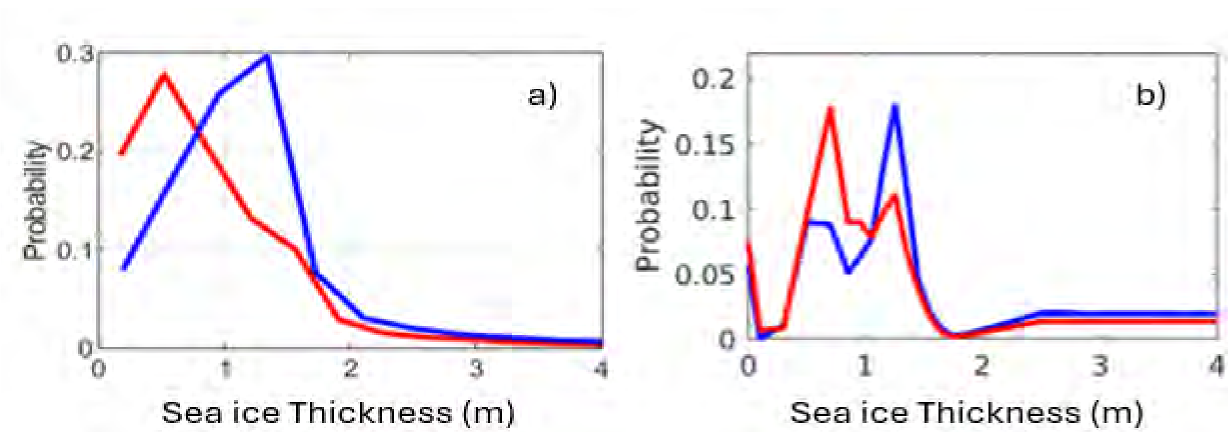

Figure 2. Observed (a) and modeled (b) sea ice thickness probability distribution under strong (red) and weak (blue) shear. In both observed modeled cases, strong shear causes a thinner ice distribution compared to weak shear. Thinner ice is weaker and easier to navigate and allows more heat exchange, affecting upper ocean acoustic performance.

Title: Eddy-Resolving Global/Basin-Scale Ocean Modeling – Ocean Forecast Compression for Resource-limited Environments
Author(s): C.B. Scarano
Affiliation(s): U.S. Naval Research Laboratory, Stennis Space Center, MS
CTA: CWO

Computer Resources: HPE Cray EX [NAVY, MS]

Research Objectives: This project uses an approach called SABRE (Selected Analogous Battlespace Reanalysis Environment) to enable reliable compression and communication of ocean forecast products to forward-operating forces over low-bit-rate data links. Each profile in an operational forecast is paired with an analogous, SABRE-identified profile sourced from 30 years of Global Ocean Forecast System (GOFS) 3.1 reanalysis and is sent to forward units in communications-limited scenarios to permit onboard reconstruction of the battlespace environment. Transmission of an integer array in lieu of a full forecast field provides compression at a ratio of 265:1 and permits the forward unit to rapidly reconstruct the battlespace domain by reindexing onboard reanalysis profiles.

Methodology: SABRE leverages 30 years of historical global ocean states onshore and onboard (1) to identify acoustic analogues and (2) to transmit their compressed indices to the warfighter for onboard reconstruction of the physical battlespace. The GOFS reanalysis profiles are clustered by water mass and acoustic properties to reduce the number of brute force searches. Each profile's analogue falls within the same cluster as its original profile based on cluster means. Then, reanalysis profiles are sorted and saved by cluster to facilitate operational searchability by a fleet subject matter expert. Forecast profiles are searched in parallel. The reanalysis profile with the same cluster designation, the same sonic layer depth, and the most similar vertical gradient of sound speed is identified. Its latitude, longitude, and time indices are converted into a single integer value. Once all corresponding analogous integers in the domain have been selected, the reconstructed sound speed and its RMSE are saved and the compressed linear index file is transmitted to the forward platform. Onboard, the deployed unit possesses regionally subsetted reanalysis sound speed and simply decodes the linear index file to rapidly reconstruct the maritime domain.

Results: Regional battlespace reconstructions were successfully completed using the SABRE process that encompasses larger geographical areas, such as the western Pacific, with favorable results. Figure shows root-mean-square error (RMSE) of vertical gradient of sound speed between an operational GOFS 3.1 forecast on January 16, 2024, and its 30-year GOFS 3.1 SABRE reconstruction for a larger western Pacific domain. While RMSE is relatively low throughout the region, it is locally high along bathymetric features, such as the coastal shelf throughout the western South China Sea. Gridlines show the bounds of each segmented 15° region. Each box is clustered and reconstructed independently, so reanalysis profiles that have been selected as the best match also lie within that same 15° region. Despite the only similarities between regions being the same global input forecast field and the same clustering-and-reconstruction scripting, there is continuity between boxes, indicating that locally high errors are due to feature presence rather than being artifacts of the SABRE methodology. A cross section of vertical gradient of sound speed along the red line indicating the Taiwan Strait in Fig. 1 is shown in Fig. 2. The subsurface feature centered around 119°E and 50 m depth is well characterized in the reconstructed field, with slightly higher errors along the seafloor.

Defense Impact/Significance: For the warfighter to effectively maintain situational awareness of the maritime domain, it is critical to maximize transmission of high-value ocean forecasts regardless of bandwidth. A robust battlespace-compression process counteracts communications-limited scenarios, reducing risk and enhancing decision making. Advanced data-compression techniques are required so that communications-disadvantaged operators can derive maximum benefit from these Navy METOC Enterprise capabilities, particularly as METOC forecast files increase in size alongside advances in forecast model resolution. Compression of METOC forecast data will enable communications-disadvantaged operators to maintain superior situational awareness and tactical advantage.

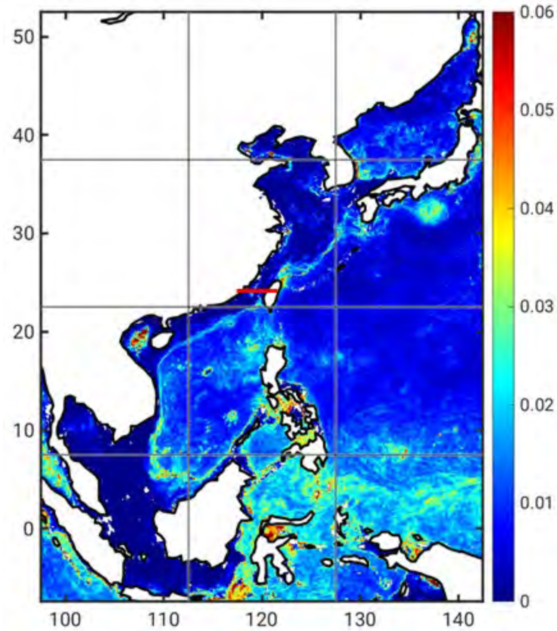

Figure 1. Root-mean-square error (RMSE) of vertical gradient of sound speed (s^{-1}) between an operational GOFS 3.1 forecast on January 16, 2024, and its 30-year GOFS 3.1 reconstruction. Gridlines denote 15° boundaries. Each box is clustered and reconstructed independently.

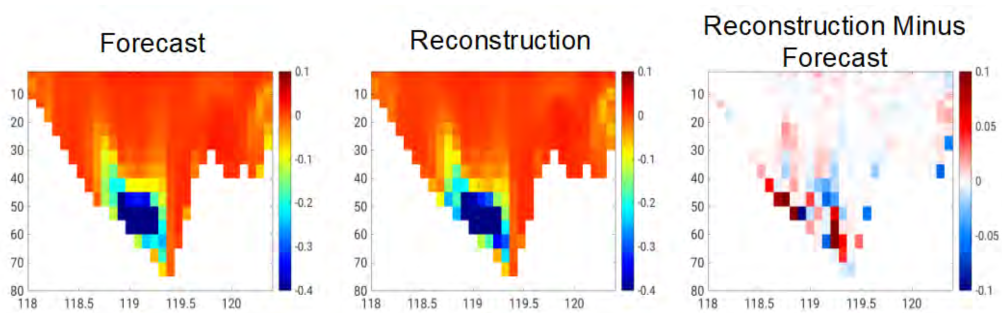

Figure 2. A vertical cross section of vertical gradient of sound speed (s^{-1}) across the Taiwan Strait along the red line denoted in Fig. 1 from an operational GOFS 3.1 forecast on January 16, 2024 (left), its reconstruction of GOFS 3.1 reanalysis profiles (middle), and the difference between the two panels (right). The vertical axis is depth (m), and the horizontal axis is longitude.

Title: Eddy-Resolving Global/Basin-Scale Ocean Modeling – Winter Mixing Intermittency and Restratification
Author(s): P.G. Thoppil and E.M. Douglass
Affiliation(s): U.S. Naval Research Laboratory, Stennis Space Center, MS
CTA: CWO

Computer Resources: HPE Cray EX [NAVY, MS]

Research Objectives: This project aims to quantify the role of submesoscale eddies in generating winter mixed-layer intermittency and to assess how atmospheric forcing modulates these processes. The long-term objectives are to determine how submesoscale dynamics influence upper-ocean convection and water-mass formation and to identify the physical mechanisms governing the spring transition from a deep ocean layer to a shallow mixed layer. By resolving these interactions, the research will provide new insight into how submesoscale processes and their coupling with atmospheric forcing alter upper-ocean stratification, mixing, and water-mass properties.

Methodology: The project employs a combination of idealized and realistic high-resolution model simulations to isolate the restratification effects resulting from submesoscale dynamics and atmospheric forcing. These simulations are complemented by high-resolution ocean observations, enabling a comprehensive assessment of how submesoscale processes and air-sea interactions shape upper-ocean stratification and mixed-layer variability.

Results: We investigated the winter mixing intermittency (WMI) events in the northeast Atlantic using HYbrid Coordinate Ocean Model (HYCOM) simulations at 1 km horizontal resolution. The simulations reveal pronounced WMI during January–May 2019. The mixed layer depth (MLD) exhibits large spatial and temporal variability, with patchy regions of shallow MLD associated with submesoscale (1–10 km) features (Fig. 1a). Elevated WMI activity appears southwest of Iceland, occurring between February and April as a series of events with differing duration and vertical structure (Fig. 1b). During these episodes, the MLD intermittently shoals from 400–600 m to 100–150 m and develops transient stratification, with warmer water overlying colder subsurface layers. These WMI periods coincide with strong ocean heat loss exceeding 100 Wm^{-2}, conditions that favor destratification rather than shoaling, indicating that surface forcing cannot explain the observed intermittency. Instead, submesoscale dynamics emerge as the primary mechanism. Vertical eddy buoyancy fluxes show that restratification is largely driven by mixed-layer eddies that advect lighter water over denser water (Fig. 1c). Argo profiles from 2018–2023 collected near modeled WMI regions corroborate the presence of intermittency; despite the 10-day sampling interval, several observed events exhibit sharp horizontal density gradients consistent with submesoscale-driven WMI.

Defense Impact/Significance: Deep mixed layers associated with wintertime ocean convection develop in regions of intense surface buoyancy loss and play a central role in setting the vertical structure of the water column. The rapid shoaling of the mixed layer during WMI events, and the resulting enhancement of upper-ocean stratification in the northeast Atlantic, have direct implications for underwater sound propagation, particularly through their influence on the sonic layer depth (SLD) and the formation of surface ducts. Insights from this research can inform improvements to the representation of upper-ocean structure in Navy forecast systems, leading to more accurate predictions of ocean acoustics.

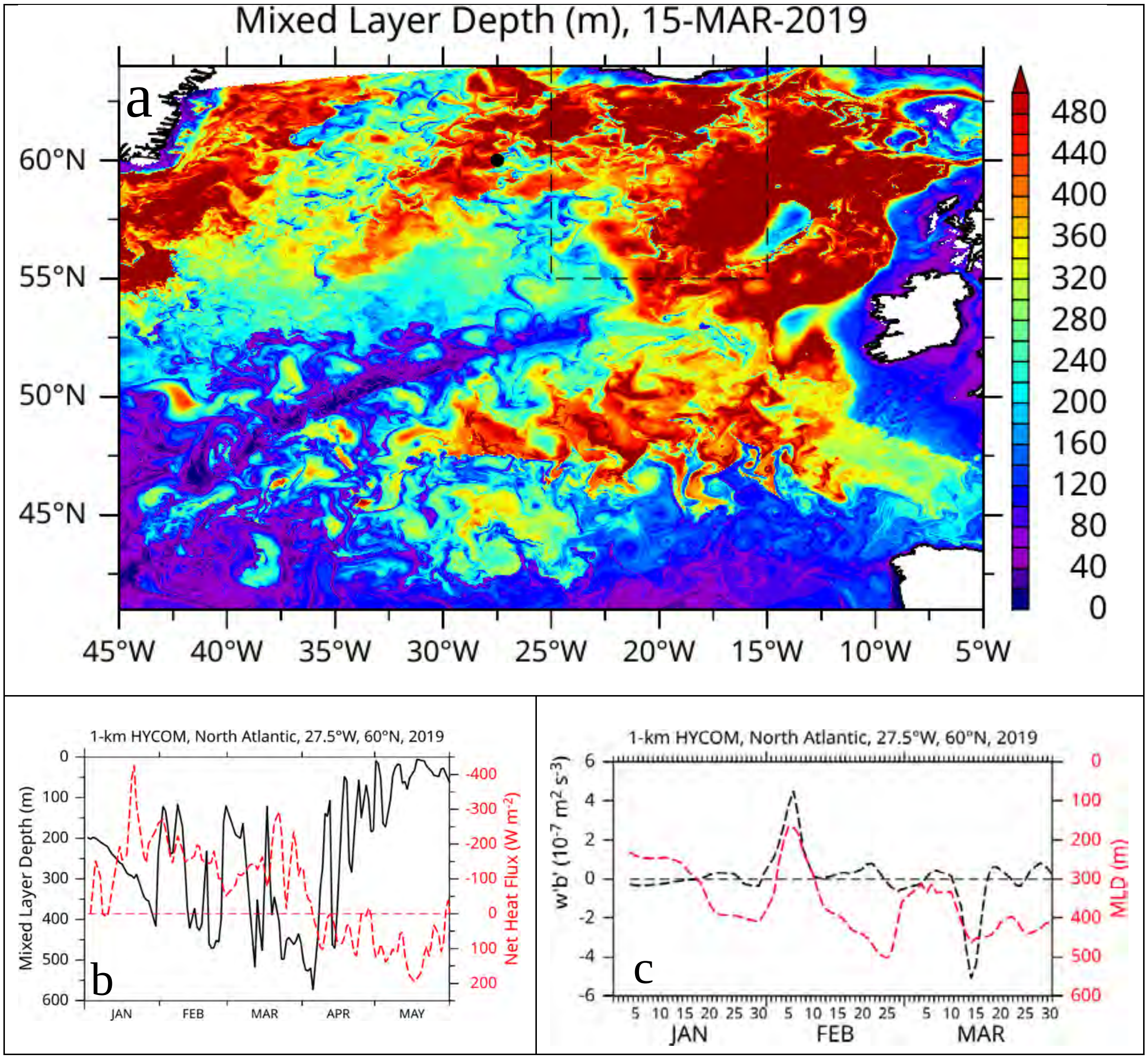

Figure 1. (a) Mixed layer depth (MLD, m) on 15 March 2019 from the 1 km-horizontal-resolution HYbrid Coordinate Ocean Model (HYCOM) simulation in the northeast Atlantic. Patchy regions of shallow MLD reflect active submesoscale eddies. (b) Time series of MLD (black) and surface net heat flux (Wm^{-2}, red) at 27.5°W, 60°N. Intermittent shoaling of the MLD marks instances of winter mixed-layer intermittency (WMI). (c) Time series of vertical eddy buoyancy flux (10^{-7} m^2s^{-3}, black) and MLD (red) at the same location. Periods of elevated buoyancy flux coincide with WMI events, indicating that submesoscale eddies contribute to mixed layer restratification. MLD is defined as the depth of the density increase equivalent to a temperature decrease of 0.3°C.

Title: Eddy-Resolving Global/Basin-Scale Ocean Modeling – Advancing Internal Tide Correction for SWOT Cal/Val: The Role of Ocean Forecasts
Author(s): J.F. Shriver and E.J. Metzger
Affiliation(s): U.S. Naval Research Laboratory, Stennis Space Center, MS
CTA: CWO

Computer Resources: HPE Cray EX [NAVY, MS]

Research Objectives: The Surface Water and Ocean Topography (SWOT) mission provides an exciting opportunity to characterize internal tides with unprecedented spatial detail. Separating tidal and nontidal oceanic signals is necessary for achieving the SWOT mission's objective of advancing our understanding of mesoscale and submesoscale processes. In this study, we evaluate the performance of a data-assimilative HYbrid Coordinate Ocean Model (HYCOM) forecast system in resolving both phase-locked and non-phase-locked internal tides during the SWOT calibration-and-validation (Cal/Val) period. The SWOT mission at present uses the High-Resolution Empirical Tide model (HRET) for internal tide corrections. This empirical method excels at removing the repeatable, phase-locked component of the internal tide (IT).

Methodology: We quantify and compare the effectiveness of empirical (HRET22) and forecast model-based (HYCOM) IT corrections during SWOT's 1-day repeat Cal/Val phase. Leveraging the expanded observational capabilities provided by SWOT, we systematically assess how well each correction method removes both phase-locked and non-phase-locked ITs from SWOT sea surface height (SSH) observations**.**

Results: The SWOT satellite operated in a 1-day repeat calibration and validation (Cal/Val) orbit from 29 March to 11 July 2023, with a ground track repeat sampling interval of 23.844 hr. During this phase, SWOT provided SSH measurements across a 120 km swath with a 20 km nadir gap and a 2 km spatial resolution along- and cross-track, covering multiple widely separated swaths throughout the global oceans (Figure 1). Designed for calibration and validation, it enables high-resolution ocean observations in both space and time.

Statistical summaries presented in Fig. 2 provide a quantitative view of correction skill. Focusing first on the phase-locked component, HYCOM and HRET exhibit broadly similar overall performance, with HYCOM's phase-locked correction showing a modest advantage. The added value of HYCOM is most evident when the non-phase-locked IT signal is included. Although the non-phase-locked correction alone contributes relatively little (median variance reduction of just 4.2%–6.8%), combining it with the phase-locked component in the HYCOM total correction leads to a substantial increase its performance. Together, the spatial and statistical analyses not only demonstrate the broad effectiveness of both HRET22 and HYCOM, but also underline that the greatest improvements in IT correction, as well as the most significant residual challenges, are concentrated in regions of dynamic tidal generation and complex oceanographic structure.

Defense Impact/Significance: Data-assimilative eddy-resolving models are important components of global ocean- and sea ice-prediction systems. Tactical decision aids (TDAs) and mission-planning tools (MPTs) based on these systems provide vital enabling capabilities for the Navy at spatial scales ranging from operational areas to entire theaters and over time horizons ranging from a few hours to many months. An estimate of the accuracy of the simulated internal tides in global HYCOM would be valuable guidance for those who would use these models as decision-making aids or boundary conditions for regional models.

References

[1] B. Yadidya, B. K. Arbic, J. F. Shriver, E. D. Zaron, M. C. Buijsman, L. Carrère, et al., "Advancing internal tide correction for SWOT Cal/Val: The role of ocean forecasts," *Earth and Space Science*, vol. 12, p. e2025EA004511, 2025, doi: 10.1029/2025EA004511.

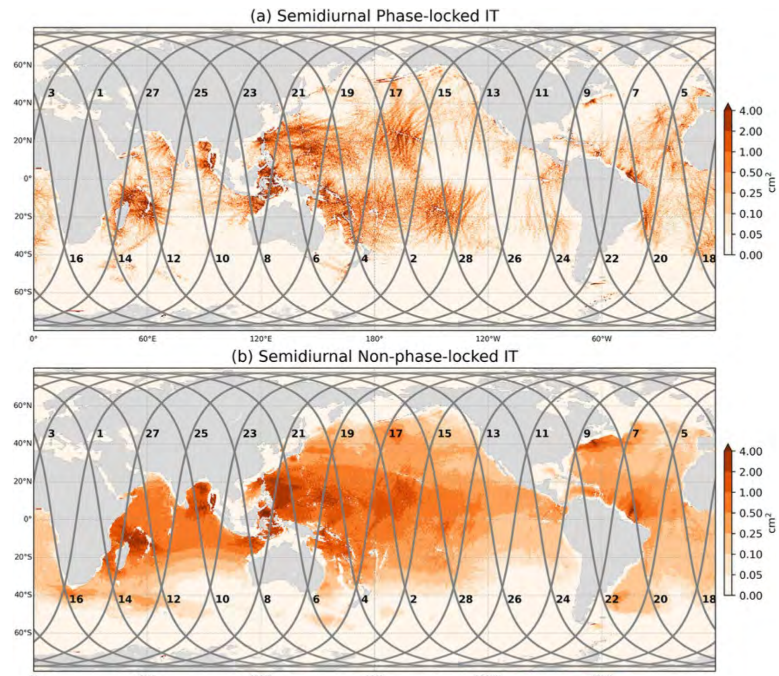

Figure 1. Temporal variance of semidiurnal (a) phase-locked IT and (b) non-phase-locked IT derived from HYCOM, with overlaid SWOT tracks corresponding to the 1-day orbit phase [1]. The pass numbers are denoted in black.

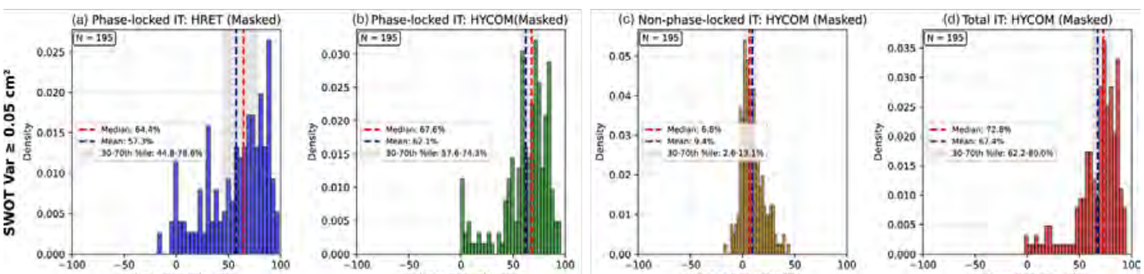

Figure 2. Statistical distributions of IT variance reduction performance across the global ocean, comparing with high-energy regions where SWOT-observed tidal variance exceeds 5. Histograms show the frequency distribution of variance reduction percentages achieved by (a) HRET phase-locked corrections, (b) HYCOM phase-locked corrections, (c) HYCOM non-phase-locked corrections, and (d) HYCOM total (phase-locked + non-phase-locked) corrections. Variance reduction is calculated as the percentage of tidal variance explained by each model relative to SWOT observations after nontidal background corrections. Vertical lines indicate median (red, dashed) and mean (blue, dashed) performance, with gray shading highlighting the 30th–70th percentile range as recommended for highly skewed distributions. Data represent 28 SWOT passes with 400 km spatial averaging and consistent quality control across all model components [1].

Title: Eddy-Resolving Global/Basin-Scale Ocean Modeling – Ocean Submesoscale Eddy Evolution
Author(s): J. May, T.A. Smith, J.M. D'Addezio, D. Hebert, and B. Krause
Affiliation(s): U.S. Naval Research Laboratory, Stennis Space Center, MS
CTA: CWO

Computer Resources: HPE Cray EX [NAVY, MS]

Research Objectives: This project aims to gain a fundamental understanding of ocean submesoscale eddy lifecycle progression. It will study the dynamics, physics, and surrounding ocean environment impacts of ocean submesoscale eddies throughout their generation, evolution, and dissipation. Long-term goals of this project are to demonstrate the seasonality of submesoscale eddies, both at the surface and at depth, to determine the key mechanism for submesoscale eddy penetration past the mixed layer and to evaluate the impact each stage of the eddy evolution has on ocean stratification, heat exchange, and vertical transport both within and below the mixed layer.

Methodology: The project utilizes idealized simulations using the Coupled Ocean/Atmosphere Mesoscale Prediction System (COAMPS®) and the Navy Coastal Ocean Model (NCOM), complemented by data analysis.

Results: To investigate and understand the impacts of submesoscale eddies both within the eddies themselves as well as on the surrounding ocean environment, high-resolution ocean model simulations must be used. We have run a 14-month 0.01° horizontal resolution ocean model simulation with 100 vertical levels over the western Pacific, the domain being located within the boundaries of a nested 3 km COAMPS atmospheric model run (Fig. 1a). This region is further divided into three regions (Fig. 1b): western Kuroshio, northern Kuroshio, and open water. For each region, submesoscale eddies are identified and isolated from the full domain field. Daily and 12-month composites of the cyclonic submesoscale eddies are then evaluated for each region to determine the seasonality of the eddy structure, extent, and characteristics within domains under different dynamical conditions. Analysis is performed on data collected both at the surface and at depth. For example, 12-month composites of the surface currents, as well as vertical cross sections of the currents throughout the water column, are shown in Fig. 1c and Fig. 1d, respectively.

For evaluating the submesoscale eddy impact within each life-cycle stage, we have also completed a 0.003°-horizontal-resolution ocean model simulation, also with 100 vertical levels and located within the 0.01° model domain. From these high-resolution (in both the horizontal and vertical) simulations, we are able to perform a sensitivity study to determine the impact horizontal resolution has on the development and progression of these submesoscale eddies. Additionally, the impact at each stage throughout the eddy's life cycle is evaluated to determine the impact on the surrounding ocean environment, with a focus on the ocean stratification, heat exchange, and vertical transport.

Defense Impact/Significance: Ocean submesoscale eddies are strong features, often with larger magnitudes compared to the mesoscale. These features exist throughout the global ocean and often extend past the mixed layer. Submesoscale eddies are areas of strong convergence zones and will impact search-and-rescue domain size and location. Additionally, submesoscale eddies change ocean stratification, which then impacts sound speed channels, sound speed gradients, and surface ducts. Improved knowledge of the interaction between submesoscale eddies and the surrounding ocean environment will lead to better representation of the effects within ocean forecasts.

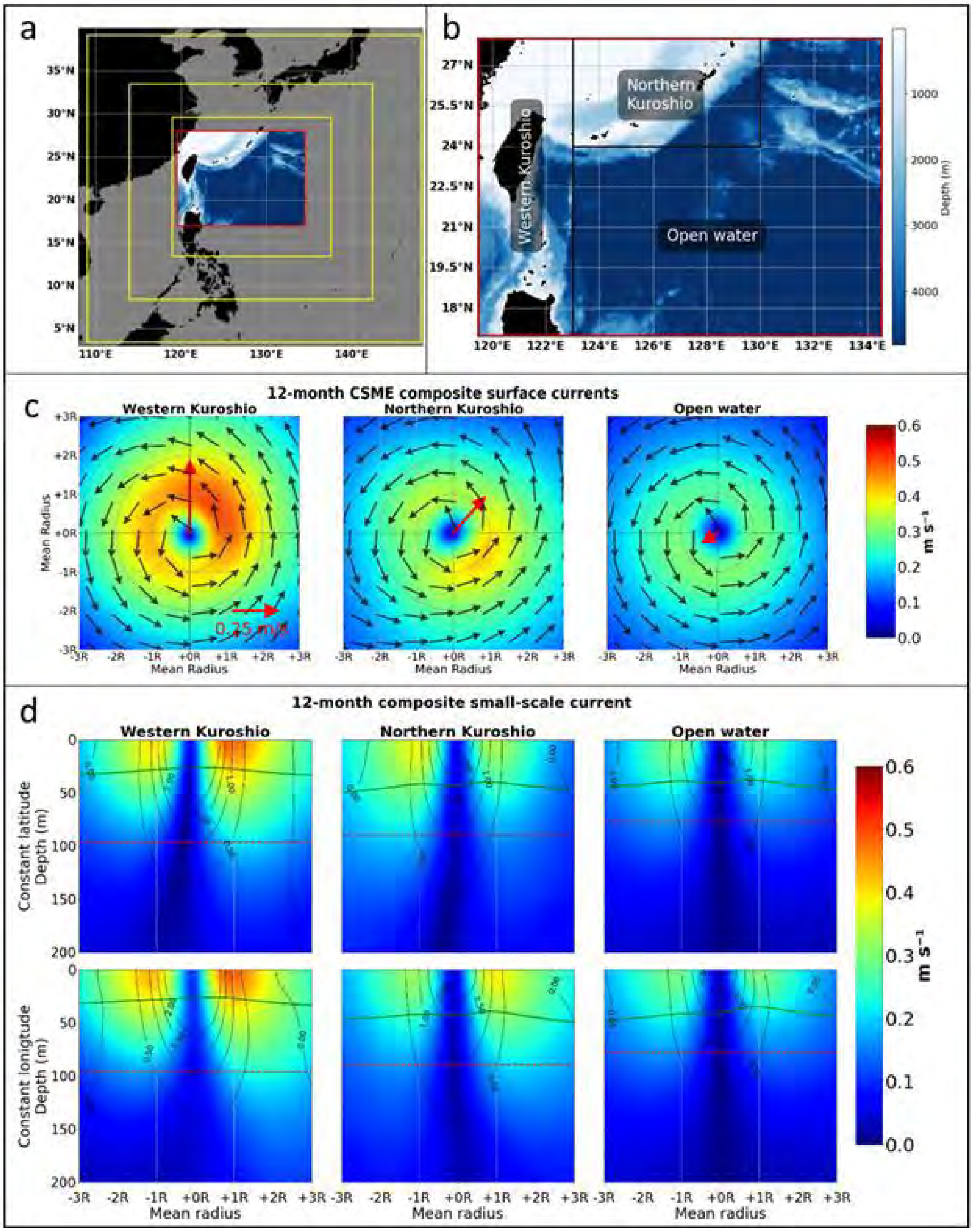

Figure 1. (A) Model domain boundaries for the COAMPS® atmospheric model (yellow boxes) and the ocean model (red box) within the western Pacific. (B) Regional domain boundaries within the 0.01° ocean model domain with model bathymetry shaded. (C) 12-month cyclonic submesoscale eddy composite of the small-scale surface currents for the three regions. The red arrows denote the direction and magnitude of the large-scale surface currents. (D) Small-scale currents vertical cross section with a constant latitude (top row) and longitude (bottom row) of the 12-month cyclonic submesoscale eddy composite for the three regions. The contours indicate vorticity, the green line represents the mixed layer depth, and the dashed, red line represents the eddy bottom depth.

Title: Resolving Northern High Latitude Water-mass Formation Mechanisms

Author(s): H. Kaur,[1] S.R. Smith,[2] and R.W. Helber[2]
Affiliation(s): [1]University of Southern Mississippi, Stennis Space Center, MS; [2]U.S. Naval Research Laboratory, Stennis Space Center, MS
CTA: CWO

Computer Resources: HPE Cray EX [NAVY, MS]

Research Objectives: The goal of this project is to determine the physical mechanisms causing deep-water formation off the coasts of southeastern Greenland and Iceland as a source of deep, dense water found exiting the Irminger and Iceland Basins. These mechanisms are believed to also be responsible for water-mass intrusions that create acoustic channels. The unique contribution of this research will be greater understanding and modeling capabilities to predict the evolution processes of high-latitude, dense water that have a significant impact on the water-mass properties in the region. This will also help us understand and quantify the kinematics and dynamics governing the evolution of high-northern-latitude-originated water and the circulation feeding the lower limb of the Atlantic Meridional Overturning Circulation.

Methodology: In recent decades, the source of deep-water formation in the North Atlantic and Arctic oceans supporting the large-scale ocean thermohaline circulation has moved southward. It has been observed that the North Atlantic's deep, dense water is now formed south of the Greenland-Scotland Ridge in the Irminger and Iceland Basins. The goal of the project is to resolve the relevant processes responsible for the formation of deep water that exits these basins at depth. The high-resolution modeling is performed off the eastern coast of Greenland (Fig. 1, Panel A) using the Navy Coastal Ocean Model (NCOM) to investigate the impact that freshwater runoff from ice melt off Greenland and Iceland has on the circulation in the region. An important feature in this region is the East Greenland Spilljet, where dense water spills over the shelf and descends to greater depths. Convection is one of the primary mechanisms responsible for deep-water-mass formation. Accurately modeling this process requires high-resolution, nonhydrostatic modeling. The MIT General Circulation Model (MITgcm) is used in the spill jet area to evaluate the advantages of nonhydrostatic modeling over hydrostatic modeling.

Results: High-resolution (1 km) NCOM and MITgcm experiments were performed off the eastern Greenland coast using HPC resources. We performed twin model experiments in which one included freshwater runoff from ice melt and the other did not. NCOM originally did not include these types of sources. Panels (A) and (B) of Fig. 1 show the mean temperature for the fall months (July, August, and September) for a 1 km NCOM simulation with runoff for the domain and the spill jet transect (black line in Panel (A)), respectively. Panel (C) in Fig. 1 shows the temperature difference between simulation with runoff and without runoff. These results reveal that runoff increases the transport of warmer water onto the shelf and results in more cold water reaching the deep ocean, while its absence keeps cold water on the shelf. Panel (D) in Fig. 1 shows the difference between idealized nonhydrostatic and hydrostatic MITgcm experiments with a vertical resolution of 10 meters and a horizontal resolution of 100 meters.

Defense Impact/Significance: The Navy needs accurate ocean forecasts and, because of amplified high-latitude warming, circulation in the tactically relevant Greenland/Iceland/United Kingdom (GIUK) gap is changing. Decreasing sea ice coverage and subsurface hydrographic changes in the seas surrounding the Arctic Ocean are altering the formation regions of Atlantic Ocean deep water. This research accounts for the variability, leading to new forecasting capabilities for high-resolution ocean circulation and sea ice predictions useful for Navy operations in the GIUK region.

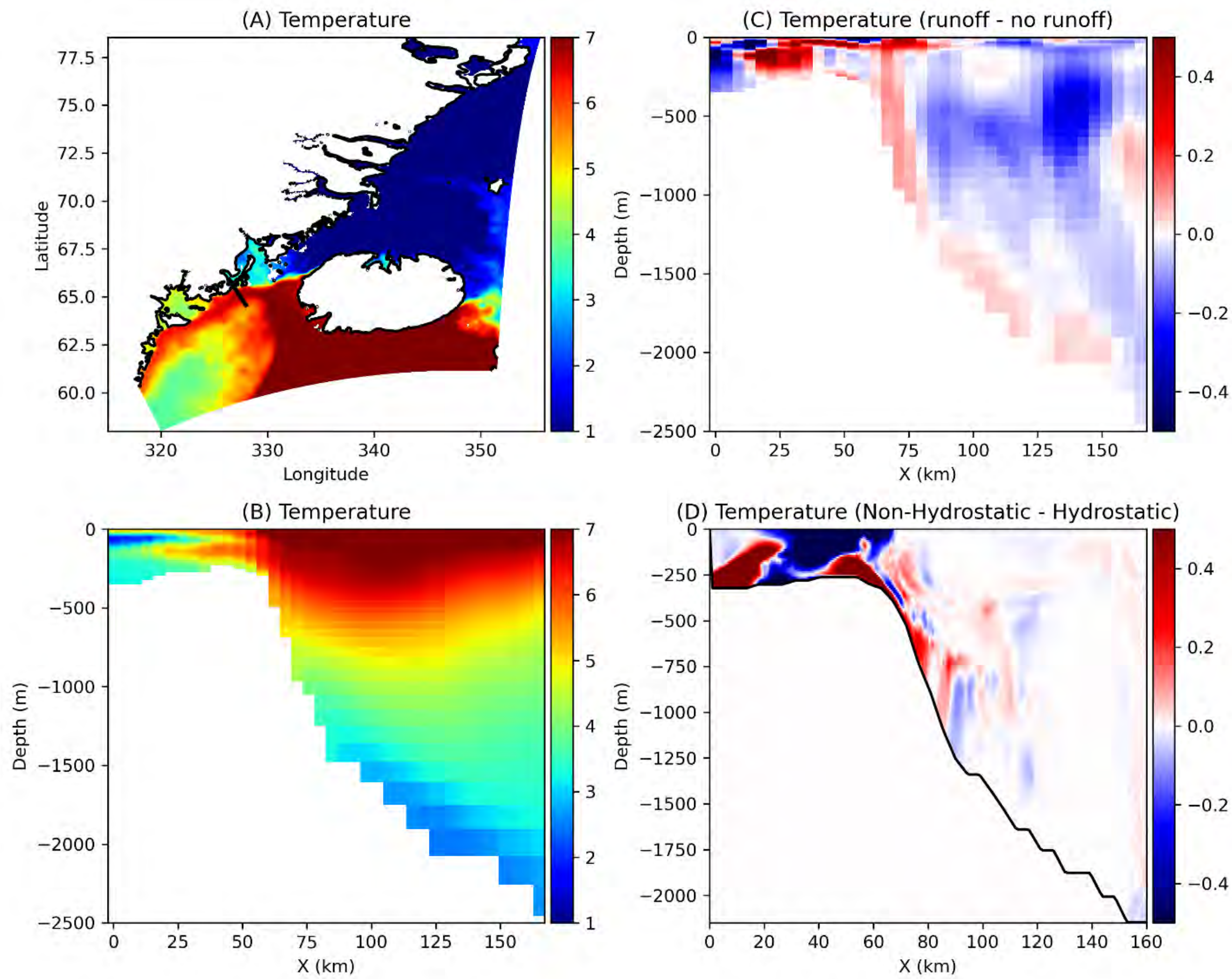

Figure 1. Panels (A) and (B) show average temperature at a depth of 309.2 m and spill jet transect (black line), respectively, for a 1 km NCOM simulation with runoff. Panel (C) shows average fall temperature differences for a 1 km NCOM simulation between with runoff and without runoff. Panel (D) shows the average temperature differences for last 5 days between nonhydrostatic and hydrostatic MITgcm simulations. Both MITgcm simulations are run for 30 days.

Title: Bio-Optical Modeling and Forecasting
Author(s): J.K. Jolliff and T.A. Smith
Affiliation(s): U.S. Naval Research Laboratory, Stennis Space Center, MS
CTA: CWO

Computer Resources: Penguin TrueHPC [NAVY, MS]

Research Objectives: The research objectives for FY25 were (1) to demonstrate how optical variability in the upper ocean is modulating radiant heating and, in turn, air-sea exchange of thermal energy in the marine boundary layer, and (2) to develop a robust capability to estimate and forecast the occurrence of subsurface optical layers in the global oceans. Our understanding of (1) has a direct impact on our ability to accurately forecast the seasonal evolution of the coupled air-sea system, which is critical for the Navy Earth System Prediction Capability (Navy-ESPC). In addition, our ability to estimate the occurrence of subsurface optical layers from a combination of satellite remote sensing and ocean circulation models, and then to forecast the subsequent occurrence and persistence of these features, is a top-tier priority for the Naval Oceanographic Office — and it has direct application to the determination of asset vulnerability in anti-submarine warfare/undersea warfare applications.

Methodology: HPC resources were directed to support the NRL Base Program 6.2 Optical Layering Impacts upon Marine Boundary Layer Physics in Stratified Upper Ocean Systems (OLYMPUS). This project involves both field observations and modeling components; however, the modeling tasks are computationally expensive. The Coupled Ocean Atmosphere Prediction System (COAMPS®) was executed in coupled ocean-atmosphere mode so that air-sea energy fluxes were dynamically represented. We have set up and executed optical sensitivity experiments using the COAMPS® in two-way coupled air-sea configuration for the Bay of Bengal to cover the summer monsoon transition in the 2024 and 2025 cases, consistent with supporting field observations coordinated with collaborators through the Office of Naval Research.

Results: COAMPS® is indeed sensitive to changes in how the solar shortwave attenuation is simulated in the Navy Coastal Ocean Model (NCOM) component (Fig. 1). In the initial part of the simulated time series, both simulations indicate upper-ocean heating above the surface mixed layer (SML). The COAMPS® simulation with higher surface optical attenuation resulted in increased surface temperatures by up to ~1°C. Since this energy was retained above the SML, the high-optical-attenuation case (B) ends up being much cooler as the upper ocean begins mixing toward the end of the simulation (toward the monsoon transition). In summary, the experiments reveal that increasing the shortwave energy retention in the surface mixed layer diminishes the total amount of heat energy in the ocean going into the monsoon transition. This is a counterintuitive result, as typically, increased attenuation increases surface ocean temperatures. However, in the Bay of Bengal, and likely in the larger Indian Ocean, the retention of thermal energy below the shallow mixed layer is also very important, as this acts as a heat reservoir that can be released back to the atmosphere when mixing across the base of the SML occurs. This is a time-delayed sensitivity issue we have not been able to identify in models previous to this project. This preliminary finding may offer some insight into why ocean models in the Indian Ocean generally are too cold during the monsoon transition.

Defense Impact/Significance: Improving the performance of operational ocean models impacts a wide array of naval activities that use environmental forecasts for support. COAMPS® model executions are also used to support basic research into coastal envrionmental variability that eventually translates into applied physical battlespace characterization and prediction. Remote detection and prediction of subsurface optical layers further impacts a wide array of asset vulnerability products.

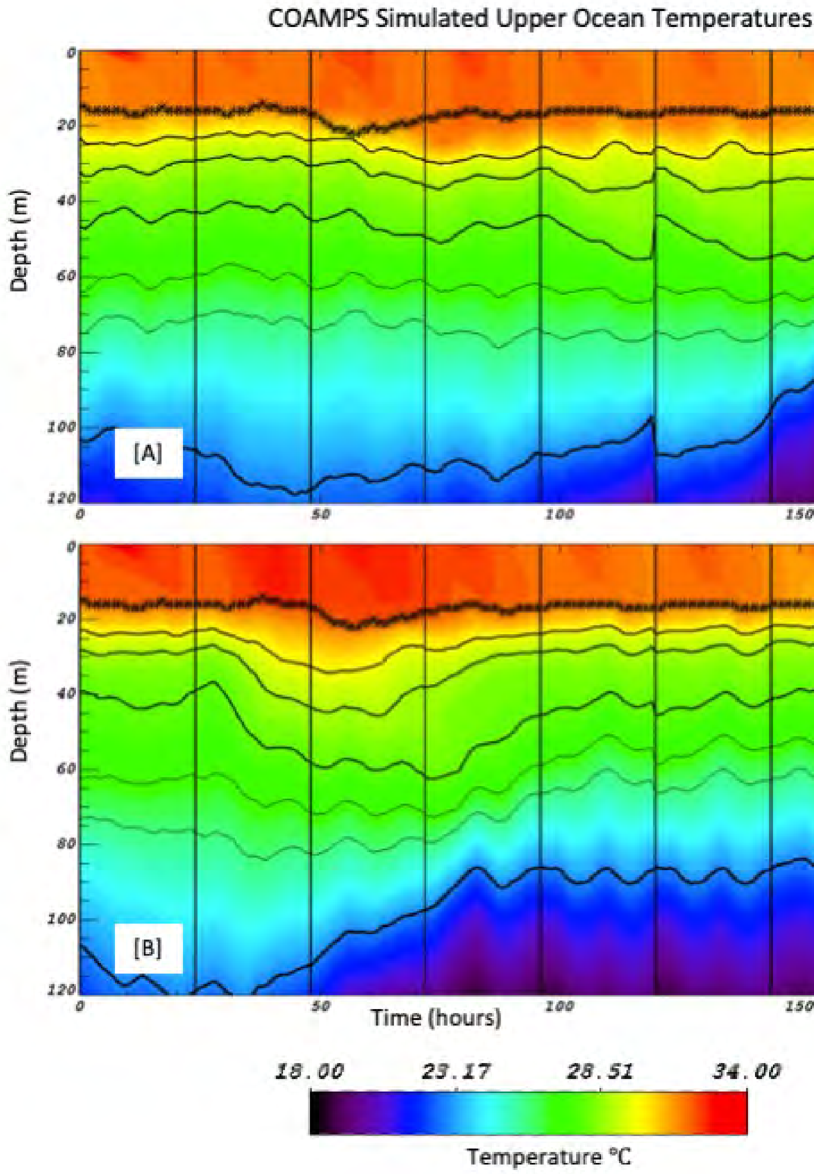

Figure 1. [A] COAMPS® results for the low-optical-attenuation case, upper ocean temperatures during the prelude to the monsoon transition; [B] results as in previous panel but for the high-optical-attenuation case. Simulations are for the June 2024 Bay of Bengal COAMPS® domain with only the optical attenuation changes in the respective model executions.

Title: Data Assimilation Studies Project
Author(s): J.S. Tsu and W.F Campbell
Affiliation(s): U.S. Naval Research Laboratory, Monterey, CA
CTA: CWO

Computer Resources: HPE Cray EX, Penguin TrueHPC [NAVY, MS]

Research Objectives: Our objective is to improve the quality of numerical weather predictions (NWP) by leveraging vast quantities of observations. Data assimilation (DA) corrects model analyses of the atmosphere, the ocean, or the surface using a nonhomogenous collection of observations. This project develops, tests, and improves 1) the development version of the U.S. Navy operational atmospheric global Hybrid 4D-Var assimilation system, which is coupled to our global model NAVGEM (Navy Global Environmental Model), 2) fully ensemble-based data assimilation, 3) coupled ocean-atmosphere global data assimilation, 4) the next-generation global model, the Navy Environmental Prediction System Utilizing a Nonhydrostatic Engine (NEPTUNE) data-assimilation system, and 5) the next-generation Joint Effort for Data Assimilation Integration (JEDI) Local Ensemble Transform Kalman Filter (LETKF) data-assimilation system within the Next-generation Ionosphere Model for Operations (NIMO); it also prepares for and tests new assimilation methods and new observational data types. Our goal is to assimilate traditional data (generally in situ, i.e., weather balloon, ship, or buoy reports) as well as data from a variety of new sources (often spaceborne) efficiently and effectively, to provide the best environmental analysis and, ultimately, to improve numerical weather forecast performance. HPC resources are a critical testbed for assimilation studies to move to next-generation fully coupled atmosphere/land/ocean/sea ice systems.

Methodology: A variety of experimental setups are designed to both develop and test the global and regional models and the associated data-assimilation systems. These require, at a minimum, porting and compiling the code to the various HPC platforms, as well as maintenance of large Earth observation repositories covering several years to be accessed by the various researchers, which include in situ and satellite-based observations as well as initial conditions of the modeling systems.

Results: Since DA has a multitude of applications, numerous types of research take place under this project using the Navy's latest global (Hybrid Ensemble NAVGEM, NEPTUNE) and mesoscale (COAMPS®) models, along with our global (NAVDAS-AR, hybrid NAVDAS-AR, and coupled hybrid NAVDAS-AR, JEDI) and mesoscale (COAMPS-AR) data-assimilation systems. Results from research performed in FY25 include the following: 1) a CI/CD workflow to continuously test the Atmospheric Data Preprocessor (ADP), enabling early bug detection and rapid resolution for all code changes, 2) a novel approach to selecting observations to assimilate using graph theoretic adaptive thinning in observation space to optimize real-time satellite observation selection for evolving weather threats such as atmospheric rivers (Ars) and tropical cyclones (TCs), simultaneously addressing a critical inefficiency that forces U.S. Navy weather-prediction systems to discard over 90% of satellite observations, 3) the capability to assimilate new aerosol-related observations, including VIIRS products for replacement of MODIS, infrared dust products, and High Spectral Resolution Lidar (HSRL) measurements, 4) the ability to run expanded ensembles in ENAAPSv1.1, 5) assimilating GNSS and airborne RO observations (Spire, PlanetIQ, GeoOptics, FY3x, Yunyao, Tianmu) from the Radio Occultation Modeling Experiment (ROMEX) utilizing a two-dimensional (2D) forward operator yielded significant improvements in NAVGEM forecasts of low- to midlevel moisture, NH geopotential height, temperature and wind speed, and 6) the implementation of Desrozier's diagnostic to estimate satellite observation errors significantly improved 5-day global NAVGEM forecasts of geopotential height, temperature and moisture compared to the current operational system.

Defense Impact/Significance: The computing platforms provided by the HPCMP offer incredible computational resources that make possible the running of experiments involving millions of observations. These resources also provide a common environment for collaboration and the rapid development of NRL's multiple data-assimilation systems. Large, common datasets can be stored and accessed by many researchers, greatly facilitating collaboration between NRL scientists at different locations (Monterey, Stennis, and DC) and scientists in academia, government, and other laboratories. The advancements of the NEPTUNE, JEDI, NAVDAS-AR, NAVGEM, and COAMPS-AR systems would not have been possible without the HPCMP systems. The core and future of Navy data-assimilation capabilities are being mostly, and in many cases solely, developed using the resources provided by HPCMP. In summary, the ability to access the HPCMP resources is critical to prepare technology for successful transfer to operations.

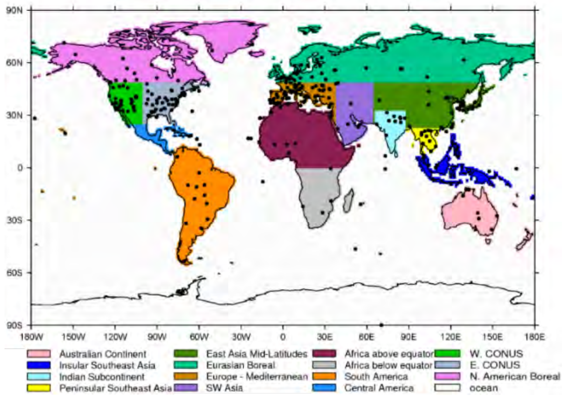

Figure 1. Verification regions used for ENAAPS evaluation.

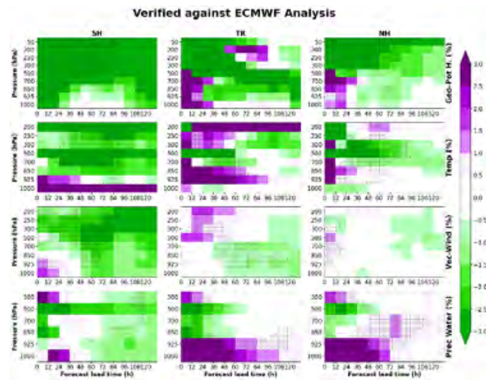

Figure 2. Assimilation of all ROMEX data with a bias correction significantly improves nearly all NAVGEM model variable forecasts out to 5 days

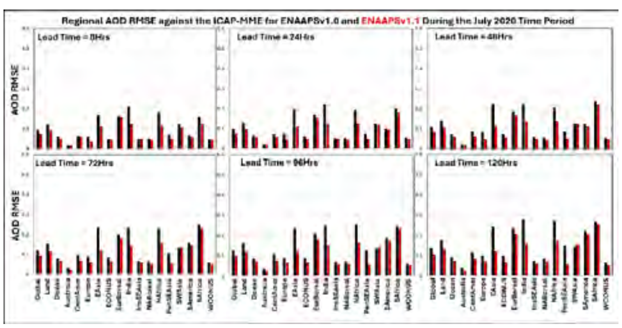

Figure 3. Regional aerosol optical depth (AOD) root-mean-square error (RMSE) for ENAAPSv1.0 (black) and ENAAPS v1.1 (red) as a function of forecast lead time.

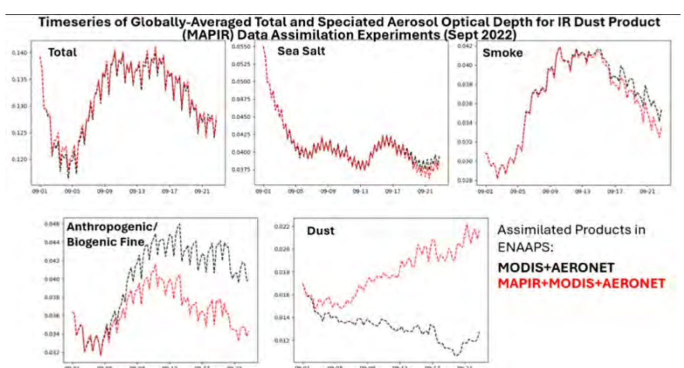

Figure 4. Globally averaged AOD time series (total + speciated) for ENAAPSv1.1 assimilation experiments in which Mineral Aerosol Profiling from Infrared Radiances (MAPIR) dust products were assimilated in addition to standard MODIS and AERONET AOD products and were compared to a baseline MODIS + AERONET assimilation run. While inclusion of MAPIR did not influence the overall total AOD, it did have a significant impact on aerosol speciation. All experiment runs were conducted on DSRC Narwhal using DA project hours.

THIS PAGE INTENTIONALLY LEFT BLANK

SAS

Space and Astrophysical Science

The Space and Astrophysical Science (SAS) CTA advances the understanding and prediction of the Earth's atmosphere and space environment to support military operations and to mitigate environmental impacts on operational systems. The CTA applies mathematics, computational science, and engineering to the analysis, modeling, and simulation of the space and near-space domain and the natural and artificial objects within it. This effort spans foundational discovery research, including studies of the Sun-Earth system, solar activity and its coupling to the Earth's atmosphere, ionosphere, and near-Earth space, and the unique physical processes governing celestial sources and space plasmas.

SAS integrates a broad suite of physical and empirical models with observational data to deliver increasingly predictive capabilities for defense applications in the extended operational environment. The CTA draws on expertise across atomic and molecular physics, plasma physics, applied optics, radiation effects, electronic warfare, directed-energy systems, astronautics and propulsion, orbital mechanics, space situational awareness, and remote sensing. By unifying these disciplines within a computational framework, SAS enables improved resilience, awareness, and operational effectiveness for space-enabled military systems.

Title: Searches for Millisecond Pulsars and Pulsar Emission Modeling
Author(s): P.S. Ray[1] and J. Deneva[2]
Affiliation(s): [1]U.S. Naval Research Laboratory, Washington, DC; [2]George Mason University, Fairfax, VA, resident at U.S. Naval Research Laboratory, Washington, DC
CTA: SAS

Computer Resources: Penguin TrueHPC [NAVY, MS]

Research Objectives: The first goal of this project is to search for millisecond pulsars in ground-based data from the Robert C. Byrd Green Bank Telescope (GBT) in West Virginia as well as a backlog of survey data from the decommissioned Arecibo Telescope in Puerto Rico. These searches require high-performance computing resources because of the massive parameter spaces that must be searched.

Methodology: We use custom codes to search for pulsations in our radio data sets. These correct for frequency-dependent delays caused by interstellar dispersion and variable Doppler shifts caused by orbital acceleration in a binary system, then search over a broad range of candidate frequencies using very large Fourier transforms and harmonic summing. We split up the trials over a set of nodes on the cluster. In the case of targeted searches of a small number of sources (like our GBT projects), a pulsation search selects few enough candidate signals that it is feasible to examine by eye the diagnostic plots made for all of them and to pick out any new pulsars among spurious candidates due to noise or terrestrial interference. In the case of surveys that cover a very large sky area (like our Arecibo 327 MHz pulsar survey) the pulsation search code finds millions of candidate signals over the entire survey data set, the vast majority of which are spurious. The set of candidate signals is too large for the corresponding diagnostic plots to be examined by eye. In this case, we apply a separate classification code to the candidates in order to rank them based on the likelihood that they are pulsars and then examine by eye the diagnostics for the highest-ranked candidates.

Results: On Nautilus at Navy DSRC, we processed GBT data on 41 targets. Some of them were selected by their locations within the error ellipses of Fermi-unidentified sources with pulsar-like gamma-ray spectra, and others were selected based on their steep, pulsar-like radio spectra in data from the VLA Low-band Ionosphere and Transient Experiment (VLITE). We also finished processing backlog data from the Arecibo 327 MHz drift survey for pulsars and transients (AO327) and discovered nine new pulsars and rotating radio transients (RRATs). This brings up the total number of AO327 discoveries to 105 [1]. Even though data reduction is completed for the AO327 survey data set, we expect more new discoveries as we experiment with applying different automated classification and ranking algorithms to the large, survey-wide set of candidate signals.

Defense Impact/Significance: The main goal is to identify millisecond pulsars that are very stable rotators and therefore useful for detecting gravitational waves with a pulsar timing array (PTA). Among the roughly 4300 known pulsars, only 35 fit this criterion, and any addition to this set is a significant contribution to the nanohertz gravitational wave detection effort, as it improves the sensitivity of the PTA. The PTA approach to gravitational wave detection is complementary to LIGO and sensitive to a different range of gravitational wave frequencies. The first PTA detection of the nanohertz gravitational wave background was published in 2023. An additional goal of our GBT pulsar searches is to determine the nature of an excess of gamma-ray emission from the Galactic Center region that was discovered by the Fermi spacecraft. Currently, there are two competing hypotheses for its origin: a population of gamma-emitting millisecond pulsars, or annihilation of dark matter particles.

References

[1] NANOGrav, “AO327 New Pulsars,” AO327 Survey. [Online]. Available: http://ao327.nanograv.org/newpulsars [Accessed: Feb. 19, 2026].

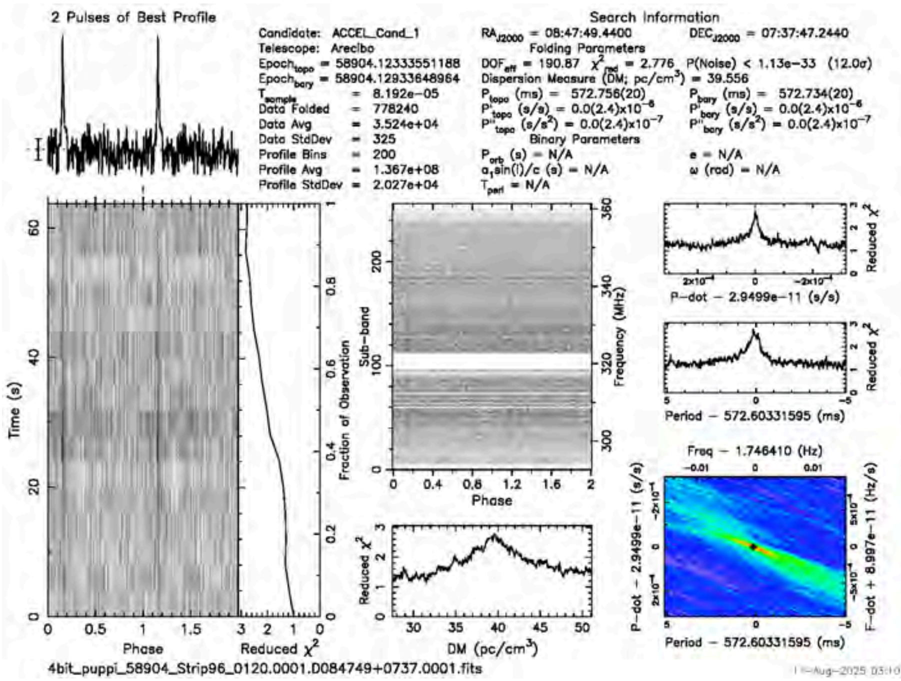

Figure 1. Discovery of PSR J0847+07, with a 0.572 s rotation period, in data from the AO327 survey. This pulsar was found by the Fourier-based periodicity search part of our code, as it emits consistently and there are many pulses within the 1-minute integration time. The white, horizontal bands in the frequency subband vs. pulse phase (middle top) panel correspond to narrowband terrestrial interference that was excised during data reduction.

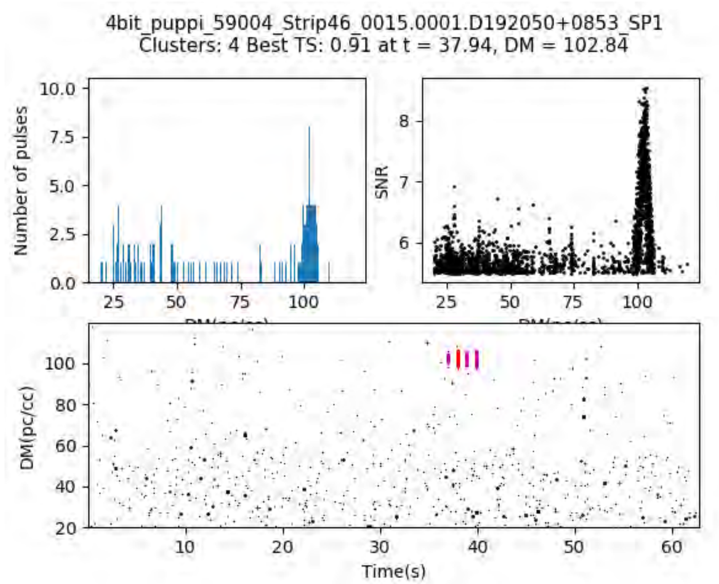

Figure 2. Discovery of PSR J1920+08, with a rotation period of 0.955 s, in data from the AO327 survey. This pulsar was found by the single-pulse search part of our code tailored to detect astrophysical radio transients. This pulsar appears to emit only very infrequently — here, only four pulses within the 1-minute integration time. The bottom panel shows the pulses in the search space defined by trial dispersion measure (DM) on the vertical axis and time on the horizontal axis. The pulses are color-coded to indicate they have the dispersion signature characteristic of astrophysical signals. The many black dots in the panel correspond to events that do not exhibit this signature.

Title: Modeling Ionospheric Irregularities due to Geomagnetic Storms
Author(s): J. Haiducek,[1] H. Trung,[2] and J. Helmboldt[1]
Affiliation(s): [1]U.S. Naval Research Laboratory, Washington, DC; [2]National Research Council Postdoctoral Research Associate at the U.S. Naval Research Laboratory, Washington, DC
CTA: SAS

Computer Resources: HPE Cray EX, Penguin TrueHPC [NAVY, MS]

Research Objectives: We plan to use the SAMI3 (SAMI3 is Also a Model of the Ionosphere) to simulate ionospheric irregularities generated during geomagnetic storms in conjunction with the Space Weather Modeling Framework (SWMF). Observations by GPS receiver networks, the NRL-sponsored Very Large Array (VLA) Low-band Ionosphere and Transient Experiment (VLITE) and the Deployable Low-band Ionosphere and Transient Experiment (DLITE) will be used to validate and improve the models.

Methodology: Storm-time ionospheric irregularities depend strongly on magnetospheric driving, including particle precipitation and magnetospherically imposed potentials. We plan to model the effects of these processes by developing a coupling interface that passes magnetospheric potentials and precipitation rates from the SWMF into SAMI3, replacing the climatological precipitation and potential estimates currently used within SAMI3. This affords several advantages, including potentially better ability to capture storm-time dynamics, higher time resolution (compared with the 3-hour time resolution of the Kp index, which drives the empirical particle precipitation model). The design of the coupling interface involves using the AMIE file format, which is also used by other magnetospheric models and observational datasets, opening up the possibility of using the same interface to conduct comparative experiments in which we assess the relative effectiveness of various models and datasets in conjunction with SAMI3.

Results: We have identified existing software programs that can convert the required SWMF outputs into an appropriate form for use within SAMI3 and are in the process of modifying SAMI3 to read these SWMF outputs from disk for a file-based, one-way coupling. Because the coupling is file-based and one-way, we can run the SWMF simulations ahead of completing the SAMI3 coupling interface, and we have already done so for several storm events of interest. For each storm, we ran an SWMF simulation using observed solar wind inputs from the L1 Lagrange point and a second simulation using forecasted solar wind inputs derived from heliospheric simulations. The simulated solar wind input provides a longer forecast lead time (days versus hours) but with reduced accuracy. We have also performed a multifluid simulation using SWMF to assess the influence of ionospheric outflow on the lunar region.

Defense Impact/Significance: Ionospheric irregularities can impact defense operations by altering radio signals used for radar and communications. The simulation tools and techniques developed in this program will provide insights into how these irregularities develop and will influence the future advancement of ionospheric forecasting capabilities.

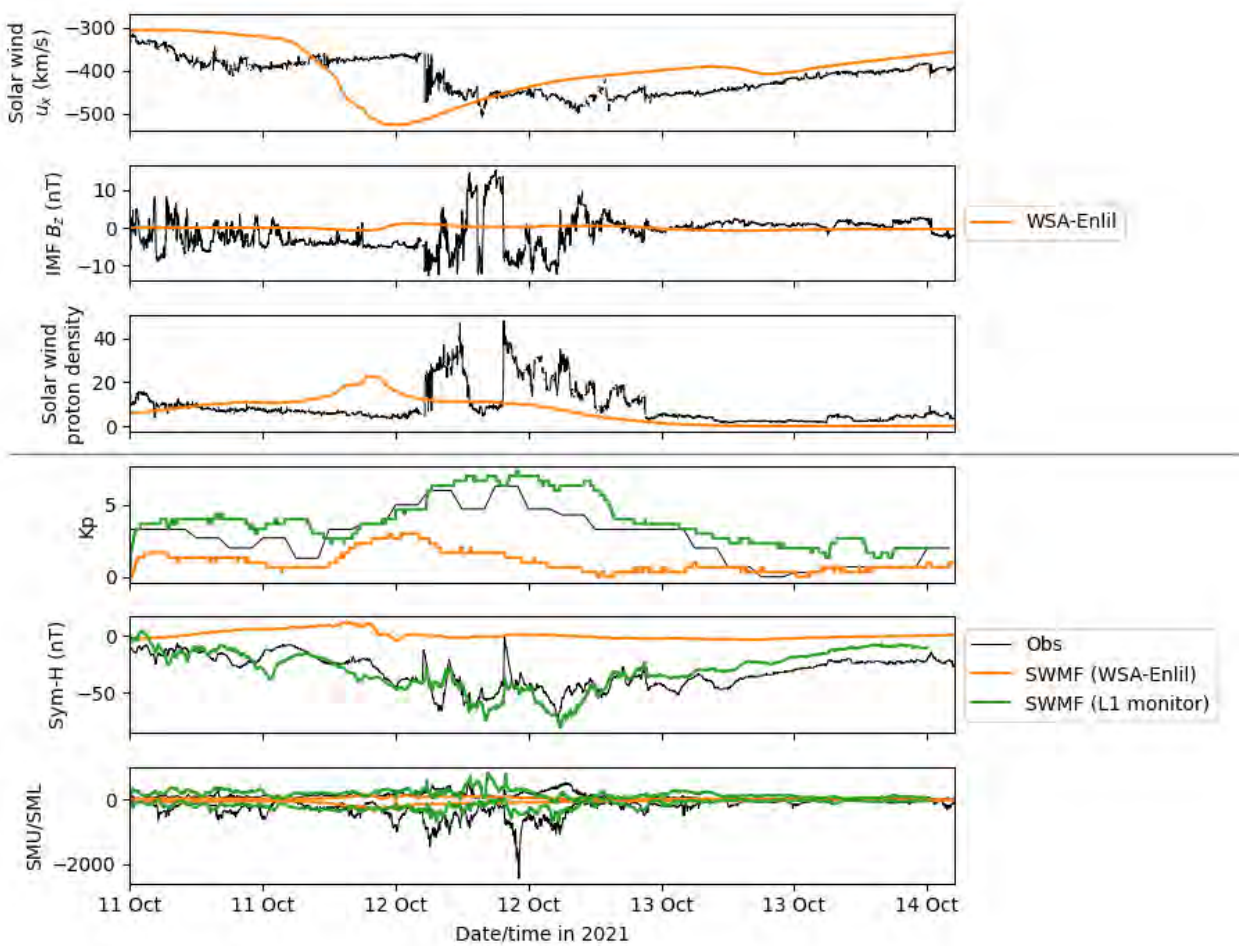

Figure 1. Plots of SWMF inputs (solar wind parameters) and outputs (geomagnetic indices) for a geomagnetic storm on October 12–13, 2021. Observed values (in black) are compared with an SWMF model run driven by simulated solar wind from the WSA-Enlil heliosphere model (orange) and an SWMF model run driven by observed solar wind parameters obtained from spacecraft at the Sun-Earth L1 Lagrange point (green). From top to bottom: X-component of solar wind velocity, Z-component of the interplanetary magnetic field (IMF) carried by the solar wind, solar wind proton density, Kp index (a geomagnetic index computed observationally from ground-based magnetometers), Sym-H (a geomagnetic index computed observationally from equatorial-zone ground-based magnetometers), and SMU/SML (geomagnetic indices computed observationally from auroral-zone ground-based magnetometers).

Title: Particle-in-Cell Simulations of Plasma Waves and Turbulence
Author(s): A.R. Soto-Chavez, C. Brown and J.D. Huba
Affiliation(s): U.S. Naval Research Laboratory, Washington, DC
CTA: SAS

Computer Resources: HPE Cray EX [ARL, MD]; HPE Cray EX, Penguin TrueHPC [NAVY, MS]

Research Objectives: 1) Support the US NRL, SMART (launching February 2026) and Vanguard Romeo (VR) experiment programs by developing the capability to simulate near-Earth space plasmas on both a kinetic scale and a macroscopic scale in order to predict and assess possible scenarios. 2) Gain deeper understanding of the nonlinear induced scattering process in a turbulent plasma in the ionosphere. 3) Also, support the U.S. NRL Space Chamber Experiments and the IARPA-SINTRA program by performing nonlinear simulations of plasma-beam instabilities and plasma solitons, and apply the understanding of turbulence gained from the SMART experiment to the turbulence in the solar wind. 4) Finally, validate global wave propagation models against test cases provided by nature, such as lightning-generated whistler waves, and determine the volume and location of the whistler cavity formed when VLF sources launch waves into the quiet plasmasphere, utilizing realistic ionospheric density gradients using the code SAMI3.

Methodology: We used the Tristan-MP code, which is a massively parallel (MP) particle-in-cell (PIC) code that has been tested on HPC systems for the kinetic physics and the 3D SAMI3 code for the global ionosphere physics. We solved highly nonlinear partial differential equations using dual computational approaches: spectral and finite difference algorithms. We also performed PIC simulations to investigate the formation of lower-hybrid (LH) waves in complex multiring plasma systems. We successfully developed and carefully implemented multiple ring distributions in a PIC simulation.

Results: We developed and tested an advanced simulation code to solve the two-dimensional (2D) electron magnetohydrodynamics (MHD) equations with a source in order to explain electromagnetic (EM) soliton structures in the whistler frequency range. EM solitons are more resistant to resonant damping interactions in typical ionospheric plasmas, making them more likely to be observable. This work pioneered numerical solutions to critical nonlinear interactions with applications to the IARPA-SINTRA program and to support the NRL Space Chamber. Results demonstrated both dynamical and topological soliton-like structures in the whistler frequency range; see Fig. 1. A manuscript is being prepared for publication submission. The PIC simulations revealed that LH waves generated in these systems efficiently scatter into whistler waves, a key finding toward better understanding the actual SMART experiment; see Fig 2. We also continued the work of LH generation and whistler wave scattering in solar flare environments with PIC simulations, which was invited for a presentation. In order to validate methods for global wave propagation, we used the HPC to track the final distribution of the massive ray ensemble, and we identified the boundaries of the whistler cavity formed by a localized source (see Fig. 3). We found that the trapped ray fronts concentrated in a specific L-shell range ($L \approx 2-3$) and spanned a significant longitudinal extent.

Defense Impact/Significance: The SMART experiment and associated simulations will ultimately demonstrate the formation of turbulence and its coupling between the ionosphere and the magnetosphere. The production of whistler waves and their impact on the magnetospheric particles is an active area of research in the space physics community. It is within Earth’s magnetosphere that most defense activities and U.S. Navy space-based assets operate. Thus, we must be able to extrapolate these local measurements to a global scale. This work demonstrates that coupling the self-consistent, physics-based SAMI3 model with large-scale ray tracing allows us to infer global wave propagation effects and for different plasmasphere states. Therefore, understanding both processes in the space environment gives the Department of the Navy new capabilities to predict, prepare for, respond to, and recover from space weather events. In summary, this work addresses the threat of orbital debris impact to space missions, communication infrastructure, and national security assets.

(a) (b)

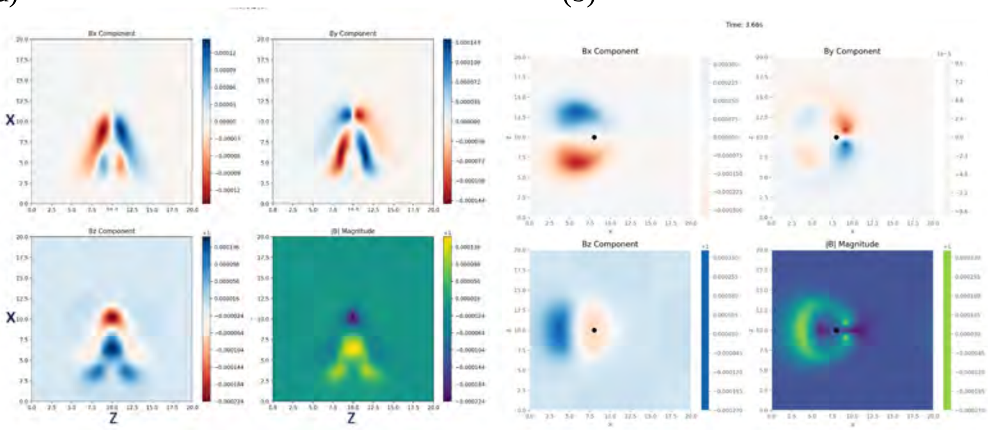

(c)

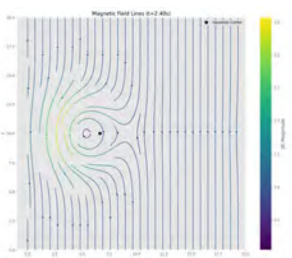

Figure 1. (a) The magnetic field components showing soliton-like structures along with the magnetic field |B|, in the whistler frequency range, from the 2D electron MHD simulation. (b) Similar to (a), but here the source is launched perpendicularly to the magnetic field. (c) The magnetic field streamlines as the Gaussian source moves perpendicularly through them.

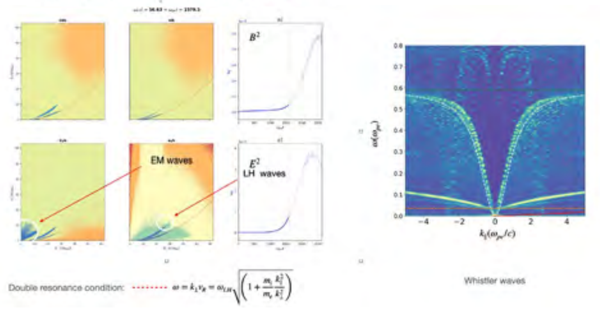

Figure 2. Left: 2D Spectral plots in k-space of the magnetic and electric field component (bottom row) indicating that the LH waves and EM waves are generated in the multiring simulation. Right: Spectrogram of the EM wave in frequency and k-space indicating the scattered whistler waves are formed.

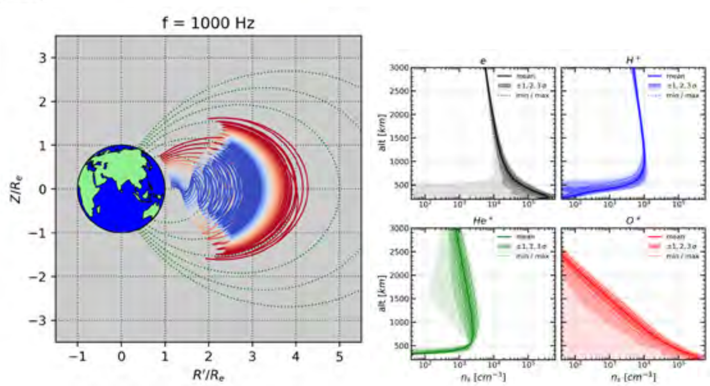

Figure 3. Left: 2D visualization of ray-propagation trajectories for a modeled lightning strike for a single frequency of 1000 Hz. Right: 1D altitude profiles of SAMI3 density data for four species (e^-, H^+, He^+, O^+).

Title: Global Kinetic Simulations of Space Plasma Waves and Turbulence
Author(s): C. Crabtree, C. Brown, E. Lichko, A.R. Soto-Chavez, and V. Tangri
Affiliation(s): U.S. Naval Research Laboratory, Washington DC
CTA: SAS

Computer Resources: HPE Cray EX [ARL, OH], [NAVY, MS]; Penguin TrueHPC [NAVY, MS]

Research Objectives: 1) Support the US NRL, SMART (launching Feb 2026) and Vanguard Romeo (VR) experimental programs by developing a new method of kinetic plasma simulation called wave-in-cell (WIC). This method treats waves and resonant particles as computational particles in a particle-in-cell (PIC)-type algorithm. It requires a significant amount of both PIC and WIC simulations both to determine critical mission parameters rapidly and to understand the measured physical processes after the experiments are performed. 2) Support the IARPA SINTRA program in simulating the interactions between charged orbital debris and background ionospheric plasmas. 3) Study the lower-hybrid turbulence of highly compressed current sheets and the impact on magnetic reconnection that controls Earth's space weather.

Methodology: We used the VPIC, Tristan massively parallel (MP) PIC code, the GKeyll multifluid code, the three-dimensional (3D) SAMI3 global ionospheric physics code, and a homegrown whistler wave ray-tracing code.

Results: 1. Validating methods for global wave propagation: using the HPC to track the propagation of a massive ensemble of whistler wave ray trajectories through a numerically simulated global ionosphere/plasmasphere using SAMI3, we successfully reproduced the observed spectrogram as recorded by the NASA Van Allen Probes mission of a lightning-generated whistler wave train (see Fig. 1). These ray trajectories are a critical component of a new wave-kinetic code that self-consistently evolves waves and resonant particles on global scales. The comparison of observations with computational artifacts is an important step in developing this new simulation capability. 2. We performed two-fluid simulations with the Gkeyll multifluid code to investigate lower-hybrid wave generation in current sheets compressed below the ion gyroradius and found quantitative agreement with analytical theory (see Fig. 2). The simulations show that sheared electron flows driven by ambipolar electric fields provide the free energy for lower-hybrid turbulence, with implications for anomalous resistivity, viscosity, and magnetic reconnection dynamics. Magnetic reconnection in the Earth's magnetosphere is one of the primary controllers of space weather that can impact defense space assets. 3. We used high-resolution VPIC particle-in-cell simulations of field-aligned, sheared ion flows with realistic mass ratio and resolved kinetic scales to study the long-term evolution of electrostatic fluctuations in magnetized plasmas. The simulations show (see Fig. 3) that such flows self-consistently generate broadband, multimode ion-cyclotron harmonics and multiscale coherent structures consistent with theory, while ongoing parameter scans examine harmonic amplitudes, critical shear effects, and electron temperature sensitivity. These simulations show how shared flow around orbital debris impacts the plasma waves, which may be used as a surrogate detection method for orbital debris.

Defense Impact/Significance: The SMART experiment and associated simulations will ultimately demonstrate the formation of turbulence and its coupling between the ionosphere and the magnetosphere. The production of whistler waves and their impact on the magnetospheric particles is an active area of research in the space physics community. It is within Earth's magnetosphere that most defense activities and U.S. Navy space-based assets operate. This work demonstrates that coupling the self-consistent, physics-based SAMI3 model with large-scale ray tracing allows us to infer global wave propagation effects for different plasmasphere states. Therefore, understanding both processes in the space environment gives the Department of the Navy new capabilities to predict, prepare for, respond to, and recover from space weather events.

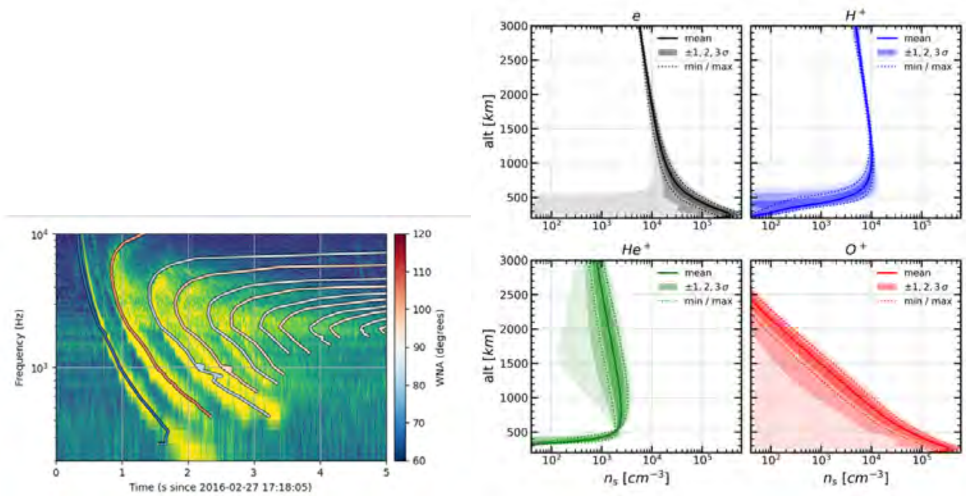

Figure 1. Left: Spectrogram created from ray-propagation trajectories for a modeled lightning strike for a single frequency of 1000 Hz. Right: 1D altitude profiles of SAMI3 density data for four species (e^-, H^+, He^+, O^+).

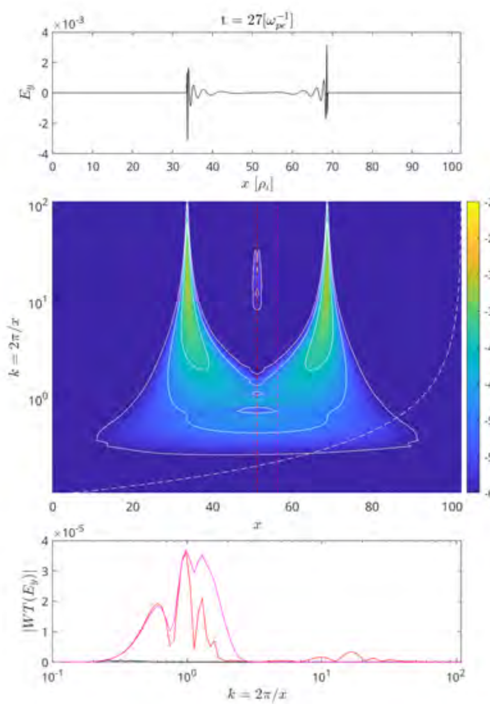

Figure 2. (top) Wave electric field profile across the current sheet. (middle) wavenumber vs. wavelength x. (bottom) wave energy density vs. wavenumber.

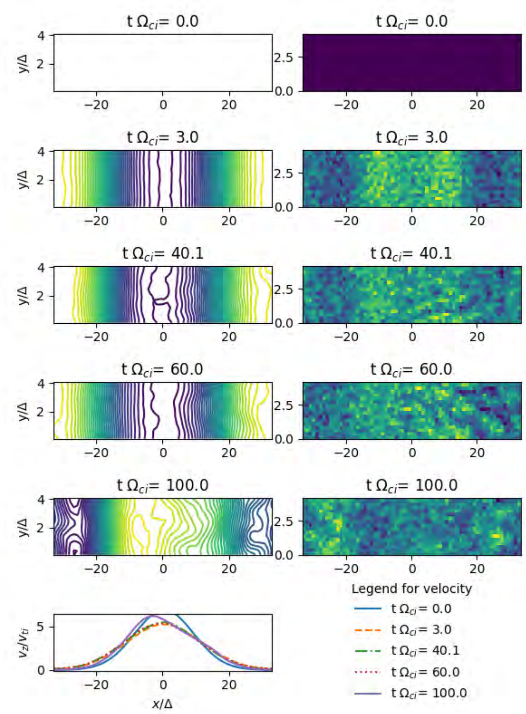

Figure 3. Plasma density around a flow layer at different times showing turbulence generation.

Title: Navy Ionosphere Model for Operations
Author(s): M.R. Burleigh,[1] S.E. McDonald,[1] J.L. Tate[2], and E. Morgan[1]
Affiliation(s): [1]U.S. Naval Research Laboratory, Washington, DC; [2]Computational Physics, Inc., Springfield, VA
CTA: SAS

Computer Resources: HPE Cray EX [ARL, OH], [NAVY, MS]; Penguin TrueHPC [NAVY, MS]

Research Objectives: The objective of this effort is to develop and improve a physics-based ionosphere model coupled to an ionospheric data-assimilation system that provides global and regional electron density specifications and short-term forecasts (0–24 hours). This capability forms the basis of a Navy operational ionospheric forecasting system that runs at multiple resolutions and is fully coupled to operational atmospheric forecast models. In FY25, the main objectives were to continue development and testing of incremental releases of the Next-generation Ionosphere Model for Operations (NIMO) and to continue to improve our understanding of the lower atmospheric effects on the ionosphere using SAMI3 (Another Model of the Ionosphere) coupled to whole-atmosphere models.

Methodology: NIMO consists of the physics-based ionosphere model, SAMI3, and a three-dimensional variational (3DVAR) data-assimilation system (IDA4D) that can ingest a wide variety of ionospheric datasets. NIMO utilizes the Earth System Modeling Framework (ESMF) for interpolating between the ionosphere and data-assimilation grids. For current testing and development, NIMO uses an empirical thermosphere comprising NRLMSIS 2.0 and HWM.

NIMO 2.0 includes enhancements to the SAMI model driver, to include an ensemble-like approach to reduce model bias, and the implementation of a new data-assimilation system, ANCHOR, which extracts and assimilates "anchor points" from data into horizontal maps of the ionospheric parameters.

To investigate lower-atmospheric effects on the ionosphere, SAMI3 is coupled to several whole-atmosphere models, including the Whole Atmosphere Community Climate Model Extended (WACCM-X), the Thermosphere Ionosphere Mesosphere Electrodynamics General Circulation Model (TIME-GCM), and the Navy Environmental Prediction System Utilizing the NUMA Engine (NEPTUNE).

Results: In FY25, HPC resources were used to perform multiple real-time and historical simulations with NIMO and supported the successful transitions of NIMO v1.2.0 and NIMO 1.2.1 into operations. The use of these resources allowed us to provide critical ad hoc support for naval operations during operational outages and to simulate hotfixes for application support ahead of operational promotions to ensure smooth transitions into the operational environment. We produced and investigated near-real-time operational verification products to monitor ionospheric product quality, providing essential statistics for both operations and research and development. Additional simulations were performed to investigate the impacts of novel observations for model enhancements, further increasing the capability of NIMO to produce quality nowcasts of the ionosphere.

In addition, multiple historic simulations were run with HPC resources to support and validate the development of NIMO 2.0, the next ionospheric model system, which will be transitioned to operations in FY26. These runs allowed us to evaluate changes to both the forecast model and the data-assimilation model to facilitate development and to quantify improvements over the current operational model system.

HPC resources were also used to run several simulations of SAMI3 coupled to a variety of whole-atmosphere models, such as WACCM-X, TIME-GCM, and NEPTUNE, to investigate lower-atmospheric effects on the ionosphere. Results from these simulations, as well as the NIMO work discussed above, identified areas of model improvement for SAMI3 that have been implemented.

Defense Impact/Significance: Development of an operational ionospheric forecast model will aid in the numerical forecasting of high-frequency (HF) radio wave propagation through the Earth's atmosphere and ionosphere across the range of conditions relevant to defense and Navy operations.

Acknowledgment: This research is supported by the Office of Naval Research.

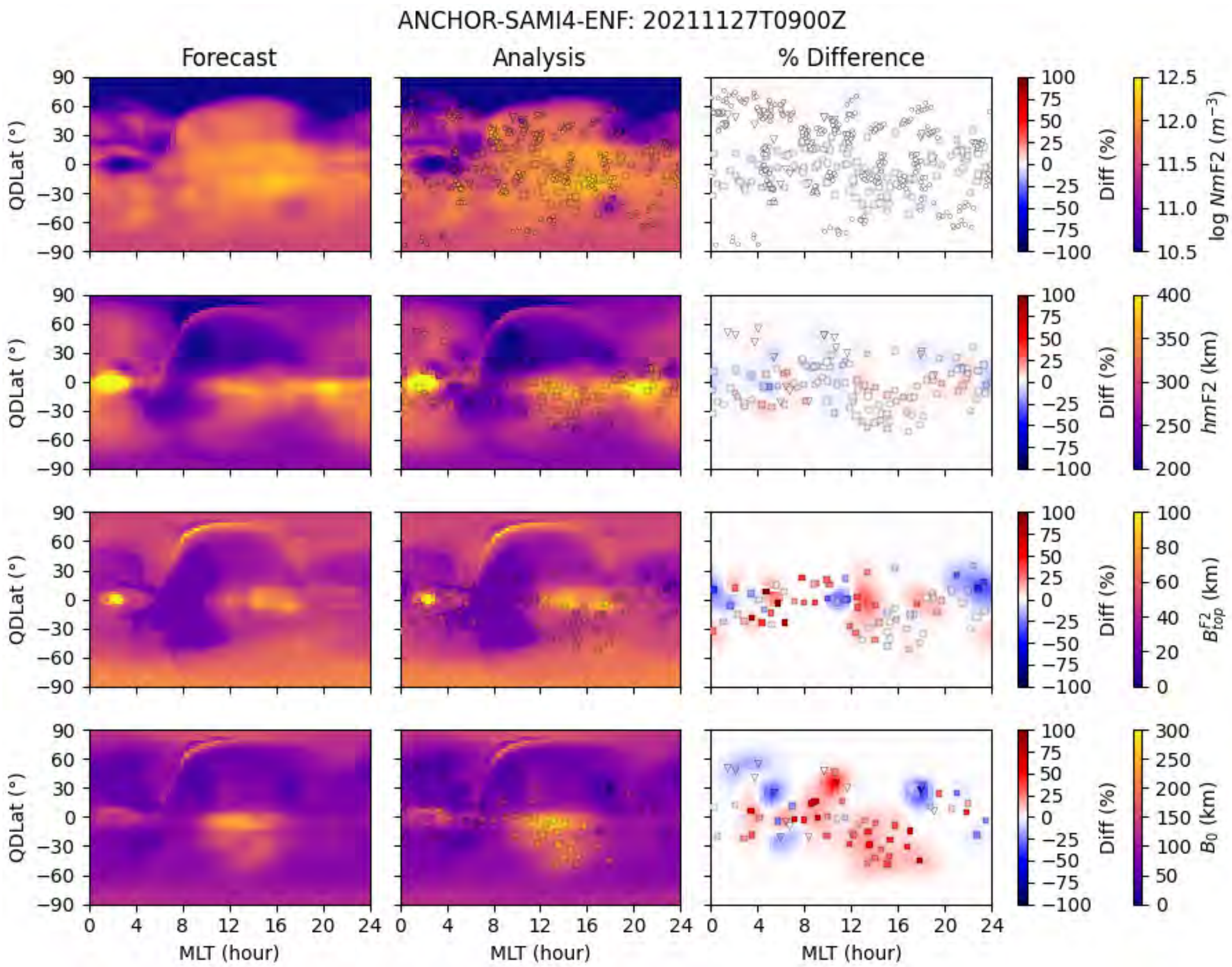

Figure 1. Results of ANCHOR assimilation for ionospheric analysis specification at 0900Z on November 27, 2021. The four rows correspond to four "anchor point" parameters used to reconstruct an electron density profile for the ionosphere.

Title: Thermosphere & Ionosphere Numerical Models and Ensemble Methods
Author(s): D.P. Drob, M. Jones, and J. Emmert
Affiliation(s): U.S. Naval Research Laboratory, Washington, DC
CTA: SAS

Computer Resources: HPE Cray EX [ARL, OH], [NAVY, MS]; Penguin TrueHPC [NAVY, MS]

Research Objectives: The prediction of space weather effects is required for US Navy tactical planning purposes to maximize the effectiveness of affected systems by adapting to the variable environment. The behavior of the ionosphere at high and polar latitudes has important effects on the performance of HF radio communication and over-the-horizon radar systems. This year's effort improves the high-latitude model physics within the US Navy's Next-Generation Ionosphere Model for Operations (NIMO 2.0) ensemble specification and forecasting system.

Methodology: To date, operational NIMO specification and forecast products have been limited to the low- and midlatitude ionosphere. To represent the high-latitude/polar ionosphere, particularly during geomagnetic storms, improvements to the SAMI4 physics-based model component of the NIMO 2.0 system are required. First, an accurate and computationally efficient way to specify the time-dependent evolution of the transition between open and closed geomagnetic field lines within SAMI4 is required. This time dependence results from the interaction of the variable solar wind plasma and the embedded solar magnetic field with the Earth's magnetic field as the Earth rotates. Second, the subsequent effects of ionizing energetic particle precipitation along open geomagnetic field lines are needed. Particle precipitation is particularly enhanced in both energy and particle density near the plasmapause boundary, resulting in the Earth's auroral ovals. Soft-particle precipitation also sustains a weak steady-state ionosphere across the entire polar cap, even during continuous polar nighttime winter conditions.

Results: To specify the time-dependent location of the plasmapause boundary, an observationally driven empirical model that is a function of measured geomagnetic field fluctuations, longitude, and time of day was integrated into the SAMI4 model. In tandem, the existing legacy particle precipitation model for electron impact ionization and electron temperature heating at high latitudes was updated to account for electron impact ionization as a function of the atmospheric column, based on an observationally driven empirical model of the average and total energy fluxes at the top of the atmosphere. Figure 1 shows ionospheric auroral electron density enhancements at 110 km altitude compared to dayside photoproduction at low- to midlatitudes. The left panel shows typical quiet geomagnetic conditions, while the right panel shows an example of the expansion and intense auroral precipitation during disturbed geomagnetic storm-time conditions. Figure 2 shows the corresponding typical quiet-time extent of the plasmasphere (left), while the right panel shows its compression and contraction due to the expansion of the auroral oval and the opening of closed geomagnetic field lines to the solar wind plasma. These new approaches were tested for numerical stability and then were tuned for geophysical accuracy. The additional run-time costs were then evaluated for operational efficacy directly within the NIMO 2.0 system. Importantly, the new model physics reduced the NIMO 2.0 system forecast model wall-clock run times. This is because previously, anomalously low plasma densities and associated strong temperature gradients near the plasmapause boundary resulted in pockets of anomalously high supersonic polar ion outflow velocities that subsequently required smaller numerical integration time steps to maintain numerical model accuracy and stability.

Defense Impact/Significance: The effort addresses the Navy and defense long-term need for environmental prediction of space weather effects for tactical planning purposes, as well as the maximization of defense-relevant space systems' performance through adaptation to the variable environment according to SECNAVINST 2400.2A.

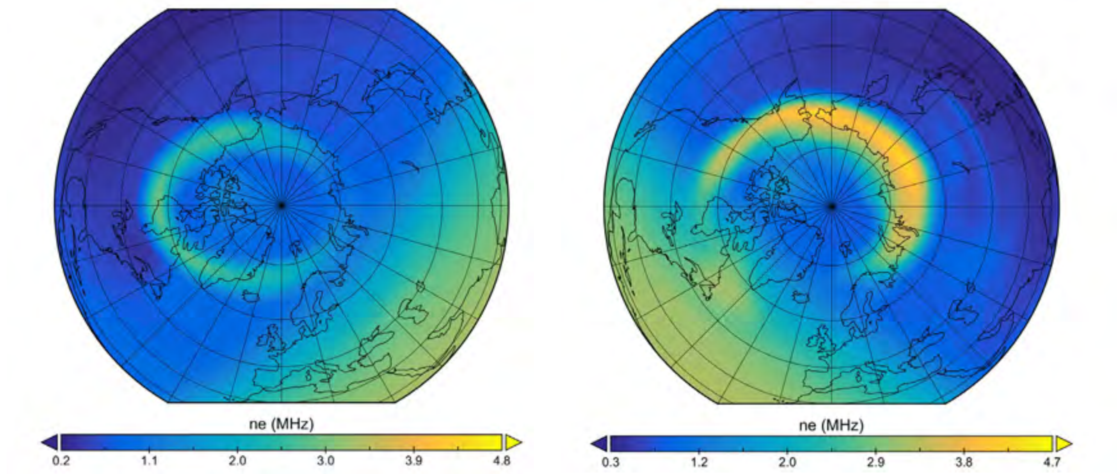

Figure 1. Ionospheric auroral electron density enhancements at 110 km altitude compared to dayside photoproduction at low- to midlatitudes. The left panel shows typical, quiet geomagnetic conditions, while the right panel shows an example of the expansion and intense auroral precipitation during disturbed geomagnetic storm-time conditions.

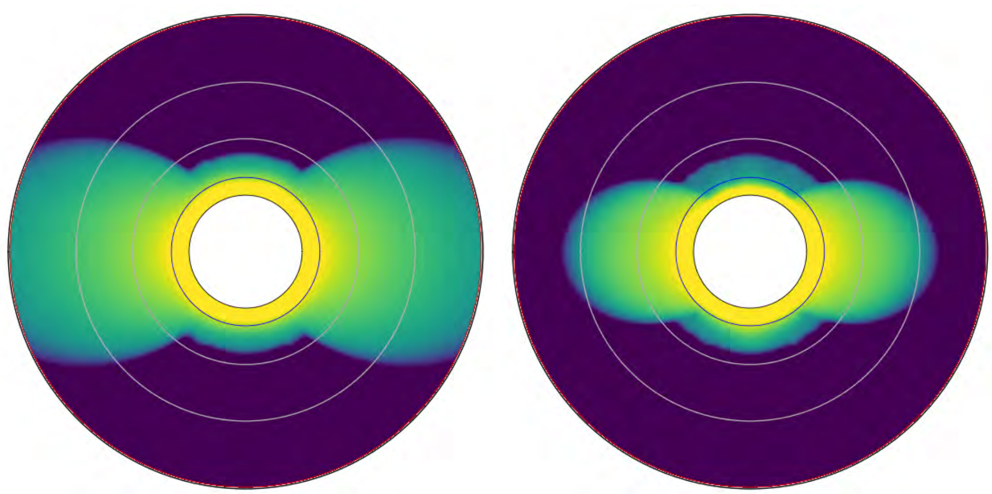

Figure 2. The left panel shows the corresponding typical quiet-time extent of the plasmasphere. The right panel shows its compression and contraction, a result of the auroral oval's expansion and the opening of closed geomagnetic field lines to the solar wind plasma. The apex altitude of the plasmasphere typically extends out to 6 R_e (Earth radii) during undisturbed geomagnetic conditions and can be compressed to approximately 2 R_e during a geomagnetic storm. The outer extent of the images corresponds to the altitude of a geostationary satellite (stated as 20,200 km or 4.2 R_e). Plasma density ranges from 1×10^6 electrons/cm^3 to 1×10^4 electrons/cm^3 in the ionosphere below approximately 500 km altitude. The plasmasphere's density ranges from 2×10^2 electrons/cm^3 to 1×10^4 electrons/cm^3. Across the plasmapause, plasma density rapidly falls to less than 10 electrons/cm^3.

THIS PAGE INTENTIONALLY LEFT BLANK

EQM

Environmental Quality Modeling and Simulation

The Environmental Quality Modeling and Simulation (EQM) CTA supports the assessment of interactions between the activities of the defense community and the natural environment, including both the environmental impacts of defense operations and the effects of environmental conditions on mission execution. EQM focuses on high-resolution, physics-based modeling of coupled hydrologic, geophysical, and geochemical processes across the atmosphere, the land surface, and the subsurface. These models capture multiconstituent fate and transport and their interactions with ecological systems and human activities, enabling comprehensive analysis of complex environmental systems.

Within the defense community, EQM capabilities support a wide range of applications, from environmental stewardship and restoration of natural and cultural resources on military installations to evaluation of environmental constraints on mobility and operations in contested and austere environments. By providing predictive, integrated environmental assessments, EQM enables informed decision-making that balances operational effectiveness with long-term environmental sustainability.

Title: Data-Driven Prediction of Global Seabed Environmental Properties
Author(s): B.J. Phrampus and T.R. Lee
Affiliation(s): U.S. Naval Research Laboratory, Stennis Space Center, MS
CTA: EQM

Computer Resources: HPE Cray EX [NAVY, MS]

Research objectives: NRL's Geology/Geophysics section aims to build, sustain, and update a data-driven, global, digital seabed model with estimates of Navy-relevant hydrological, biological, and geological properties. The prediction of high-resolution products and/or the utilization of large ("big data") datasets require the use of HPC systems to produce these models in an acceptable time frame. The objective of this effort is to utilize HPC capabilities available to the defense community to facilitate the production of necessary models, to build deliverables, and to maintain/test the scalability of future code development in support of the operational Navy. Such a capability allows the Navy to have a fast, repeatable method for providing critical environmental information for mission planning, in situ performance prediction, and deployment planning.

Methodology: We have developed a geospatial machine learning (GML) system to utilize seabed data to predict global properties. GML is used to link the production of geospatial statistics, machine learning (ML), and deep learning (DL) prediction of environmental parameters, as well as simulation of geophysical properties, into one, modular codebase. GML is currently used to produce regional to global databases and deliverables for use in the operational Navy. Here, we aim to leverage the HPC computational capabilities to improve upon the GML codebase to produce models at higher global resolutions (i.e., global 1 arc-minute), to utilize larger datasets, and to use more advanced ML/DL algorithms. These efforts will accelerate the production of Navy-relevant properties with more accurate and realistic deliverables.

Results: The HPC system at Navy DSRC is used with the GML framework to produce global and regional grids of geophysical and geoacoustic significance. This process is iterative and involves prediction-optimization and feature-selection methodologies, which can take significant computational power to complete. The HPC allows these methods to complete in reasonable and tactically useful timeframes. We continue to work, in conjunction with the High Performance Computing Modernization Program's Productivity and Enhancement Training (PET) team, to streamline and optimize our workflow to more rapidly and accurately produce environmental parameters. These results are used in products that are publicly published (e.g., Fig. 1), but most importantly, some products are used in support of both NAVO and NRL efforts to produce updated products for OPNAV. Finally, NAVOCEANO personnel utilize GML and the HPC in conjunction with NRL to update products, databases, and TDAs.

Defense Impact/Significance: The computational resources provided by the HPC for the defense community are in direct support of the Navy's seafloor prediction capabilities. Further, this project is aligned with FY26 OPNAV N2N6E Naval Oceanography RDT&E Priorities for Sensing, Data Processing and Dissemination Technologies: "Techniques to enable absolute seafloor characterization …" and "Techniques to enable global bathymetric model generation …" Results from this project have produced and will continue to produce updated and high-resolution environmental properties in support of the operational Navy. Development on the HPC enables not only NRL, but also NAVOCEANO, to advance and maintain state-of-the-art capabilities in support of battlespace awareness across several warfare areas.

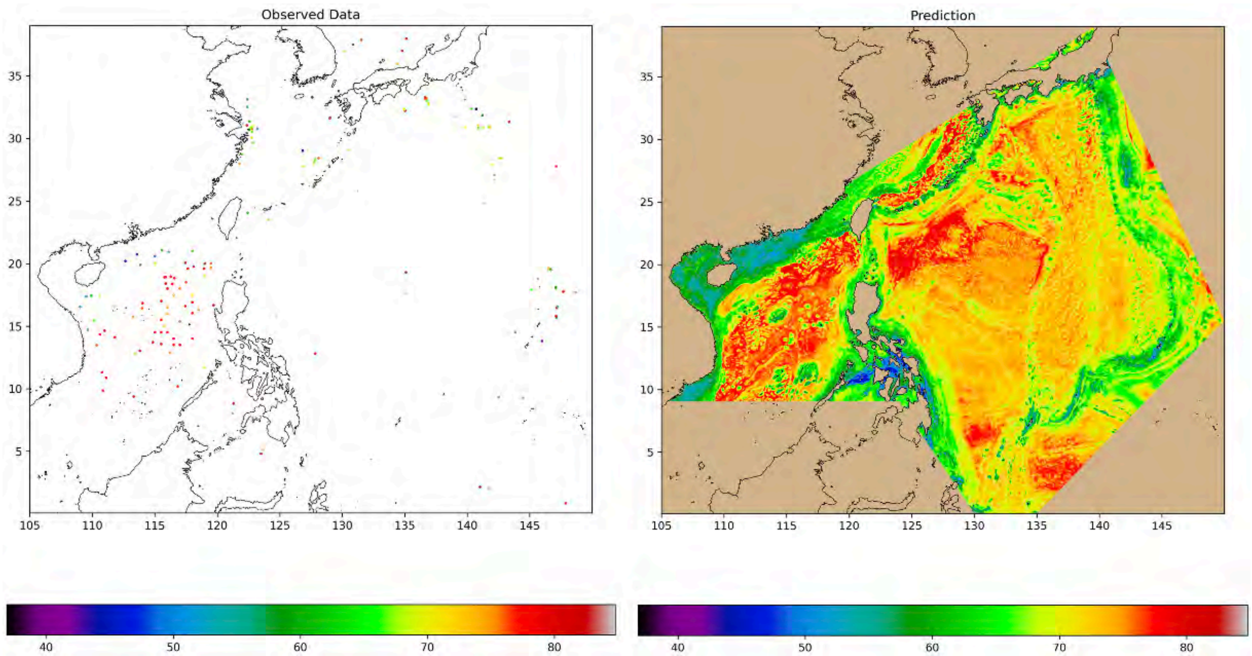

Figure 1. (left) Sparse distribution of seafloor porosity observations. (right) Continuous map of seafloor porosity using geospatial machine learning. Porosity is a measure of sediment water content, defined as the volume of pore space per unit volume of total sediment, and has direct control over physical properties such as sediment strength and seafloor density.

THIS PAGE INTENTIONALLY LEFT BLANK

DDA

Data and Decision Analytics

The Data and Decision Analytics (DDA) CTA concentrates on leveraging state-of-the-art supercomputing to advance large-scale data analytics and machine learning. Rapid progress in machine learning algorithms now makes it possible to extract insight from and to act on the vast, increasingly accessible data repositories maintained by the defense community and available to the public. Representative applications include financial optimization using defense-relevant records, predictive analysis of helicopter maintenance based on operational data, and the design of novel peptides derived from public protein databases. The CTA places particular emphasis on enabling the analysis of high-dimensional data sets that were previously intractable, as well as on developing new algorithms for graph analytics and machine learning.

In addition to algorithmic innovation, the CTA addresses the full research-and-deployment workflow, encompassing software, hardware, storage, and networking infrastructure. Its objectives are to streamline data aggregation, to accelerate the development of advanced analytic and machine learning capabilities, and to ensure seamless integration of results into operational decision-making processes.

Title: Synthetic Aperture Radar Foundation Machine Learning Model
Author(s): M. Naughton-Rockwell, R. Fiedler, T. Cox, and B. Shelters
Affiliation(s): U.S. Naval Research Laboratory, Washington, DC
CTA: DDA

Computer Resources: Penguin Open Compute Platform (OCP) [AFRL, OH]; Penguin TrueHPC [NAVY, MS]

Research Objectives: Synthetic aperture radar (SAR) is mission critical due to its ability to acquire imagery regardless of weather or time of day; however, the machine learning (ML) tools for analyzing SAR imagery lag behind their optical counterparts. The prevailing method to train SAR-based ATR algorithms is to perform transfer learning with open-source foundation models trained exclusively on electro-optical (EO) data. A challenge with this approach is that content in SAR imagery fundamentally differs from that in EO imagery because SAR is collected in the range-angle domain in the microwave band, while optical imagery is collected in the angle-angle domain in the visual spectrum. Therefore, algorithm performance can be limited, as the underlying image features and relationships on which an EO foundation model is trained do not hold for SAR imagery. We propose a set of generic foundation models for SAR imagery that can be applied to a wide variety of downstream tasks, for example, image detection, classification, and segmentation.

Methodology: A proof-of-concept Vision Transformer (ViT) model was pretrained with full scene data from spaceborne commercial SAR platforms via the masked autoencoding (MAE) technique (MAE ViT); the encoder transforms a 64 × 64 input image into 16 patches of 16 pixels ×16 pixels, and then only gives the encoder 25% of the patches (i.e., effectively masking the patches). The decoder then learns to recreate the input image from the subset of patches. We modified the MAE to take a 1 channel as input, versus the classic RGB 3 channel image, to support the grayscale nature of SAR. Additionally, we introduced image augmentations that are SAR specific, allowing for our model to capture SAR features. We use a unique method of developing a training dataset for this study. The training dataset consists of about 6,000 publicly available Sensor Independent Complex Data (SICD) files, containing mainly water for our model's anticipated maritime applications.

Results: A proof-of-concept MAE ViT model was pretrained with full scene data from spaceborne commercial SAR platforms. An ablation study of EO and SAR foundation models was performed to compare performance in several downstream target classification tasks. Preliminary results indicate that the prototype SAR foundation model performs comparably against state-of-the-art (SOTA) EO models even though the SAR model was only trained for approximately half of the time of the EO model. The performance trends achieved with a small quantity of training data encourage full-scale training with a large volume of data. It is predicted that ATRs developed from a SAR native foundation model starting point will outperform those developed from EO foundations. Additionally, transfer learning from a SAR (vs. EO) foundation model will provide increased insight into the quantity and characteristics of training data required to develop mission-specific ATR algorithms.

Defense Impact/Significance: Future operational concepts for long-range fires rely on timely situational awareness data provided by machine learning (ML)-based automatic target recognition (ATR) algorithms. Reliable ATRs for SAR data are critical for target custody maintenance in any weather condition, day, or night.

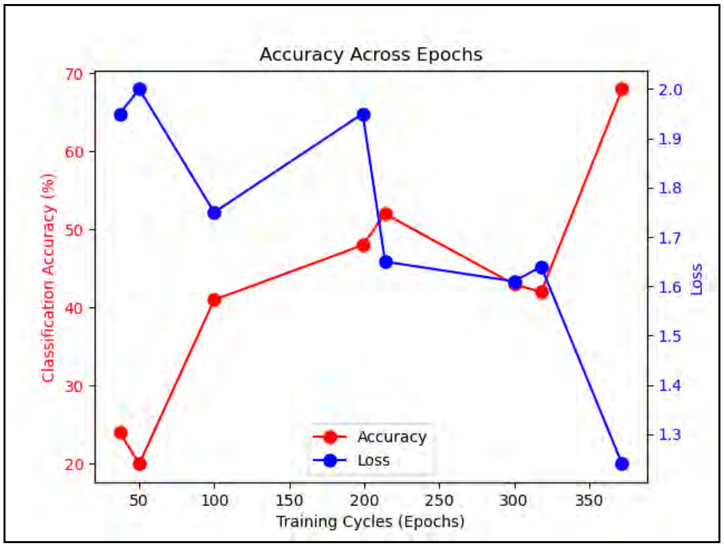

Figure 1. Testing accuracy across epochs: The shape of the accuracy curve across epochs is a key indicator of training progress. When the accuracy of the testing dataset plateaus and stops increasing, the model has learned all it can from the data and is done training. The substantial, consistently rising curve of accuracy in Fig. 1 strongly indicates that the prototype SAR foundation model has not reached its potential. Further, ViT models, such as the one trained in this experiment, are known for their scalability; their performance generally improves with increased dataset size and training time.

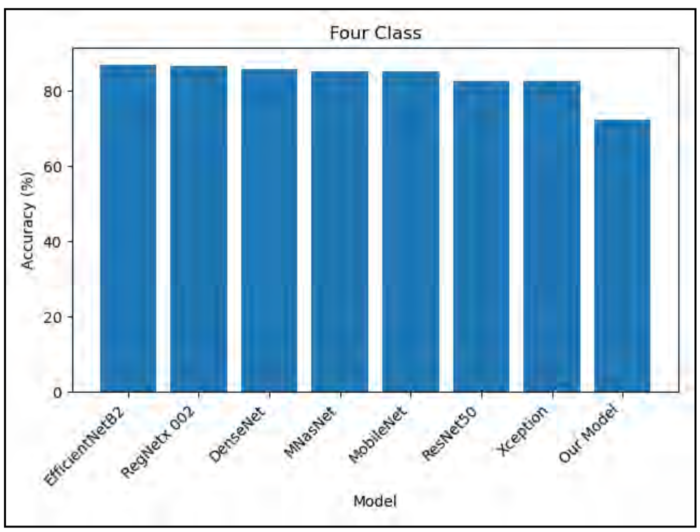

Figure 2. Comparative analysis of the classification performance on the Four Class dataset. EfficientNet, the top-performing model, achieved an accuracy of 87%. In contrast, our SAR model achieved an accuracy of 72%. The performance difference warrants further training and analysis of the SAR foundation model.

THIS PAGE INTENTIONALLY LEFT BLANK

Other

Work that is not easily categorized as one of the other CTAs.

Title: Characterization of some TI benchmarks on HPC Systems
Author(s): Y.Y. Khine
Affiliation(s): U.S. Naval Research Laboratory, Washington, DC
CTA: OTH

Computer Resources: HPE Cray EX [ARL, MD], [NAVY, MS]; Penguin TrueHPC [NAVY, MS]

Research Objectives: The goal of this project is to identify the tools required for performance testing of benchmarks on two recently available HPC systems: Penguin Computing TrueHPC system Nautilus (AMD Genoa CPUs with HPE Slingshot network at Navy DSRC) and HPE Cray EX4000 Carpenter (AMD Milan CPUs with HDR InfiniBand network at ERDC DSRC), and to apply them to a selection of representative codes, including some of the High Performance Computing Modernization Program's (HPCMP) technology insertion (TI) benchmark suites.

Methodology: The TI benchmark suite used in the past by HPCMP includes a representative collection of codes for various computational areas. In this project, we have chosen the open-source HYbrid Coordinate Ocean Model (HYCOM), which is a general ocean-modeling code widely used by the Navy and is available publicly [1], and the General Atomic and Molecular Electronic Structure System (GAMESS) by the Ames Laboratory, which is a general ab initio quantum chemistry package [2]. This project explored ways for more effectively benchmarking HPCMP systems using roofline model that is a visual performance-analysis tool that illustrates the relationship between a system's computational capability and memory bandwidth [3]. More effective approaches for collecting performance counters that are hardware registers that record low-level events such as cache misses, branch predictions, and instruction counts during program execution are also investigated in this project [4]. They provide detailed quantitative data that help developers analyze bottlenecks, identify inefficiencies, and optimize software performance on specific hardware architecture.

Results: Some sample results for this project are presented in this section. Figure 1 presents the theoretical roofline plots of Carpenter (ERDC DSRC) and Nautilus (Navy DSRC). The horizontal lines represent the compute ceiling/peak offered by the systems. The slanted lines to the left of the horizontal peak compute are the memory bandwidth ceiling of the systems. From Fig. 1, the performance of Carpenter is slightly better than that of Nautilus.

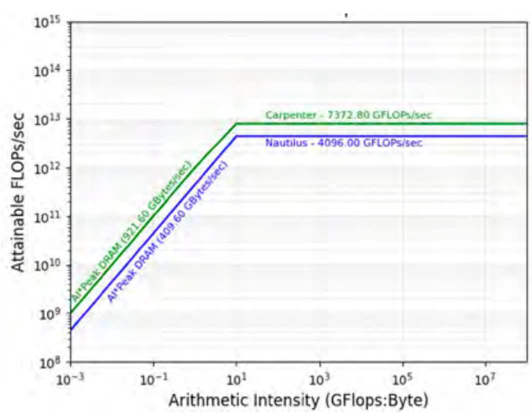

Figure 1. Theoretical roofline plots for Carpenter (ERDC DSRC) and Nautilus (Navy DSRC)

Figure 2 displays the roofline model of HYCOM on Nautilus at Navy DSRC, and HYCOM is widely used by Navy as the ocean component of a global coupled ocean-atmosphere-ice-wave prediction system. In a roofline model, the horizontal orange line represents the compute ceiling of the hardware, while the slanted lines on the left of the horizontal line represent peak memory bandwidth. On Nautilus, the performance of HYCOM (large, blue square) lies under the orange horizontal line, so the overall code performs under the compute ceiling of the hardware. This suggests that the performance of HYCOM could be improved to perform close to the peak compute offered by the hardware.

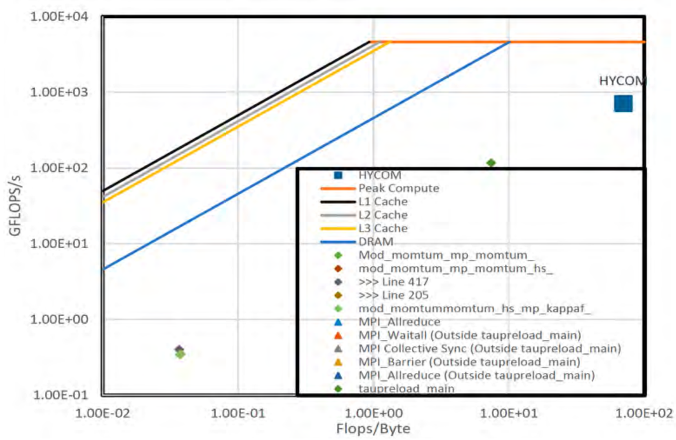

Figure 2. Roofline model of HYCOM on Nautilus at Navy DSRC

Defense Impact/Significance: The performance data from these studies provide valuable insights into how these applications perform across different systems and node counts. These insights go beyond simple runtime comparisons, helping to identify the factors that drive performance differences. They also inform how software optimizations or alternative hardware choices might improve overall performance of the widely used codes by the defense community to utilize available HPC resources efficiently. The results on the overall performance of various benchmark software on the newer HPC architecture/hardware are also important for future acquisitions of the future HPC systems.

Acknowledgment: Support on this project provided by the HPCMP PET program and the HPCMP Benchmarking Team are greatly appreciated.

References

[1] HYCOM Consortium, "HYCOM: HYbrid Coordinate Ocean Model," Online. Available: https://www.hycom.org/
[2] Ames Laboratory, "GAMESS: Open Source Quantum Chemistry Software," online. Available: https://www.ameslab.gov/gamess-open-source-quantum-chemistry-software
[3] S. Williams, A. Waterman, and D. Patterson, "Roofline: An insightful visual performance model for multicore architectures," *Communications of the ACM*, vol. 52, no. 4, pp. 65–76, Apr. 2009, doi: 10.1145/1498765.1498785.
[4] D. Zaparanuks, M. Jović, and M. Hauswirth, "Accuracy of performance counter measurements," in *Proc. 2009 IEEE International Symposium on Performance Analysis of Systems & Software (ISPASS)*, Berkeley, CA, USA, Apr. 2009, pp. 23-32, doi: 10.1109/ISPASS.2009.4919635.

Title: Application of Physics-based Machine Learning to Navy Problems
Author(s): L.N. Smith
Affiliation(s): U.S. Naval Research Laboratory, Washington, DC
CTA: OTH

Computer Resources: Penguin Open Compute Platform (OCP), HPE Cray EX [AFRL, OH]; Liqid [ARL, MD]; Penguin TrueHPC [NAVY, MS]; Nvidia H100 Cluster [NRL, DC]

Research Objectives: The overarching goal of our Improving Generalization of Neural Networks for Physics Domains project in FY25 was to investigate and develop various generalization methods across three critical physics domains: acoustics, meteorology, and materials science. Our primary focus aimed to bridge existing gaps in research and to enable neural networks to excel at physics tasks across various physical environments and boundary conditions.

Methodology: Our technical approach made significant strides in this regard. Deep learning techniques have demonstrated exceptional success in computer vision and language tasks. However, there remain significant gaps in the field's research that hinder their successful application to physics problems. Our research endeavored to fill these gaps and to provide valuable insights into the fundamental workings of neural networks in this context.

In FY25, this research program addressed three fundamental challenges in physics-informed machine learning: (1) inadequate generalization of standard deep learning techniques for physics applications, (2) requirements for models that generalize across diverse physical environments and governing equations, and (3) computational limitations of traditional numerical physics solvers. Our integrated approach combines physics-guided neural architectures, domain-specific generalization strategies, and scalable neural operator frameworks to achieve robust, high-fidelity predictions across complex physical systems.

Results: Our research focuses primarily on wave propagation phenomena governed by the Helmholtz equation, with applications spanning sonar acoustic modeling, radio frequency (RF) propagation, and structural health monitoring. We investigated neural operators — a class of deep learning models that learn mappings between function spaces — to improve the generalization of neural surrogates for the Helmholtz equation governing wave propagation in inhomogeneous media (underwater acoustics, electromagnetic waves in atmospheric environments, and elastic waves in metallic structures). Due to their significant, but underexplored, potential, neural operator frameworks were our primary technical focus in FY25 and will continue to be our primary focus throughout FY26.

In addition to our research efforts, we also examined the use of the Python library JAX and torch.compile (in PyTorch) to obtain substantial speedups of our neural network implementations.

Defense Impact/Significance: Our work demonstrates that applying machine learning to a variety of physics problems is sound. We are now applying machine learning methods to solve other challenges in various physics domains in order to enable substantially improved environmental and situational understanding by our fleet. In addition, the understanding gained by the experiments on the HPC GPU servers builds on all the previous understandings gained from previous experiments, and this understanding is crucial for our future progress in the field.

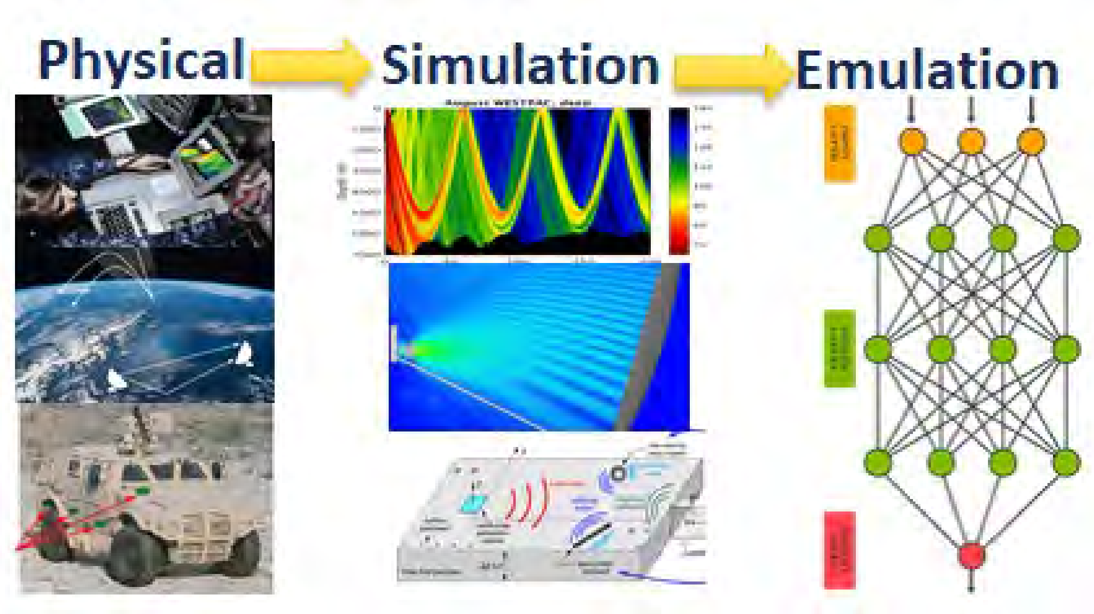

Figure 1. This figure represents the concept of using generative neural network models to emulate the results of a computationally expensive physics simulator. Our emulations run orders of magnitude faster than physics simulations, providing a substantial advantage for warfighters in computationally constrained environments.

Title: Simulation of High Energy-Radiation Environments
Author(s): J.D. Finke
Affiliation(s): U.S. Naval Research Laboratory, Washington, DC
CTA: OTH

Computer Resources: HPE Cray EX [AFRL, OH], [NAVY, MS]

Research Objectives: Our objective is to apply an improved model of the extragalactic background light (EBL), computed on HPC machines, to new gamma-ray absorption data. The EBL is the background light from all the stars that have existed in the Universe. It contains information about star formation, stellar initial mass function (IMF), the expansion rate of the Universe, dust extinction, and other quantities of astronomical interest. It can absorb gamma rays at energies greater than approximately 10 GeV, allowing for a method of measuring it complementary to galaxy counts. The model was applied to gamma-ray data from: (1) the Fermi Large Area Telescope (in Earth orbit), on 1574 AGN; the 15 years of data are sensitive to the 10 GeV–1 TeV energy range, extending out to redshift 4.3, and (2) 403 gamma-ray spectra from 73 AGN out to redshift 0.95 detected with ground-based imaging atmospheric gamma-ray telescopes; these spectra are in the energy range of 100 GeV to 30 TeV. This is a significant improvement over the previous sample used in 2018.

Methodology: We have created a model for the extragalactic background light (EBL). This model makes use of the PEGASE stellar spectra library and includes physically realistic star formation, dust extinction, and dust reradiation. This model has been applied to a variety of gamma-ray absorption data from blazars, measured by the Fermi Large Area Telescope and ground-based imaging atmospheric Cherenkov telescopes. Using a Markov chain Monte Carlo (MCMC) technique, the model can be applied to these data and the EBL intensity, and the cosmic star-formation history can be measured. In this application, the free parameters are associated with star formation and dust radiation. The IMF and dust-extinction parameters were fixed. In addition, a simple empirical model was used to fit the data. This model used a series of log-parabola components for the luminosity density, which were then convolved to find the EBL intensity and gamma-ray opacity to compare with data. This provides a model-independent constraint on the EBL.

Results: The MCMC technique has resulted in updated constraints on the EBL intensity (see Fig. 1). We are able to measure the star-formation history going back to when the Universe was about 1.1 billion years old. For comparison, the Universe is about 13.8 billion years old now; thus, we can measure the star formation for more than 90% of the Universe's history. The measurement is consistent with complementary measurements from galaxy surveys. This more precise measurement, and comparison with results from galaxy counts, can help determine whether there is another component to the EBL from, for example, interhalo light from galaxies or dark matter annihilation. The empirical model allowed for a more robust measurement, although with less physical interpretation. With fewer physical constraints, the empirical model applied to these data resulted in larger uncertainties. The recent results are a bit higher than the results from 2018, likely due to the inclusion of new, lower limits on the EBL intensity.

Defense Impact/Significance: Understanding the transparency of the Universe is crucial to studying GRBs, AGN, and other astrophysical objects that accelerate particles. Understanding particle acceleration in these sources can give insight into how particles accelerated elsewhere can impact defense space assets.

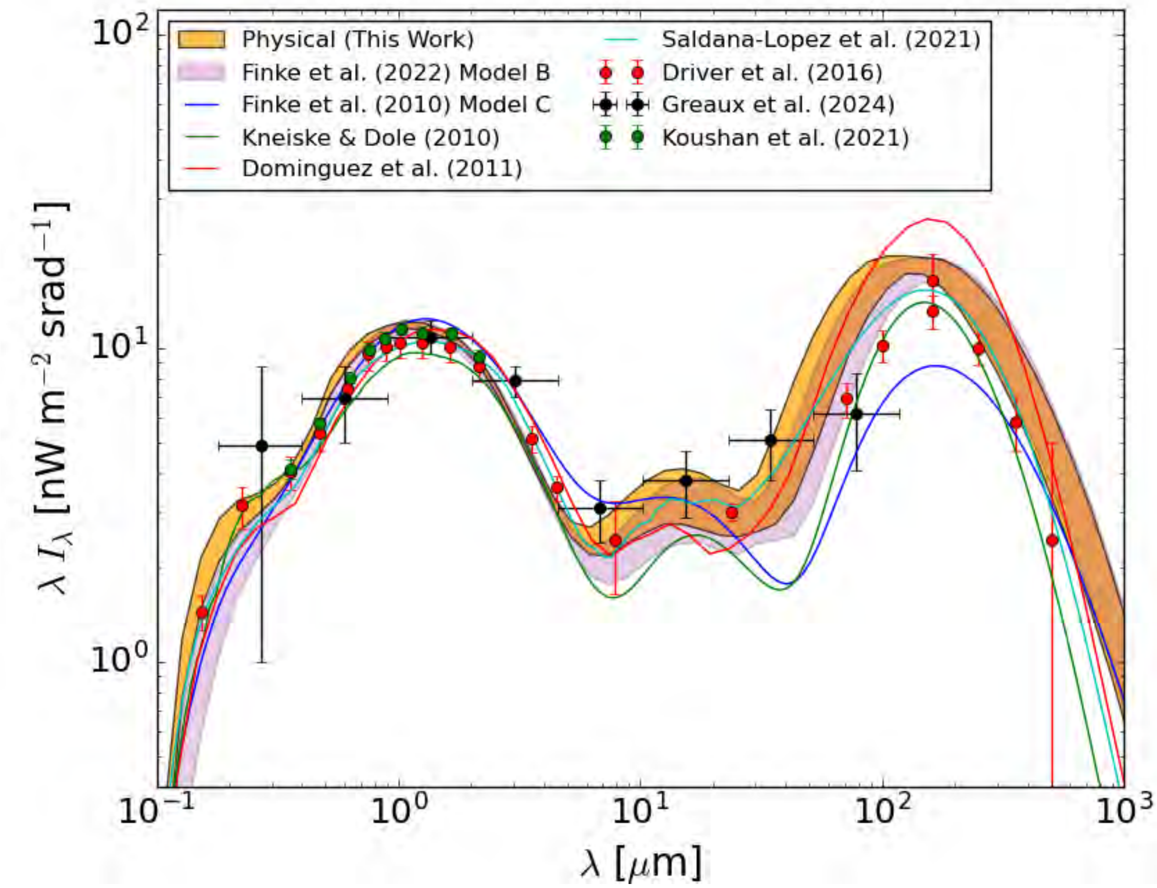

Figure 1. The EBL intensity from several measurements and models from the literature, as described in the legend. The most recent ***preliminary*** result is labeled "Physical (This Work)".

THIS PAGE INTENTIONALLY LEFT BLANK

Author Index

Author Index

Division/Branch Index

Center for Biomolecular Science and Engineering (Code 6900)

Ocean and Atmospheric Science and Technology Directorate (Code 7000)

Acoustics Division (Code 7100)

Remote Sensing Division (Code 7200)

Ocean Sciences Division (Code 7300)

Marine Meteorology Division (Code 7500)

Space Science Division (Code 7600)

Site Index

DSRCs

This page intentionally left blank